SOIL UPTAKE OF MOLECULAR HYDROGEN & REMOTE SENSING OF SOIL FREEZE AND THAW

Thesis by

Nicole V Smith Downey

In Partial Fulfillment of the Requirements for the

degree of

Doctor of Philosophy

CALIFORNIA INSTITUTE OF TECHNOLOGY

Pasadena, California

2006

(Defended July 20, 2006)

© 2007

Nicole Smith Downey

All Rights Reserved

ACKNOWLEDGEMENTS

First I would like to thank my advisor, Jim Randerson, for his support and inspiration over the past five years. I have never met anyone with so many ideas about science and the enthusiasm to be involved in such a wide range of projects. I admire Jim's open attitude toward sharing ideas and I am continually impressed by his ability to know exactly what figure will clarify the point I am trying to make.

John Eiler first got me into the hydrogen problem by giving an ESE seminar, to which I remember writing an e-mail saying "I am building a model of soil carbon fluxes, adding hydrogen shouldn't be that hard". As I soon discovered that it was going to be harder than I thought, John provided lab advice, a good dose of reality and encouragement.

Dianne Newman convinced me not to leave Caltech a long time ago, and I will be forever grateful for her support and advice during my first year.

Sassan Saatchi first came up with the idea of detecting soil freeze and thaw with microwave satellite data, and helped guide me through my first "scientific endeavor". Thanks for your encouragement!

Jared Leadbetter provided the TA3000R instrument to measure H_2 and lab space.

For my field measurements, I thank Brad Berger, William Bretz, the staff of the James Reserve, and the University of California Natural Reserve System for providing field sites and infrastructure. I also thank Lisa Welp for helpful advice and for letting me 'borrow' her field equipment for my measurements. Stan Tyler first suggested the plastic syringe approach to storing my field gas samples. Paul Novelli gave me a crash course in what to expect from my H_2 analyzer.

In the lab, where I started out knowing nothing, I am grateful for assistance from Prosenjit Ghosh, Julie O'Leary, Hagit Afek, and Max Child. Kathleen Treseder collected soil samples near Delta Junction, AK for my lab experiments, and Xiaomei Xu helped me analyze soils for organic carbon and nitrogen content at UC Irvine.

Prasad Kasibhatla generously invited me to Duke University to learn GEOS-CHEM, and provided me with computational support for my simulations of H_2 anomalies in the atmosphere. Hiroko Kato and Dorothy Hall provided me with data for my global H_2 model and Mark Flanner came through with a last minute save on snow depth data.

Nathan Downey helped me develop the finite difference scheme that is the basis of my global hydrogen model and dug a few holes in the field.

Outside of my research, I am indebted to my husbando Nathan, who is the greatest, and my parents, who have always loved me. My friends Angie, Laura, Marcin and TJ keep me sane and give me something to look forward to. Chris, David, Elisabeth, JD, Julie, Laura, Lydia, Tanja – you are all amazing. Thanks for the walks to Peet's, BC, and all the fun times.

I also thank Caltech, the EPA STAR fellowship program, General Motors, the Davidow family, and the University of California Dean's Initiative for funding support.

ABSTRACT

Soils play a large role in the cycling of atmospheric trace gases and are an important component of the climate system. The bulk of my thesis was directed at the role of soils in the global molecular hydrogen (H_2) cycle. I conducted field measurements of H_2 uptake in three Southern California ecosystems, and found that both the diffusion of H_2 into soils and the distribution of biological activity with depth controlled uptake rates at the surface. I then moved into the laboratory, where I mapped out the temperature and moisture controls on the biological uptake of H_2 in both desert and boreal forest soils. These experiments yielded simple relationships between moisture, temperature, and uptake rate, which I then used to constrain H_2 uptake by soils in a mechanistic model. The model is based on the 1D diffusion equation with a sink term, and is driven by a combination of remote sensing products and land surface modeling output. I calculated a mean annual soil H_2 sink of 67.3 ± 5.5 Tg. The model was able to reproduce the seasonal cycle at high northern latitudes, and implies that seasonal variability in snow cover is a key process controlling H_2 uptake. I found that snow cover and soil moisture control the uptake of H_2 globally, which may have important implications for the hydrogen budget in future climate change scenarios.

My second thesis topic involved the development of a remote sensing technique using passive microwave brightness temperatures to identify the freeze-thaw status of soils, which I applied to areas north of 45°N. I found a significant increase in the growing season length in North America by 3.8 days/decade, driven by both an earlier spring thaw and later fall freeze. The lengthening of the growing season may affect the carbon and hydrogen cycles at high northern latitudes, and is a new metric of global change.

TABLE OF CONTENTS

Acknowledgements iii
Abstract v
Table of Contents vi
Chapter I: Introduction 1
Chapter II: Field Observations of molecular hydrogen (H_2) uptake in three California ecosystems 7
Abstract 7
Introduction 8
Methods 10
Results 14
Discussion and Conclusions 16
Tables and Figures 19
Chapter III: Temperature and moisture dependence of soil H_2 uptake measured in the laboratory 29
Abstract 29
Introduction 29
Methods 32
Results 35
Discussion and Conclusions 37
Figures 40
Chapter IV: A Global mechanistic model of molecular hydrogen (H_2) uptake by soils 46
Abstract 46
Introduction 46
Global H_2 Model 48
Model Results 53
Discussion and Conclusions 55
Figures 58
Chapter V: Trends in high northern latitude freeze and thaw cycles from 1988 to 2002 64
Abstract 65
Introduction 66
Methods 68
Results 76
Discussion 79
Conclusions 83
Tables and Figures 84
Appendix I: Update to "Trends in high northern latitude freeze and thaw cycles from 1988 to 2002" 97

Bibliography 100

Chapter 1

Introduction

Soils are an important component of the climate system and act as an interface between the biological cycling of trace gases and the atmosphere. My thesis concentrated on two separate components of this interface. The major focus of my thesis was to investigate the role of soils in the destruction of atmospheric molecular hydrogen (H_2). By conducting field and laboratory experiments, I was able to describe the environmental controls of soil H_2 uptake and develop a mechanistic model of global H_2 consumption by soils. The model allowed me to estimate the annual total hydrogen consumption by soils globally, to identify the importance of different environmental driving variables and to simulate the seasonal cycle of H_2 at high northern latitudes. My second project involved developing a remote sensing technique to detect the freezing and thawing of soils. Using this product, I quantified changes in the onset of spring thaw, fall freeze and the growing season length at high northern latitudes from 1988 to 2005 and discussed potential impacts to the carbon cycle. Both of these projects have important implications for the cycling of atmospheric trace gases with the biosphere, and highlight the importance of soils in the climate system. My thesis is comprised of the papers resulting from my work at Caltech.

Molecular Hydrogen Uptake by Soils

Molecular hydrogen (H_2) is the 9th most abundant gas in earth's atmosphere, and the 2nd most abundant reduced gas after methane (CH_4). The mean global concentration of H_2 was ~530 ppb in the 1990s and it has a mean tropospheric lifetime of 2 years [*Novelli, et al.*, 1999]. H_2 is produced by fossil fuel combustion, biomass burning, and

the oxidation of methane and non-methane hydrocarbons. The two primary sinks of H_2 are uptake by soils and loss to OH (Figure 1) [*Novelli, et al.*, 1999]. The latitudinal distribution of H_2 is rather unique, as the concentration is lower in the northern hemisphere than the southern hemisphere even though most H_2 sources are in the northern hemisphere. This is attributed to the dominance of the soil sink, which is concentrated in the northern hemisphere. There is a strong seasonal cycle in the atmospheric H_2 record at northern latitudes, with a peak in late spring and a minimum in fall (Figure 2).

Recent concerns regarding the loss of stratospheric ozone due to increases in anthropogenic H_2 emissions in a hydrogen economy have stimulated significant interest in the global H_2 budget [*Schultz, et al.*, 2003; *Tromp, et al.*, 2003; *Warwick, et al.*, 2004]. The possibility (or reality) of global warming due to greenhouse gas emissions has forced governments and energy providers to seek new sources of energy that do not rely on fossil fuels. One option is to replace fossil fuels with hydrogen fuel cells, which, in theory, generates water as its only waste product. Apart from the environmental impacts of generating H_2 for this application, significant increases in anthropogenic emissions of H_2 due to leaks may increase the tropospheric H_2 burden. Hydrogen mixes freely across the tropopause, and once in the stratosphere it is converted to water, which leads to ozone loss [*Tromp, et al.*, 2003; *Warwick, et al.*, 2004]. The magnitude of this impact will be directly controlled by the soil sink, which may respond to both changes in emissions and future climate conditions.

Although it has long been recognized that soils are the dominant loss mechanism for H_2 (e.g. [*Seiler*, 1987]), the environmental controls and global distribution of soil H_2

uptake are not well understood and estimates of the proportional loss of H_2 due to soils range from 62 to 92% [*Seiler*, 1987; *Warneck*, 1988; *Ehhalt*, 1999; *Novelli, et al.*, 1999; *Hauglustaine and Ehhalt*, 2002; *Rhee, et al.*, 2006]. A model analysis of the complete hydrogen cycle was unable to predict the seasonal cycle of H_2 at northern latitudes, which was attributed to poor understanding of the soil sink [*Hauglustaine and Ehhalt*, 2002].

There are several studies including field measurements of H_2 uptake by soils [*Conrad and Seiler*, 1985; *Yonemura, et al.*, 1999, 2000a; *Rahn, et al.*, 2002] and multiple laboratory experiments aimed at identifying the microbes or enzymes responsible for the destruction of H_2 and their response to changes in environmental conditions [*Conrad and Seiler*, 1981; *Schuler and Conrad*, 1990, 1991; *Haring and Conrad*, 1994; *Haring, et al.*, 1994; *Godde, et al.*, 2000; *Dong and Layzell*, 2001]. These studies point to the importance of temperature and moisture on H_2 uptake rates, and suggest that diffusion of H_2 into soils controls flux rates at some locations [*Yonemura, et al.*, 2000a; *Yonemura, et al.*, 2000b].

My thesis was aimed at rigorously defining the temperature, moisture and diffusion controls on H_2 uptake and combining these into a global mechanistic model of soil H_2 fluxes. This involved three stages: first I conducted field measurements in three Southern California ecosystems between September 2004 and July 2005 (Chapter 2); next I moved into the laboratory and measured the temperature and moisture response of H_2 uptake in soils from the boreal forest and the Mojave Desert (Chapter 3); finally, I combined the information from my field and laboratory studies in a global model of soil hydrogen uptake (Chapter 4). Using this model, I was able to reconstruct the seasonal

cycle of H_2 in the atmosphere at northern latitudes, and calculated a mean total soil sink of 67.3 ± 5.5 Tg H_2 yr^{-1}.

Soil Freeze and Thaw

The annual freezing and thawing of soils is a significant phase transition that controls both respiration from soils, the onset of photosynthesis, and the capacity of soils to consume H_2. I developed a technique to detect the timing of soil freeze and thaw between 1988 and 2002 using passive microwave brightness temperatures from the Nimbus-7 Scanning Multichannel Microwave Radiometer (SMMR) and DMSP Special Sensor Microwave/Imager (SSM/I) (Chapter 5). North of 45°N, I found that the growing season length (the length of time between spring thaw and fall freeze) increased in North America between 1988 and 2002, as a result of both an earlier thaw and later freeze. In Eurasia, I found that both the spring thaw and fall freeze were shifting forward in time, yielding no net change in the growing season length, but changing the timing of carbon uptake by photosynthesis and release by respiration. The interannual variability in soil freeze and thaw was correlated with variations in surface air temperature. Since the publication of my original paper in 2004, three more years of SSM/I data have become available, and updated estimates of the trends in thaw, freeze and growing season length are included in Appendix I.

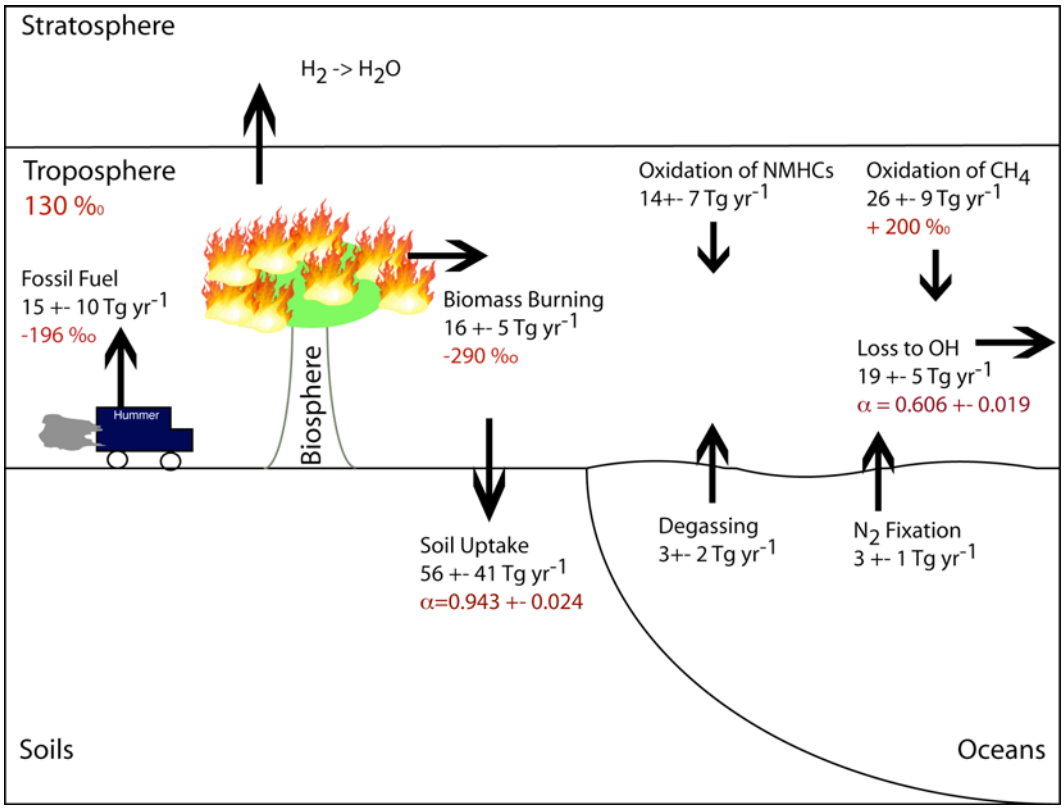

Figure 1. Simplified schematic of the molecular hydrogen (H_2) cycle. Arrows represent fluxes from one 'box' to another. Data are from *Novelli et al*. [1999], *Gerst and Quay* [2001] and *Rahn et al.* [2002].

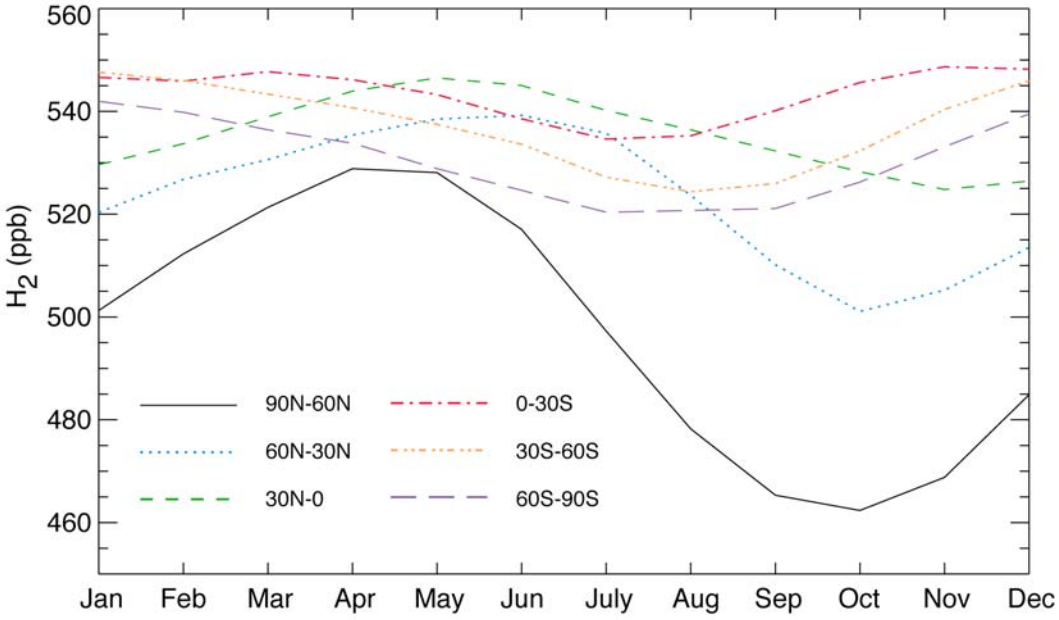

Figure 2. Mean seasonal cycle of H_2 at separated by latitude band. Data are from *Novelli et al.* [1999].

Chapter 2

Field observations of molecular hydrogen (H_2) uptake in three California ecosystems

In preparation for Journal of Geophysical Research - Biogeosciences

Nicole Smith Downey and James T. Randerson

Abstract

The largest sink of molecular hydrogen (H_2) in the atmosphere is uptake by soils. The mechanism and environmental controls on H_2 uptake by soils are, however, not well understood. Field observations of soil H_2 uptake are limited, and we present the results from a series of field experiments in forest, desert and marsh ecosystems in Southern California. We measured soil H_2 fluxes using chambers from September 2004 to July 2005. The mean H_2 flux rate into soils was -8.3 ± 4.6, -8.2 ± 4.3 and -6.0 ± 2.7 nmol/m^2/s for the forest, desert and marsh respectively. We did not observe a seasonal cycle at our sites. Soil profile measurements of [H_2] suggest that the vertical distribution of H_2 uptake capacity changes in response to soil moisture and that the majority of H_2 uptake occurs in the top 10 cm of the soil surface. Soil removal experiments in the forest showed that the litter layer did not actively take up H_2, and that aeration of soils increased their uptake capacity. Similar experiments at the desert site showed that the top layer of soil did not consume H_2, and that fluxes at the surface increased when this layer was removed. Measurements of the vertical profile of [H_2] support this result, and suggest that the depth of the 'inactive' layer increased as surface soils dried out. Our experiments highlight the importance of H_2 diffusion into soils and a minimum moisture requirement for biological activation of H_2 uptake.

1. Introduction

The uptake of molecular hydrogen (H_2) by soils accounts for between 62% to 92% of the total atmospheric sink [*Seiler*, 1987; *Warneck*, 1988; *Ehhalt*, 1999; *Novelli, et al.*, 1999; *Gerst and Quay*, 2001; *Hauglustaine and Ehhalt*, 2002; *Rhee, et al.*, 2006] and there are relatively few field measurements of soil H_2 uptake with which to improve these estimates. Recently, the atmospheric H_2 budget has received substantial attention due to the possibility of increased H_2 emissions and subsequent decreases in stratospheric ozone in a hydrogen economy [*Schultz, et al.*, 2003; *Tromp, et al.*, 2003; 2004]. With the current level of understanding, it is impossible to estimate how the soil sink will change in response to increases in emissions or changes in climate.

The uptake of H_2 by soils is a biological process that is inhibited at very low soil moistures [*Fallon*, 1982; *Conrad and Seiler*, 1985; *Smith-Downey, et al.*, in press], and decreases at high soil moisture levels due to limitation of H_2 diffusion into soils [*Yonemura, et al.*, 1999; *Yonemura, et al.*, 2000b]. The temperature dependence of the surface flux of H_2 into soils is not consistent between studies, and in many cases there is no observable correlation between soil temperature and H_2 flux rate. Laboratory measurements suggest that H_2 uptake is sensitive to changes in temperature from -4°C to 15°C, after which a broad temperature optimum is observed [*Smith-Downey, et al.*, in press]. Field measurements of soil H_2 uptake have been conducted in a boreal forest [*Rahn, et al.*, 2002], subtropical regions of South Africa [*Conrad and Seiler*, 1985], temperate sites in Europe [*Conrad and Seiler*, 1985], and an arable field and forest in Japan [*Yonemura, et al.*, 1999, 2000a]. More field observations of H_2 uptake by soils are

needed to sufficiently describe the response of soil H_2 uptake to environmental conditions.

Here we describe a series of field experiments conducted in three different California ecosystems between September 2004 and July 2005. We measured H_2 flux rates and distribution in the soil profile at forest, desert, and marsh field sites. We performed a series of soil removal experiments to determine how soils at different depths responded to H_2, and measured two near-surface atmospheric profiles of H_2 at night. CO_2 flux rates were also measured at the forest and desert sites and continuous measurements of soil temperature and soil moisture were recorded from February 2005 through July 2005.

We found that H_2 flux rates did not vary considerably between our forest and desert sites (-8.3 ± 4.6 and -8.2 ± 4.3 nmol m^{-2} s^{-1} respectively), and that the mean flux rates at the marsh were slightly lower (-6.0 ± 2.7 nmol m^{-2} s^{-1}). We did not observe a seasonal cycle of H_2 uptake, but our results suggest that the vertical distribution of H_2 uptake capacity is moisture dependent.

Our soil profile measurements show that H_2 is virtually eliminated within the top 10 cm of soil at the forest and desert sites. Over the course of the year, the 'active' layer of hydrogen uptake moved further down the soil profile at the forest and desert sites due to moisture limitation. At the marsh site, a hydrogen source was observed at 40 cm depth, which is consistent with anaerobic production of H_2 in saturated anoxic soils. Soil removal experiments showed that surface vegetation and litter do not contribute to the flux of H_2. Nighttime atmospheric profiles revealed a drawdown of H_2 accompanied by a

buildup of CO_2, which suggests that H_2 flux can be estimated at tower sites when the flux of CO_2 and atmospheric profiles of CO_2 and H_2 are measured.

2. Methods

2.1 Site Descriptions

We measured hydrogen uptake by soils at three sites in Southern California (Figure 1, Table 1) from September 2004 to July 2005. Each site was located in a different biome including a mixed conifer and hardwood forest in the San Jacinto Mountains (33°48′N, 116°46′W), the Mojave Desert (34°N, 116°W), and a freshwater marsh (33°39′N, 117°51′W), hereafter referred to as the forest, desert and marsh sites respectively. The forest and desert soil were sand and coarse sand, whereas the marsh soils were clay topped with organic material. At the forest site, three replicate flux chambers and soil gas samplers were installed near a streambed and on a hillside. At the desert site, two replicate flux chambers and soil gas samplers were installed at three locations along a gradient extending out from oak shrubs to bare sand to capture variability in organic carbon content of soils. At the marsh site, three replicate flux chambers and soil gas samplers were installed near a seasonal pond and in a reed dominated marsh. The water table was at approximately 40 cm at the marsh site in October 2004. In February 2005, both of these sites flooded, so a third site was established near the edge of a pond in April 2005.

2.2 Sample storage and H_2 analysis

For hydrogen measurements, gas samples were collected with 10 mL plastic syringes fitted with 3-way valves and stored in a cooler filled with dry ice. Storing the samples at sub-zero temperatures preserved the hydrogen concentration for several hours,

and laboratory tests showed a leak rate of approximately 2 ppb / hour for syringes filled with hydrogen free air. All samples were immediately returned to the lab and measured within 10 hours of sample collection. Samples were injected into a TA3000R Reducing Gas Analyzer (Ametek Process Instruments, Newark, DE) through a 5 mL sample loop connected to a 6-port valve (Valco Instruments, Houston, TX). The TA3000R RGA is a continuous flow instrument with a Unibead 1S and an MS 13X column for separation of H_2 and CO.

2.3 Flux chambers

Soil collars were constructed from 20 cm diameter PVC pipe cut into 10 cm deep sections and fitted with an acrylic collar (Figure 2a). These collars were permanently installed at each site and remained in place through the course of our field measurements. A flux chamber was constructed from acrylic and included a syringe port for removal of gas samples. A ¼" thick viton o-ring was placed between the soil collar and the flux chamber to ensure that the chamber was sealed. Once the collars were capped with the flux chamber, 10 mL gas samples were withdrawn immediately (after flushing the syringe twice), and at 1, 2, 4, and 8 minute intervals using plastic syringes. Exponential curves were fit to each uptake experiment (e.g. Figure 3)

$$H_2(t) = H_2(0) \cdot e^{-bt} \qquad (1)$$

where t is time, and the flux of hydrogen into the soil (nmol/m^2/s) was calculated as:

$$F_{H_2} = H_2(0) \cdot (-b) \cdot \frac{P \cdot V}{R \cdot T} \cdot \frac{1}{A} \qquad (2)$$

where $H_2(0)$ is the concentration of H_2 at time = 0s, P is atmospheric pressure (Pa) at each site, V is the volume of the flux chamber (0.01318 m^3), R is the gas constant, T is temperature (K), A is the area inside the soil collar (0.0324 m^2) and b is the constant from

equation (1). We made measurements of soil CO_2 flux rates several times at the forest and desert sites over the course of our experiments as well. The same soil collars were used, but the syringe port was removed from the flux chamber and replaced with a ¼" tube fitting that allowed continuous circulation of air through the chamber. A 0.5L pneumatic pump (KNF Neuberger, Trenton, NJ) pulled air from the flux chamber through a filter, a LI-800 Gas Hound CO_2 analyzer (Licor, Lincoln, NE) and finally pushed air back into the flux chamber through a tube fitting at the top of the chamber. The CO_2 efflux was measured for approximately three minutes increased linearly with respect to time. The CO_2 flux rate was calculated as:

$$F_{CO_2} = m \cdot \frac{P \cdot V}{R \cdot T} \cdot \frac{1}{A} \qquad (3)$$

where P, V, R, T and A are defined above, and m is the slope of the CO_2 growth curve.

2.4 Soil Profiles

Soil profiles of $[H_2]$ with depth were measured using soil gas samplers that were buried and left in place over the entire course of our field study (Figure 2b). The gas samplers were constructed from 25 mL disposable plastic pipets with 1/8" holes drilled in three sides and 1/32" inner diameter tubing leading to the surface. We dug soil pits to ~50 cm depth, and used a soil corer to remove horizontal plugs of soil at 2.5, 5, 10, 20 and 40 cm depth along the open face of the pit. The soil gas samplers were placed horizontally into the holes and the pit was back-filled with tubes leading to the surface. Soil gas samples were extracted with 10 mL plastic syringes fitted with a three-way valve and a luer stub adaptor (BD, Franklin Lakes, NJ). First 5 mL of air was removed from the gas samplers and was flushed out of the syringe and valve then a full 10 mL was withdrawn, the valve was closed, and the syringes were placed in a dry-ice filled cooler.

2.5 Soil Removal Experiments

We conducted a set of soil removal experiments at the forest and desert sites in April of 2005. A 30 cm deep soil collar was inserted into the soil (Figure 2a) and the H_2 flux was measured as described in section 2.3. Next, the vegetation contained in the collars was removed, and placed in a close-bottomed soil collar, and the H_2 flux was measured. We then re-measured the flux of H_2 in the soil collar, and removed one layer of soil. That layer of soil was placed in the closed-bottomed soil collar and the H_2 flux was measured. This process was repeated several times to establish the H_2 uptake capacity of individual soil layers, and the remaining soil profile.

2.6 Atmospheric Profiles

Atmospheric profiles of [H_2] and [CO_2] were measured at night at the Forest and Marsh sites in April of 2005. Tubes for H_2 and CO_2 sampling were placed at 0, 0.25, 0.5, 1, 2 and 4 m height on a sampling tower. H_2 samples were drawn through 1/32" tygon tubing and stored in 10 mL plastic syringes. CO_2 samples were pulled into a LI-800 Gashound CO_2 analyzer with a 0.5 L pneumatic pump (KNF Neuberger, Trenton, NJ).

2.7 Soil Temperature and Moisture

Soil temperature and moisture were measured continuously after February 2005 at the forest and desert sites using integrating temperature sensors from 0 to 5 cm depth (Model 107-L, Cambpell Scientific, Logan, UT) and time-domain reflectometry (TDR) sensors at 5 and 20 cm depth (Model 616-L, Cambpell Scientific, Logan, UT). Data were averaged every ½ hour and stored on CR10X dataloggers (Campbell Scientific, Logan, UT). Southern California received an anomalously high amount of precipitation over the winter of 2005, and our sites received 100 cm (forest), 21 cm (desert), and 40 cm (marsh)

of precipitation between September 2004 and May 2005 (Western Regional Climate Center (WRCC) station observations from Idyllwild, CA, Twentynine Palms, CA, and Newport Beach, CA available online at http://www.wrcc.dri.edu/clim-sum.html).

3 Results

The flux of H_2 into soils was first-order, and most of the hydrogen was removed from our flux chamber within 8 minutes (e.g. Figure 3). The forest and desert H_2 fluxes exhibited the same range of variability (-2 to -15 nmol m^{-2} s^{-1}, negative to indicate flux into soil), but a clear seasonal cycle was not evident from our data (Figure 4a and 4b). The decrease in the forest streambed flux rate after January 2005 corresponded with a flooding event that deposited ~5 cm of litter and sediment over our collars. In March 2005, the fluxes at the desert site were substantially higher than at any other time, and corresponded with relatively warmer soil temperatures and higher soil moisture (Figure 4). Fluxes at the marsh were generally lower (-5 to -8 nmol m^{-2} s^{-1}) than at the forest and desert sites (Figure 4c, Table 2). CO_2 fluxes were higher at the forest streambed site than the hillside site (Figure 4d, Table 2). At the desert site, CO_2 fluxes were substantially higher directly under the shrubs, and were lowest in the bare sand (Figure 4e), but no consistent pattern existed for H_2 fluxes. Soil temperature steadily increased at the forest and desert sites between January and July (Figures 4f and 4g). Volumetric water content of soils decreased at the forest site after rain ceased in May 2005 (Figure 4h), and decreased at the desert site after March 2005 (Figure 4i). At both sites the soil moisture was higher at 20 cm depth than at 5 cm depth. We were unable to fit significant relationships between soil temperature, soil moisture and H_2 flux at the surface.

Our soil profile measurements showed that, at the forest and desert sites, [H_2] concentrations decreased rapidly with depth and at all measurement periods H_2 was less than 10% of atmospheric levels at a depth of 40 cm (Figure 5). From April 2005 to July 2005, [H_2] at the desert site penetrated progressively deeper into the soil profile, which coincided with a decrease in the surface H_2 flux after March 2005 (Figure 6a). The concentration of H_2 at 10 cm depth increased along with a decrease in the volumetric water content of soils (Figure 6b). A similar, although less dramatic change occurred at the forest site in July 2005. Steady state hydrogen concentrations were higher at the marsh site, and [H_2] increased at 40 cm depth (Figure 5c).

At the forest site, soil removal experiments showed that the topmost vegetation and litter layers did not significantly contribute to the flux of H_2 observed at the surface (Figure 7). After the litter layer was removed, the observed flux at the surface increased from -9.7 to -12.3 nmol m^{-2} s^{-1}. Each of the removed soil layers consumed more hydrogen than the intact soil profile (-24.4 and -18.9 nmol m^{-2} s^{-1} vs. -12.3 and -12.8 nmol m^{-2} s^{-1}). At the desert site, the topmost vegetation and soil layers did not consume H_2. As each layer of soil was removed, the observed surface H_2 flux increased from -5.97 to -9.70 to -14.35 nmol m^{-2} s^{-1}. We used a simple 1D diffusion model with a sink term to assess how long it would take the soil profile to re-equilibrate after the removal of layers of soil, (which exposed soil with very low H_2 to the atmosphere, increasing the concentration gradient). Our model predicted that the soil profile would re-equilibrate in less than 45 s.

Nighttime atmospheric profiles of [H_2] and [CO_2] from 0 to 4 m height were measured at the forest and marsh site in April 2005 (Figure 8). At both sites a drawdown

of H_2 and buildup of CO_2 was observed close to the soil surface. At the forest site the flux of H_2 was -19.5 nmol m^{-2} s^{-1} and the flux of CO_2 was 1.6 μmol m^{-2} s^{-1}. At the marsh the flux of H_2 was –3.2 nmol m^{-2} s^{-1} and the flux of CO_2 was 6.4 μmol m^{-2} s^{-1}.

4. Discussion and Conclusions

Our field observations imply that that ecosystem type is not a strong controller of soil H_2 flux rates and that the vertical distribution of H_2 uptake in soils may control surface flux rates. Our soil profile and soil removal experiments demonstrated that the vertical distribution of H_2 uptake with depth changed over time, and previous work suggests that H_2 uptake requires a minimum moisture level for biological activation [*Fallon*, 1982; *Conrad and Seiler*, 1985; *Smith-Downey, et al.*, in press]. The profile measurements show that the surface layer of soil at the desert site became inactive with respect to hydrogen between March and April, and continued down the soil profile through July. This corresponded with decreases in the surface flux of H_2, suggesting that the vertical structure of H_2 uptake is important for the surface flux, and that it is controlled by soil moisture (Figure 6a).

At the forest streambed site, a flooding event deposited ~ 5 cm of sediment and litter over our collars in January 2005. This led to a dramatic decrease in H_2 fluxes, which gradually recovered over time. This suggests that soil disturbance, particularly disturbance that impedes the diffusion of H_2 into soils, is a powerful control on local soil H_2 uptake.

Generally, there was little observable difference between fluxes at the forest and desert sites, but the marsh site exhibited slightly lower fluxes. We hypothesize that this is primarily due to differences in soil structure. The soils at the forest and desert site were

relatively porous sandy soil, whereas the marsh was dominated by fine grained, clay rich and less porous soil.

At the desert site, we designed our experiments to test the effect of organic carbon on H_2 fluxes by placing our soil collars along a gradient of vegetation from directly under large shrubs to bare sand. Although CO_2 fluxes were substantially higher under the shrubs, and decreased as we moved to bare sand, no such trend was apparent in the H_2 flux data. Similar patterns have been observed for the uptake of methane by desert soils [*Streig, et al.*, 1992].

Soil removal experiments showed that the litter layer at the forest site was nearly neutral with respect to H_2. We attribute the small flux we did observe to a small amount of soil that was inter-mixed with the litter in the soil collar. Once the litter layer was removed, the flux at the surface increased. We hypothesize that this is due to the removal of a diffusive barrier, which enhances the supply of H_2 to the underlying surface. When each layer of soil was scraped away from the soil profile and placed in a sealed chamber, the total flux observed increased. In removing the soil layers from the surface and transferring them to the sealed collar, we aerated them, which may have enhanced the flux of H_2.

At the desert site, we observed an 'inactive' layer of soil at the top of the profile in our soil removal experiments. When this layer was removed, the surface flux of H_2 increased from -6 nmol m^{-2} s^{-1} to -10 nmol m^{-2} s^{-1}. After a second layer of soil was removed, the surface flux increased to -14 nmol m^{-2} s^{-1}. It is possible that these increases in fluxes were due to an increased gradient in [H_2] between the atmosphere and relatively depleted soil [H_2] at depth, but our 1D diffusion model results suggest that the soil profile would

re-equilibrate in less than 45 s, supporting our hypothesis that the increased fluxes were due to the removal of a diffusive barrier.

Our results suggest that both the diffusive properties of soil, which regulate [H_2] supply to soil microbes, and uptake distribution with depth control the surface fluxes of H_2. These results are consistent with previous observations from several groups [*Conrad and Seiler*, 1985; *Yonemura, et al.*, 1999, 2000a; *Yonemura, et al.*, 2000b; *Smith-Downey, et al.*, in press] and suggest that in order to predict hydrogen fluxes, it is necessary to model both the diffusive properties of soils along with the response of biological uptake to environmental conditions.

Table 1. Mean Climate at Field Sites

	Mean Max Temp (°C)	Mean Min Temp (°C)	Mean Annual Precipitation (cm)	Elevation (m)
Forest	**13**	**-0.6**	**79**	**1650**
Desert	**28**	**11**	**11**	**1100**
Marsh	**23**	**12**	**31**	**2**

Mean temperatures and precipitation from the Western Regional Climate Center (WRCC) station observations from Idyllwild, CA, Twentynine Palms, CA, and Newport Beach, CA available online at http://www.wrcc.dri.edu/clim-sum.html

Table 2. Mean H_2 and CO_2 fluxes

		Mean H_2 Flux (nmol m^{-2} s^{-1})	Mean CO_2 Flux (μmol m^{-2} s^{-1})
Forest	Streambed	-8.00 ± 4.5	7.56 ± 2.4
	Hillside	-8.62 ± 4.8	3.60 ± 1.8
Desert	Under Bush	-6.63 ± 3.3	3.33 ± 1.6
	Grassy	-9.67 ± 5.7	1.44 ± 0.8
	Open Sand	-8.31 ± 3.8	0.64 ± 0.5
Marsh	All	-5.97 ± 2.7	NA

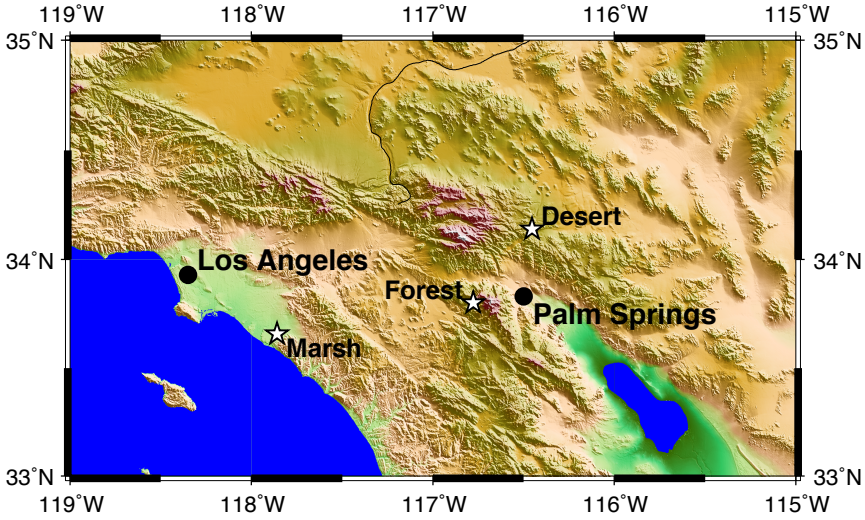

Figure 1. Map of field sites in Southern California. The Marsh site was located at the University of California, Irvine San Joaquin Freshwater Marsh Reserve near Irvine, CA. The Forest site was located at the University of California, Riverside James San Jaciento Reserve near Idyllwild, CA. The desert site was located at the University of California, Irvine Burns Piñon Reserve near Yucca Valley, CA.

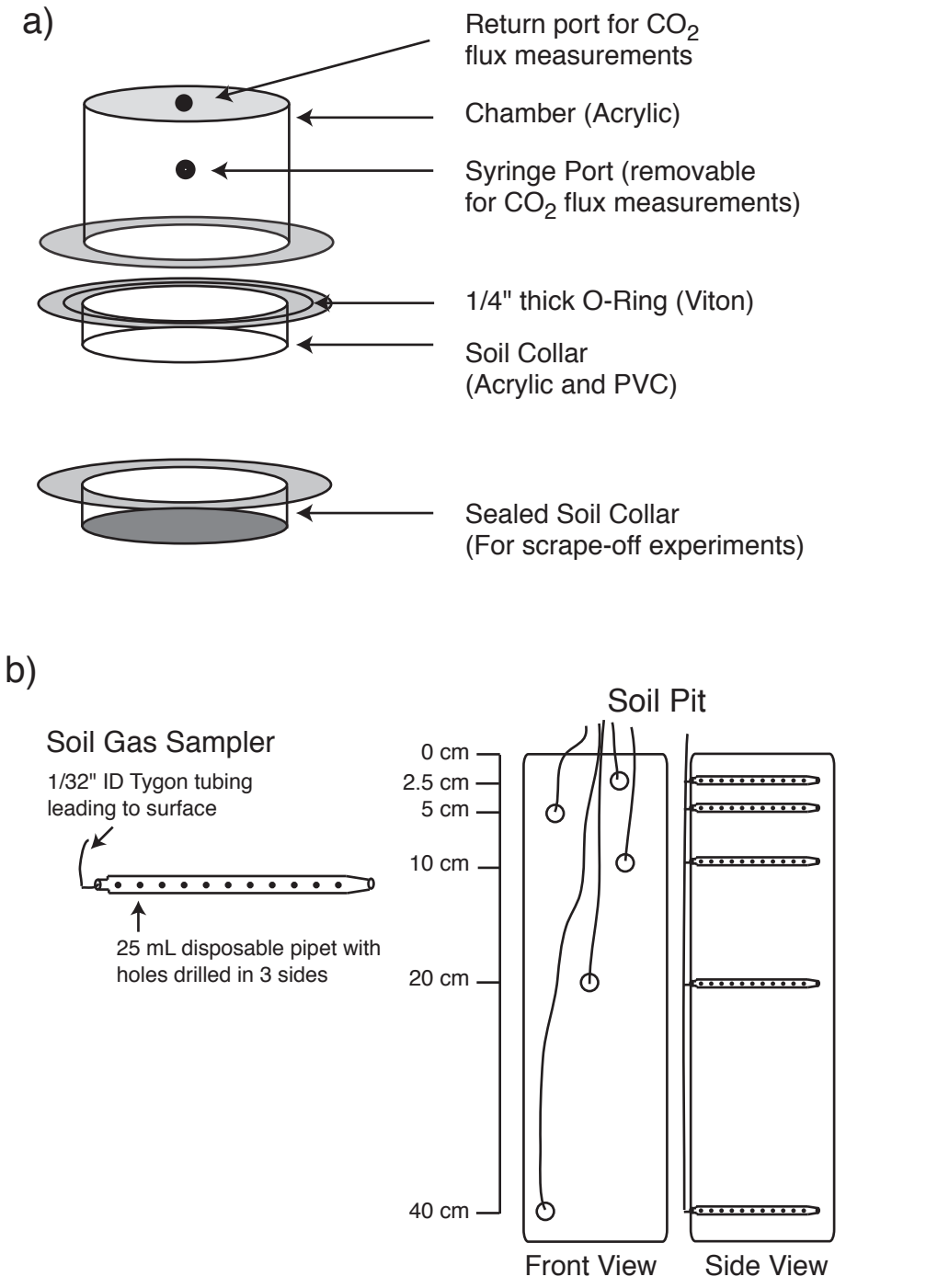

Figure 2. a) Schematic of soil flux chamber and soil collar design. b) Schematic of soil gas sampler design and placement.

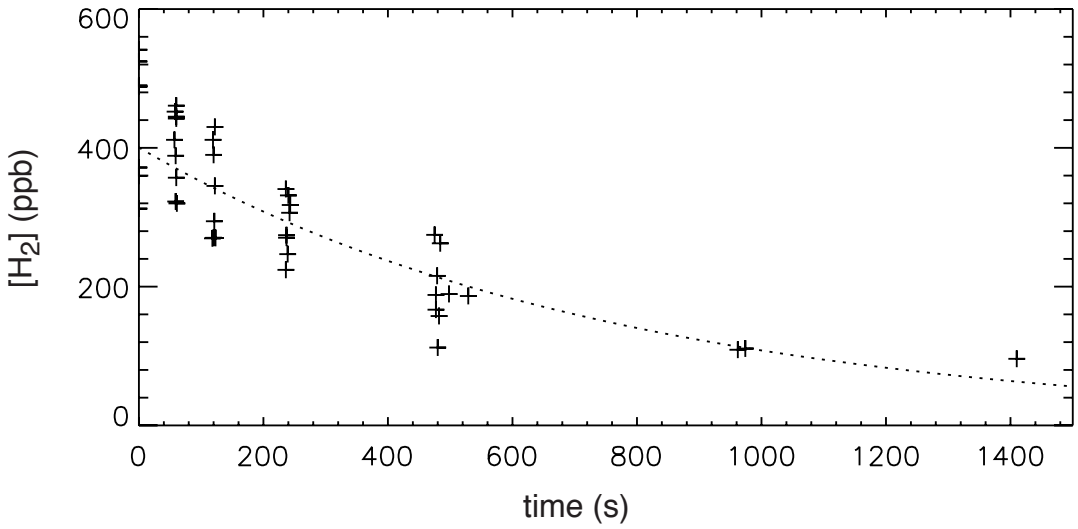

Figure 3. Example uptake curves for H_2 at the forest and desert sites in March, 2005. Symbols represent H_2 measurements and the line is the least squares exponential curve fit to the data.

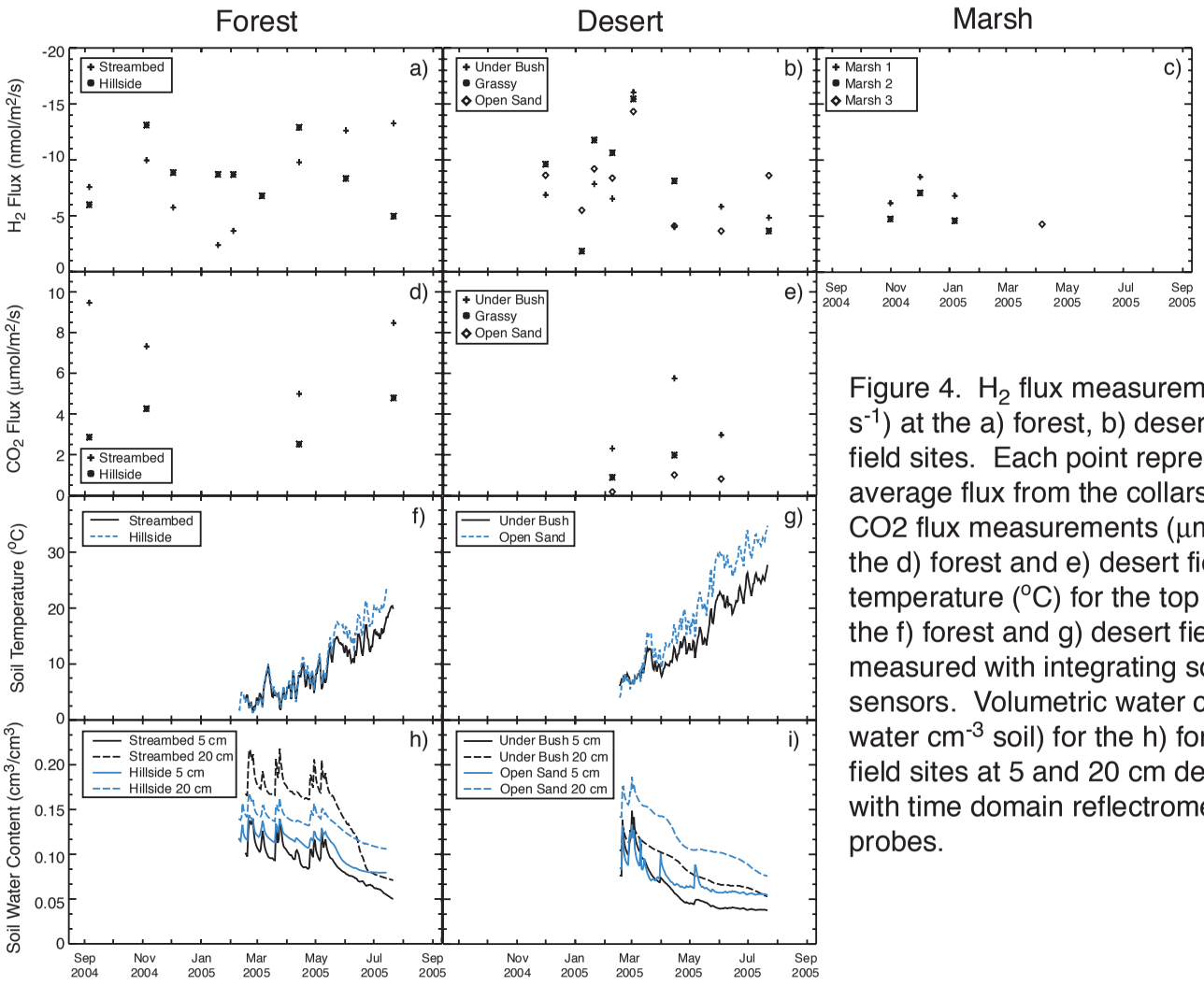

Figure 4. H_2 flux measurements (nmol m^{-2} s^{-1}) at the a) forest, b) desert and c) marsh field sites. Each point represents the average flux from the collars at each site. CO2 flux measurements (µmol m-2 s-1) at the d) forest and e) desert field sites. Soil temperature (°C) for the top 5 cm of soil at the f) forest and g) desert field sites measured with integrating soil temperature sensors. Volumetric water content (cm^3 water cm^{-3} soil) for the h) forest and i) desert field sites at 5 and 20 cm depth measured with time domain reflectrometry (TDR) probes.

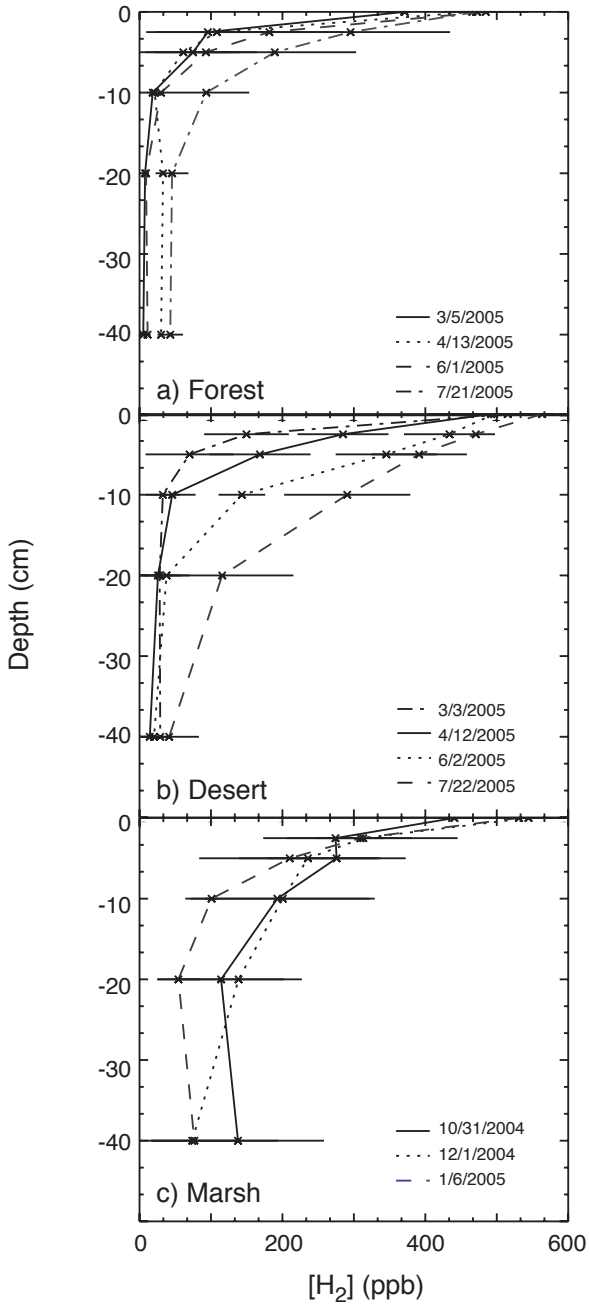

Figure 5. H_2 concentration with depth at the a) forest, b) desert and c) marsh field sites. Each line represents the average of all soil profiles measured at each site. The steady state concentration at depth appears to be non-zero, although our sampling techniques may have introduced some [H_2] into the system before samples were analyzed. Notice that in panel b) H_2 penetrates deeper into the soil from April to July 2005 due to drying and inactivation of the surface soil layers. The increased H_2 at 40 cm depth at the marsh field site (c) may be due to anaerobic production of H_2 in saturated soils below our deepest soil gas sampler.

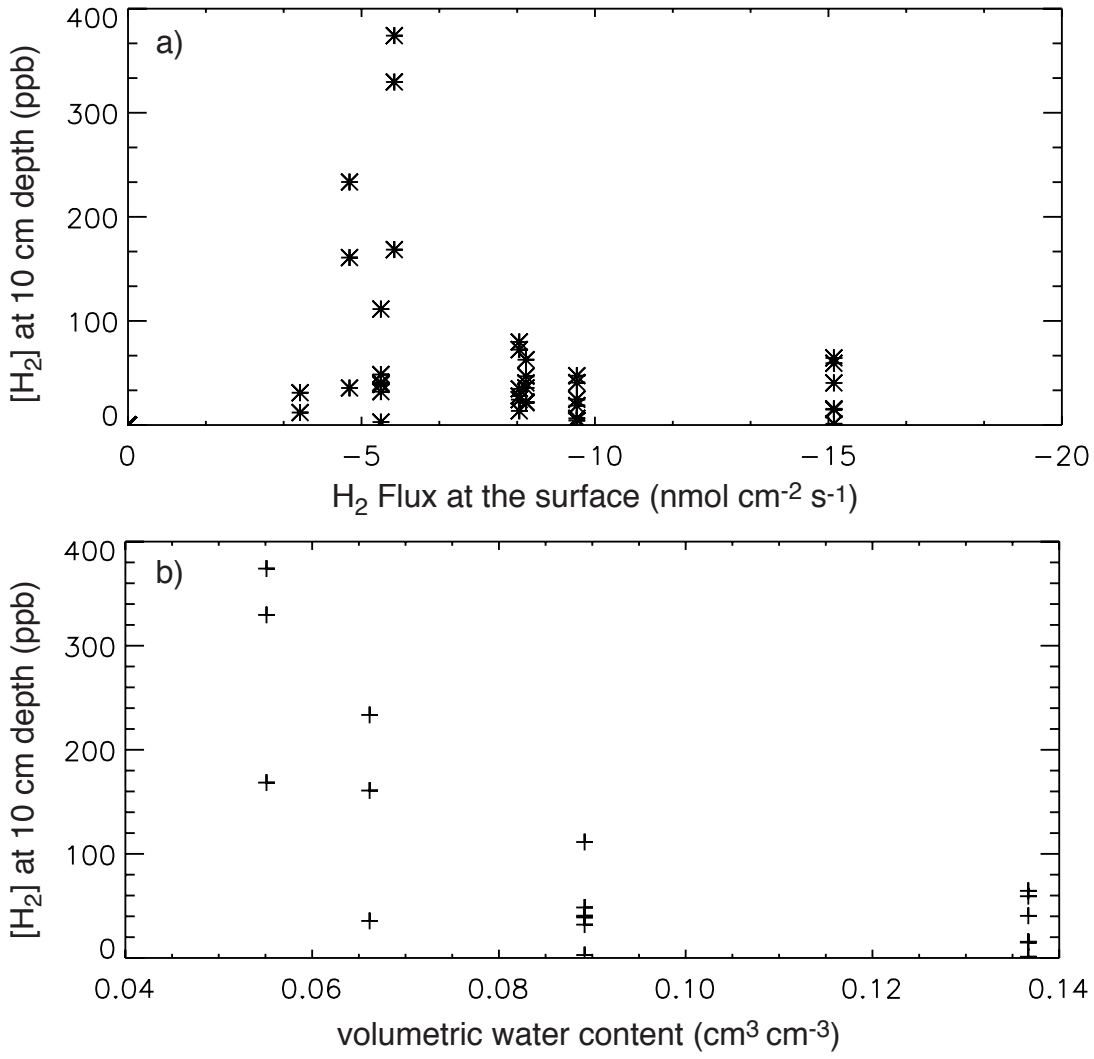

Figure 6. Steady state hydrogen concentration at 10 cm depth plotted along with a) the observed surface flux (nmol m^{-2} s^{-1}) and b) the volumetric water content averaged between 5 and 20 cm depth.

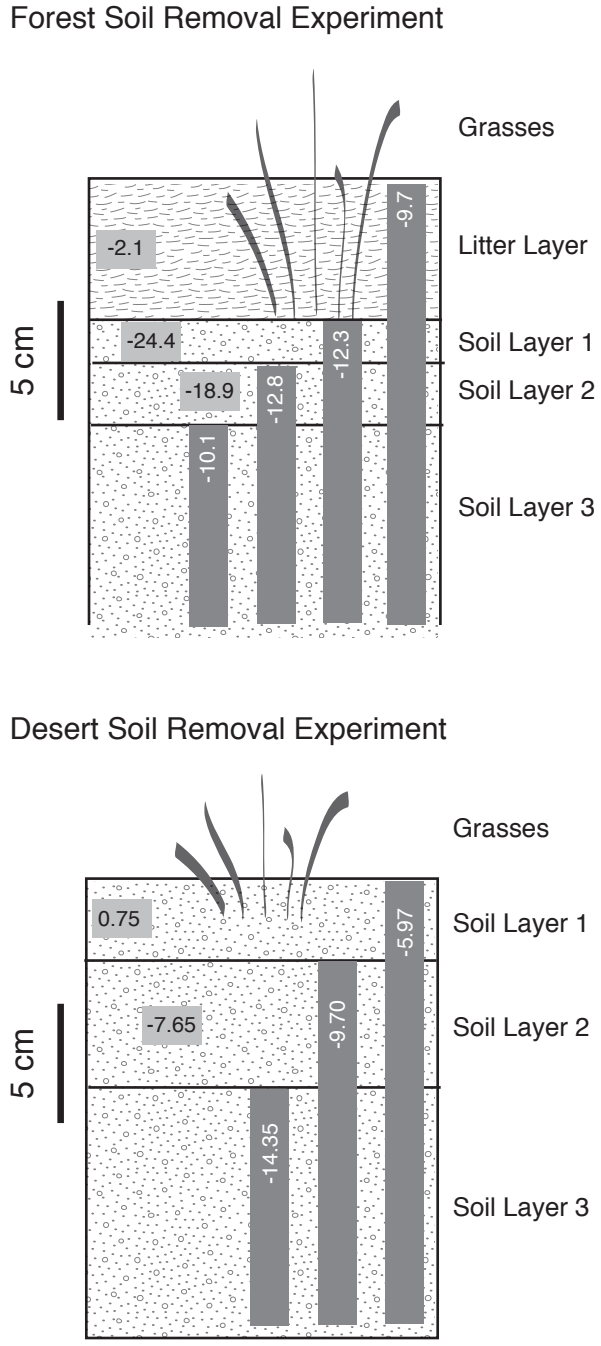

Figure 7. Soil removal experiments at the a) forest and b) desert field sites. Here, surface fluxes were measured, and successive layers of the soil profile were removed and placed in a separate flux chamber to determine the vertical distribution of uptake with depth. In both cases the grasses did not contribute to hydrogen flux. The dark vertical bars represent fluxes of the intact soil layers, and the light grey bars represent the fluxes of individual layers in the removal experiment.

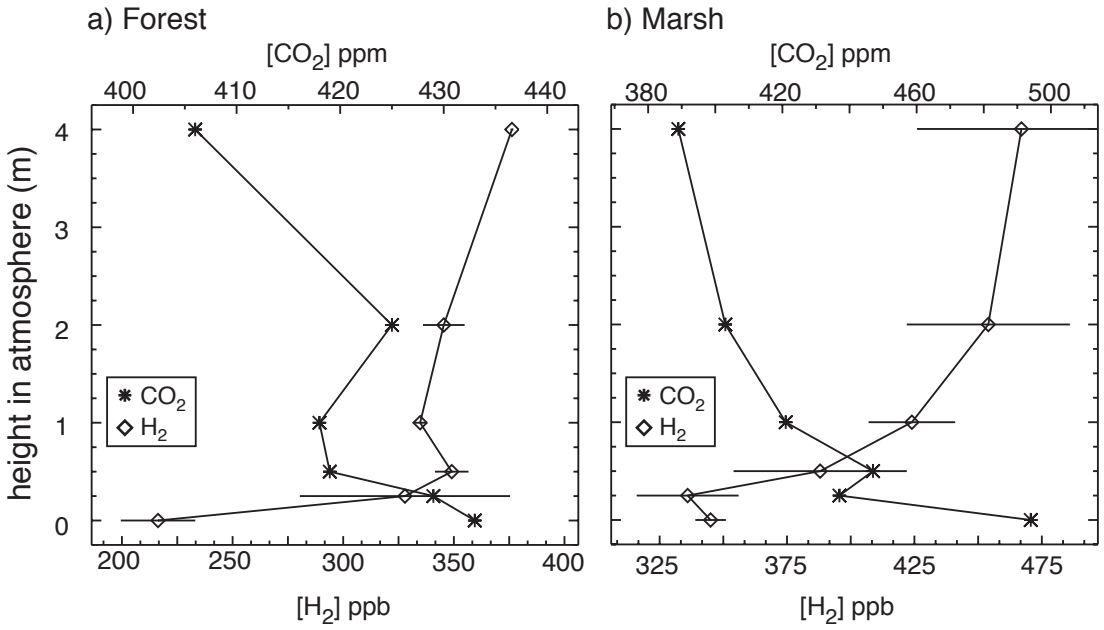

Figure 8. Nighttime atmospheric profile measurements of $[H_2]$ and $[CO_2]$ at the a) forest and b) marsh field sites. The surface fluxes of H_2 and CO_2 (measured with a flux chamber) were -19.5 nmol m^{-2} s^{-1} and 1.6 μmol m^{-2} s^{-1} respectively at the forest site, and -3.2 nmol m^{-2} s^{-1} and 6.4 μmol m^{-2} s^{-1} at the marsh site.

Chapter 3

Temperature and moisture dependence of soil H_2 uptake measured in the laboratory

In press – Geophysical Research Letters

Nicole Smith Downey, James T. Randerson, John M. Eiler

Abstract

The soil sink of molecular hydrogen is the largest and most uncertain term in the global atmospheric H_2 budget. Lack of information about the mechanisms regulating this sink limit our ability to predict how atmospheric H_2 may respond to future changes in climate or anthropogenic emissions. Here we present the results from a series of laboratory experiments designed to systematically evaluate and describe the temperature and soil moisture dependence of H_2 uptake by soils from boreal forest and desert ecosystems. We observed substantial H_2 uptake between -4°C and 0°C, a broad temperature optimum between 20°C and 30°C, a soil moisture optimum at approximately 20% saturation, and inhibition of uptake at both low and high soil moisture. A sigmoidal function described the temperature response of H_2 uptake by soils between -15°C and 40°C. Based on our results, we present a framework for a mechanistic description of the soil H_2 sink.

1. Introduction

Molecular hydrogen (H_2) is the second most abundant reduced gas in the troposphere (after methane), with a concentration of ~530 ppb during the 1990s [*Novelli, et al.*, 1999]. Sources of H_2 to the troposphere include photolysis of formaldehyde, which is primarily generated from the oxidation of methane and non-methane hydrocarbons, and

emissions from fossil fuel combustion and biomass burning. Sinks of hydrogen include oxidation by OH and uptake by soils [*Novelli, et al.*, 1999]. The soil sink is the largest and most uncertain term in the H_2 budget. Estimating the magnitude of the soil sink has proved challenging and the calculated proportion of H_2 uptake by soils to total loss has varied from 62% to 92% [*Seiler*, 1987; *Warneck*, 1988; *Ehhalt*, 1999; *Novelli, et al.*, 1999; *Gerst and Quay*, 2001; *Hauglustaine and Ehhalt*, 2002]. The prospect of a global hydrogen economy has sparked interest in the environmental impact of substantial increases in H_2 emissions. A hydrogen economy may be accompanied by reduced NO_x emissions, which would increase the atmospheric lifetimes of CH_4 and CO due to decreases in OH, and decrease tropospheric O_3 levels in polluted urban areas [*Schultz, et al.*, 2003]. *Tromp et al.* [2003] and *Warwick et al.* [2004] found that replacing fossil fuels with hydrogen fuel cells would lead to a decrease in stratospheric ozone because H_2 mixes freely across the tropopause and forms water in the stratosphere. A critical aspect of this problem is the response of the soil sink. Because neither the mechanism nor the environmental controls on soil uptake of H_2 are well defined it is difficult to predict both temporal and spatial variability in the magnitude of this sink and how it may respond to future changes in climate or anthropogenic emissions.

Schuler and Conrad [1991] studied the temperature response of H_2 uptake of soils from a temperate forest, compost bin, and a private garden. They found that at H_2 concentrations of 1 ppm, the uptake was optimized at a temperature of 30°C whereas at higher H_2 concentrations (3000 ppm) H_2 uptake was optimized at 65°C. At 1 ppm, rates of soil H_2 uptake doubled when temperature was increased from 5°C to 30°C. In an incubation experiment that measured soil uptake for H_2 concentrations between 100 and

500 ppm, *Trevors* [1985] found a lower temperature optimum (20°C) for aerobic soils at 60% water holding capacity (WHC) and observed a 3-fold increase in uptake between 5 and 20°C. Another experiment by *Yonemura et al.* [2000b] found a similar temperature optimum, and a factor of 2 difference in uptake rate between 1°C and 25°C at a single soil moisture level.

Previous work suggests that soil moisture also plays an important role in determining the uptake rate of H_2. Experiments from *Conrad and Seiler* [1981; 1985] and *Fallon* [1982], observed that in very dry soils, uptake is stimulated by the addition of water. *Gödde et al.* [2000] measured the H_2 oxidation capacity of soils from a temperate forest, agricultural field and meadow in Germany, and found that uptake was generally higher in drier soils (at 30% WHC) than in wetter soils (at 60% WHC). Field studies from a forest and arable field in Japan show that at high soil moisture levels (> 30% volumetric water content) H_2 uptake decreases with increasing soil moisture [*Yonemura, et al.*, 1999; 2000a], probably from limited H_2 diffusion through water filled soils [*Yonemura, et al.*, 2000b].

Although several experiments on the temperature and moisture response of H_2 uptake by soils exist, there are insufficient data to parameterize a mechanistic model that predicts soil H_2 fluxes across the full range of environmental conditions found in Earth's major biomes. Such a model would be useful in exploring the sources of variability in the atmospheric H_2 record and could be used to predict changes in the H_2 cycle due to changing climate or emissions. To construct a mechanistic model of H_2 soil uptake, more information is needed about the interaction between soil temperature and soil moisture, the sensitivity of soil H_2 uptake to soil moisture under unsaturated conditions, rates of

soil H_2 uptake at temperatures below 0°C, and differences in uptake between different biomes.

We measured rates of H_2 uptake by soils across a wide range of temperatures and soil moisture levels using a flow-through chamber system. In our experiments we used two different surface soils, one from a mature black spruce boreal forest in interior Alaska and another from the Mojave Desert in California. Our experiments suggest that there is 1) a strong soil temperature control on H_2 uptake, 2) a minimum soil moisture requirement for biological activation, 3) maximized uptake at approximately 20% saturation, 4) decreasing uptake at higher soil moisture levels, 5) substantial H_2 uptake occurring between -4°C and 0°C and 6) that soil type affects the shape of the moisture response. We propose a framework from which global H_2 uptake by soils can be modeled based on these data.

2. Methods

2.1 Soil collection and preparation

Approximately 500 mL of the top 5 cm of soil was collected from a black spruce (*Piceae Mariana*) forest near Delta Junction, Alaska (63°53′N, 145°44′W) and from the University of California Burns Piñon Ecological Reserve in the Mojave Desert (34°N, 116°W). From 1961 to 1990 the mean annual temperature was -2.3°C at the boreal forest site and 20°C at the Mojave Desert site. Mean annual precipitation was 30 cm/yr at the boreal forest site and 11 cm/yr at the Mojave Desert site (Western Regional Climate Center (WRCC) station observations from Big Delta, AK and Twentynine Palms, CA, available online at http://www.wrcc.dri.edu/clim-sum.html). Soils were stored in sealed containers for transport back to the lab, after which they were stored at room temperature

in jars sealed with Parafilm. The carbon and nitrogen content of the boreal forest soil was 38.5% C and 1.11% N whereas the Mojave Desert soil was 0.3% C and 0.02% N (measured with an elemental analyzer, Carlo Erba, Lakewood, NJ).

2.2 Flux measurements

Hydrogen calibration gases between 5 and 2000 ppb H_2 were generated by diluting a standard gas containing 5070 ± 25 ppm H_2 (Scott-Marrin, Riverside, CA) with ultra-pure N_2. Samples from cylinders of compressed air were measured following calibration of the instrument and these cylinders were used as secondary standards throughout the experiment.

We created a flow through apparatus for measuring H_2 uptake by insetting a ½" OD glass tube through a 2L beaker and filling the tube with soil (Figure 1). Gas from a compressed air cylinder containing 1585 ± 21 ppb H_2 flowed, in order, through a mass flow controller (MKS, Wilmington, MA), through a flask filled with water to control humidity, through the ½" glass tube filled with the soil sample, through a dry ice loop to remove moisture and finally to the inlet of a TA 3000R Reducing Gas Analyzer (Ametek Process Instruments, Newark, DE) at a rate of 10 standard cubic centimeters per minute (sccm). The TA3000R RGA is a continuous flow instrument with a Unibead 1S and an MS 13X column for separation of H_2 and CO. Ultra-torr fittings (Swagelok, Solon, OH) were used at each joint, and the system was leak tested with an 80% H_2 source. The TA 3000R instrument measures H_2 with a relative precision of 1.5%.

2.3 Temperature and moisture experiments

In preparation for the temperature and moisture manipulation experiments, soils were thinly spread out in plastic pans and allowed to dry at room temperature (23°C)

overnight. Soil samples were then split into 5 equal portions and water was added to each sample in increments. In these experiments, soil moisture was described as '% saturated', which was calculated as the ratio of water (g) contained in soils to the amount contained after soils are fully submerged in pure H_2O and allowed to drain for 10 minutes. The soils were stirred to evenly incorporate the added water and stored in 50 mL test tubes sealed with Parafilm for at least 3 days before experiments began. The manipulation of the soils may have changed the soil porosity and existing bacterial communities and, for this reason, our results may not be representative of *in situ* fluxes.

For each soil moisture level, the column was filled with 10 mL of soil with a cone of filter paper at each end. The beaker was filled with water of different temperatures, and the concentration of outgoing H_2 was measured every 3.5 minutes. Temperatures were cycled through in the following order 23, 30, 37, 10, 0, -4, -15°C (Figure 2). We used a hot plate to maintain 30°C and 37°C, a water bath with periodic ice additions to maintain 10°C, an ice water bath to maintain 0°C, an ice/salt water bath to maintain -4°C, and an ice/ethanol/water bath to maintain -15°C. The water in the beaker was drained and replaced between each temperature level to ensure a quick transition. We used a stir bar to avoid temperature stratification within the beaker. We conducted one set of temperature manipulations on soils with a thermocouple embedded in the soil and another in the water bath. The temperature of the soil equilibrated with the water bath temperature within minutes, and there was no observed temperature offset between the soil and the water bath. The thermocouple wire could not be placed in the soil during the flow through experiments because a gas-tight seal was necessary at each joint. Each

temperature/moisture level was considered stable after the outgoing H_2 concentration had remained constant for at least 30 minutes (e.g., Figure 2).

2.4 Uptake rate estimates

The uptake rate (pmol cm^{-3}_{soil} s^{-1}) of each soil sample was calculated using the measured difference between the incoming and outgoing H_2 concentrations:

$$H_2 uptake = \frac{([H_2]_{in} - [H_2]_{out}) \cdot f \cdot P}{V_{soil} \cdot R \cdot T \cdot 1 \cdot 10^9} \quad (1)$$

where f is the flow rate (cm^3/s), P is the pressure (Pa), V_{soil} is the volume of soil (cm^3), R is the gas constant and T is the temperature (K). Pressure was assumed to be 1.0135 x 10^5 Pa.

3. Results

Our experiments showed a dependence of H_2 uptake on soil moisture and temperature in both soils (Figure 3). The maximum flux from the boreal forest soil (0.8 pmol cm^{-3} soil s^{-1}) was approximately twice as large as the maximum flux rate from the Mojave Desert soil (0.35 pmol cm^{-3} soil s^{-1}). We observed a broad temperature maximum between 10°C and 35°C (Figure 3). Substantial uptake continued at -4°C (especially for intermediate soil moisture levels), but was nearly eliminated by -15°C. The uptake rate increased sharply with increasing temperature between -4°C and 0°C for the boreal forest soils at intermediate saturation levels, whereas the changes in uptake rate with temperature were more gradual in the Mojave Desert soils. In a similar experiment on soils from a California forest, fluxes decreased substantially when the temperature was increased to 65°C (Figure S1) suggesting uptake inhibition at high temperatures.

We observed both high and low soil moisture inhibition of H_2 uptake with soils from both sites (Figure 3). For the boreal forest soils, increasing the saturation level from

4% to 10% caused uptake to increase by 300% at 23°C. Similarly, increasing the saturation from 11% to 19% for the Mojave Desert soils caused the uptake rate to increase from approximately zero to the maximum uptake levels (Figure 3). The boreal forest soils continued consuming substantial H_2 at higher saturation levels than the Mojave Desert soils, and did not show evidence of moisture inhibition until 59% saturation.

We constructed normalized contour plots of the boreal forest and Mojave Desert fluxes as a function of both temperature and soil moisture (Figure 4). Contour values ranged between 0 and 1 and were scaled by the maximum observed flux at each site. The maximum flux occurred at 23°C and 23% saturation for the boreal forest soil, and at 30°C and 19% saturation for the Mojave Desert soil.

The response to temperature, when normalized to the maximum flux at each soil moisture level, was similar between the two sites and can be described by a sigmoidal function with the following parameters (Figure S2):

$$f(T) = \frac{1}{1 + \exp(-0.1718 \cdot T + 46.938)} \qquad (2)$$

where T is the temperature (K). This function is valid for temperatures between -15°C and 40°C (with an r^2 of 0.72). At temperatures above 40°C, our results suggest that uptake decreases with increasing temperature (Figure S1).

The moisture response cannot be characterized by a simple function, largely due to the effect of soil moisture on the diffusion of H_2 into soils, which varies considerably with soil type. It is clear, however, that a minimum level of soil moisture must be attained before uptake is possible. To account for the effects of soil moisture as it fills

pore space, hydrogen uptake must be modeled as a diffusion process where the uptake rate is scaled according to the results presented here:

$$\lambda_s = f(T)g(M) * \lambda_{\max} * [H_2] * \frac{P}{R*T} \quad (3)$$

where *f(T)* and *g(M)* are functions of soil temperature (T) (Equation 2) and moisture (M) respectively that range between 0 and 1, λ_{max} is the maximum possible H_2 uptake (1/s) under ideal soil temperature and moisture conditions (i.e. when *f(T) and g(M)* are equal to 1), [H_2] is the available hydrogen concentration (ppb), P is pressure (Pa), R is the gas constant, and T is temperature (K). We assumed that the reaction was first order based on chamber measurements of H_2 uptake in the field. This framework can be used to estimate H_2 uptake as a function of soil moisture and temperature.

4. Discussion and Conclusions

We systematically defined the temperature and moisture controls on soil H_2 uptake over a wide range of environmental conditions and identified, for the first time, uptake at subzero temperatures (from -4°C to 0°C). Our results provide additional evidence that a minimum moisture level is required for biological activation of microbes utilizing H_2 [e.g. *Conrad and Seiler*, 1981; *Fallon*, 1982; *Conrad and Seiler*, 1985], but that once pore spaces are filled with water, diffusion of H_2 into the soil becomes limited and fluxes decrease [e.g. *Yonemura, et al.*, 2000b]. The low soil moisture inhibition of H_2 uptake has important implications for desert soils, and may lead to maximum H_2 uptake in wetter months despite the possibility of lower temperatures.

The shape of the temperature and moisture response (Figure 4a) suggests that in boreal forest soils most of the variability in H_2 uptake by soils occurs under relatively low (-4°C to 15°C) temperatures and low soil moisture conditions. These observations may

have important implications for the seasonal cycle of H_2 uptake globally. Northern soils routinely experience shifts in temperature over the range -4°C to 15°C seasonally. The timing of the spring drawdown of H_2, (beginning in May) and buildup (beginning in October) at northern latitudes [*Novelli, et al.*, 1999] may be sensitive to the sharp increase in uptake that we observed between -4°C to 15°C (Figure S2). It is possible for northern soils to consume H_2 through the warmer parts of the winter, although the effect of snow cover, which may limit diffusion of H_2 into soils, must be measured and accounted for. Additionally, the seasonal and interannual soil moisture changes at these latitudes will affect the timing and magnitude of H_2 uptake.

Boreal forest soil fluxes are approximately twice as large as Mojave Desert soil fluxes at the same temperature and soil moisture content. We hypothesize that this is due, in part, to differences in organic carbon content and soil structure. The two soils we examined have carbon contents near the extremes observed in common soils (0.02 to 38.5%) but more data is needed to clearly define the dependence of uptake on organic carbon content of soils. Although our laboratory measurements provided evidence that on a volumetric basis, boreal soils consume more H_2 than desert soils, chamber observations at these two locations do not show a large difference between surface flux rates per m^2 ground area [*Rahn, et al.*, 2002; *Smith-Downey, et al.*, in prep]. The net uptake at the surface is a product of the maximum uptake capacity of a soil (λ_s), the temperature and moisture controls defined here, along with the diffusion of H_2 into the soil profile. It is possible that despite a higher capacity for H_2 uptake per cm^3 soil, the boreal forest uptake is diffusion limited due to higher soil moisture or differences in soil structure. Constructing a model that takes all of these factors into account will allow us

to examine sources of variability in the observed atmospheric H_2 record and to assess how climate change will influence future atmospheric levels of H_2.

Acknowledgements:

NSD thanks J. Leadbetter for lab and instrument use, K. Treseder for collecting soils in Alaska, X. Xu for assistance with the elemental analyzer, P. Ghosh, J. O'Leary, H. Afek and M. Child for help in the lab, and N. Downey. NSD received support from the NCER STAR program, EPA. JTR acknowledges support from UC Irvine's School of Physical Sciences Dean's Innovation Fund. This work was also supported by a generous gift from General Motors and William Davidow and family.

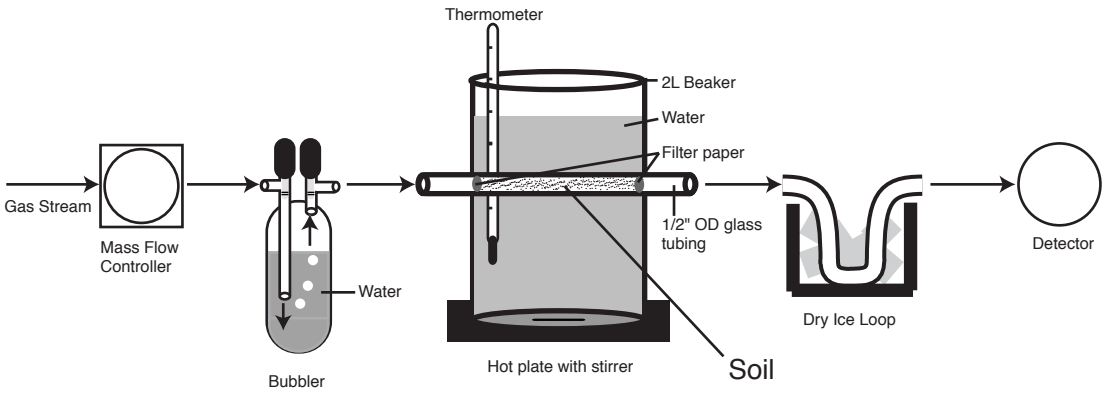

Figure 1. Experimental setup for measuring the temperature and moisture dependence of H_2 uptake by soils. Air with known [H_2] is pushed through the system from left to right and the outgoing [H_2] is measured to determine uptake in the soil column using equation 1. The bubbler hydrated the incoming gas stream slightly, which prevented desiccation of soils over the course of our experiments. The bubbler was removed from the system for the 11% saturated Mojave Desert experiment to prevent addition of water to the soil. The entire beaker apparatus was weighed both before and after each experiment to monitor changes in water content over the course of each experiment.

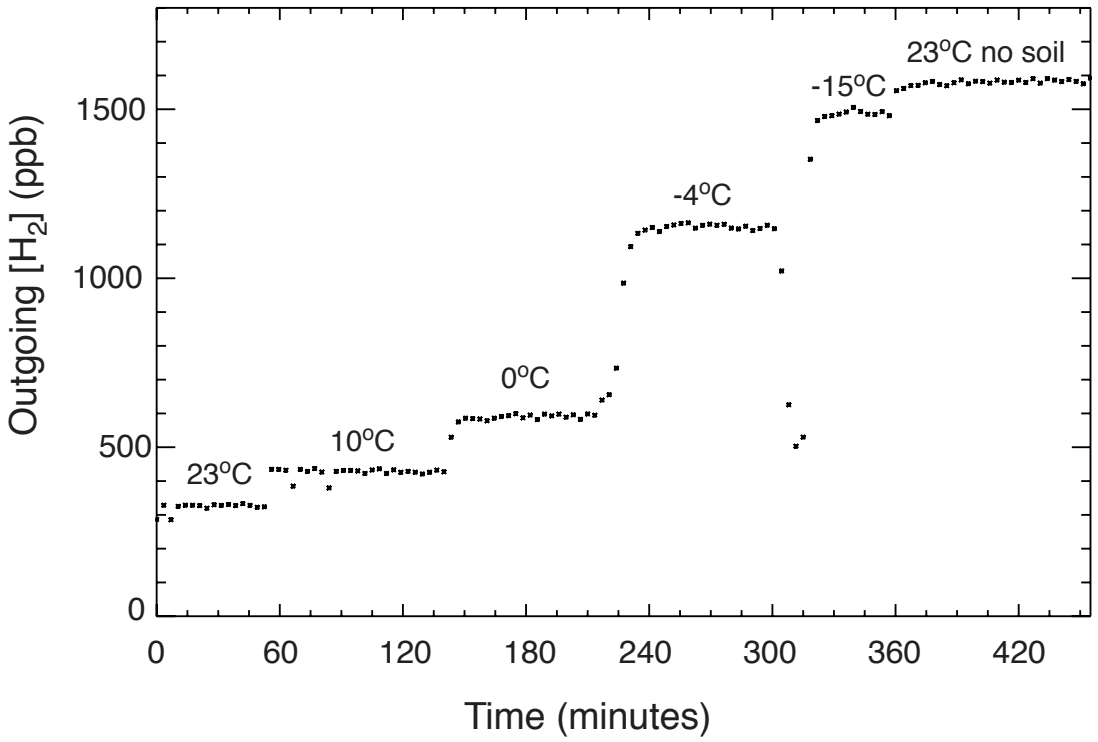

Figure 2. Time series of $[H_2]_{out}$ from a single laboratory experiment using the boreal forest soils at 23% saturation. The difference between the 23°C no soil ($[H_2]_{in}$) and $[H_2]_{out}$ was used in equation 1 to calculate the uptake of H_2 in the soil column. The drop in $[H_2]_{out}$ between -4°C and -15°C corresponds with a warm temperature excursion due to the exchange of the salt-water solution from the beaker with an ethanol/ice solution.

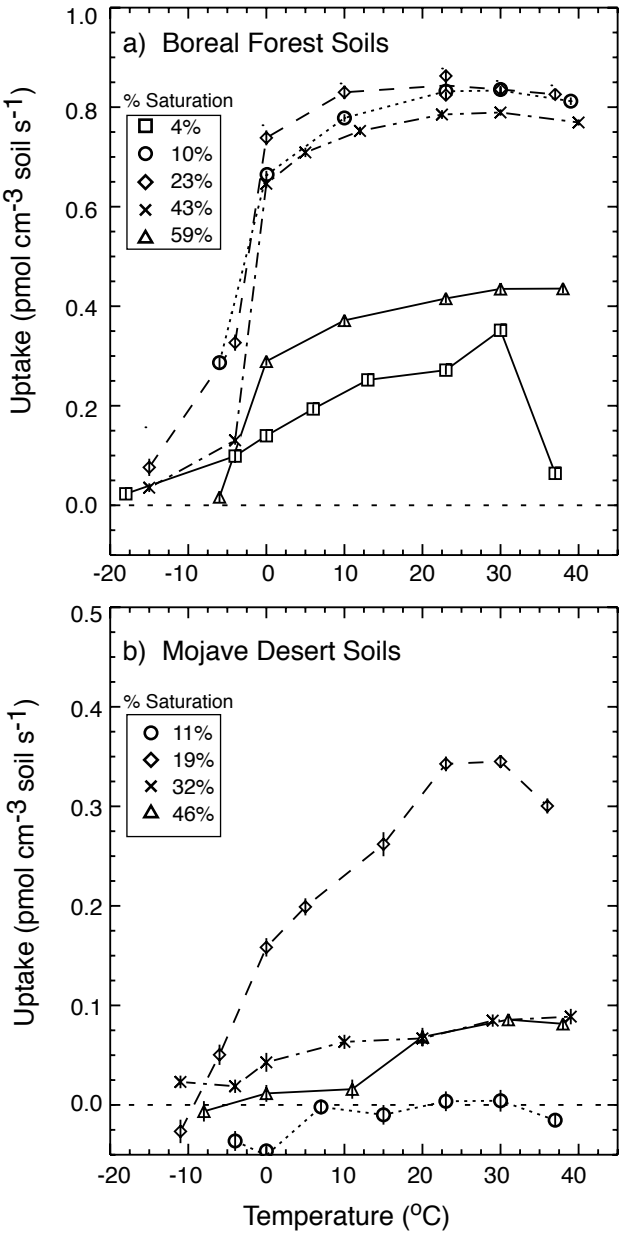

Figure 3. Hydrogen uptake rates as a function of temperature for different soil moisture levels. a) boreal forest soils collected near Delta Junction, AK and b) Mojave Desert soils collected near Yucca Valley, CA. Note that the scale in panel a is twice that of panel b. Uptake rate at 23°C was measured twice for the boreal forest soils at 10% and 23% saturation, and in both cases the difference between measurements was less than 5%. Standard deviations were calculated as $\sqrt{\sigma^2_{in} + \sigma^2_{out}}$ where σ_{in} and σ_{out} are the standard deviation of the measurement of incoming and outgoing [H_2] respectively. The negative values observed probably do not represent an actual production of H_2, but illustrate the level of internal noise in our measurement system.

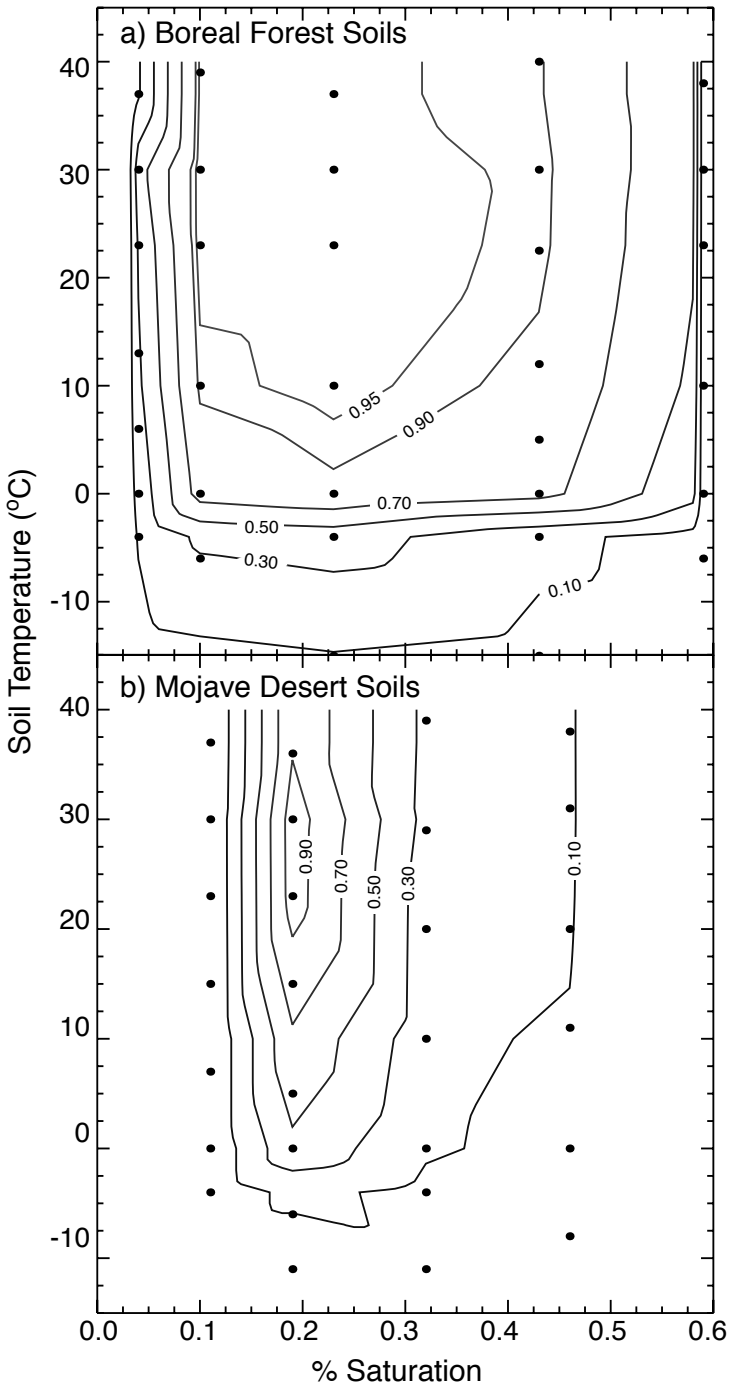

Figure 4. Contour plots of normalized uptake rate at each site as a function of temperature and moisture. Data were normalized by the maximum flux at each site. Grey dots represent locations of the data points used to generate the contour plots. a) For boreal forest soils there was a relatively strong gradient between 0% and 10% saturation and -4°C and 0°C. b) For Mojave Desert soils there was more symmetry about the moisture maximum as compared to the boreal forest soils. In constructing this plot, we assumed negative flux values measured in the Mojave Desert soils (Figure 3b) were equal to zero.

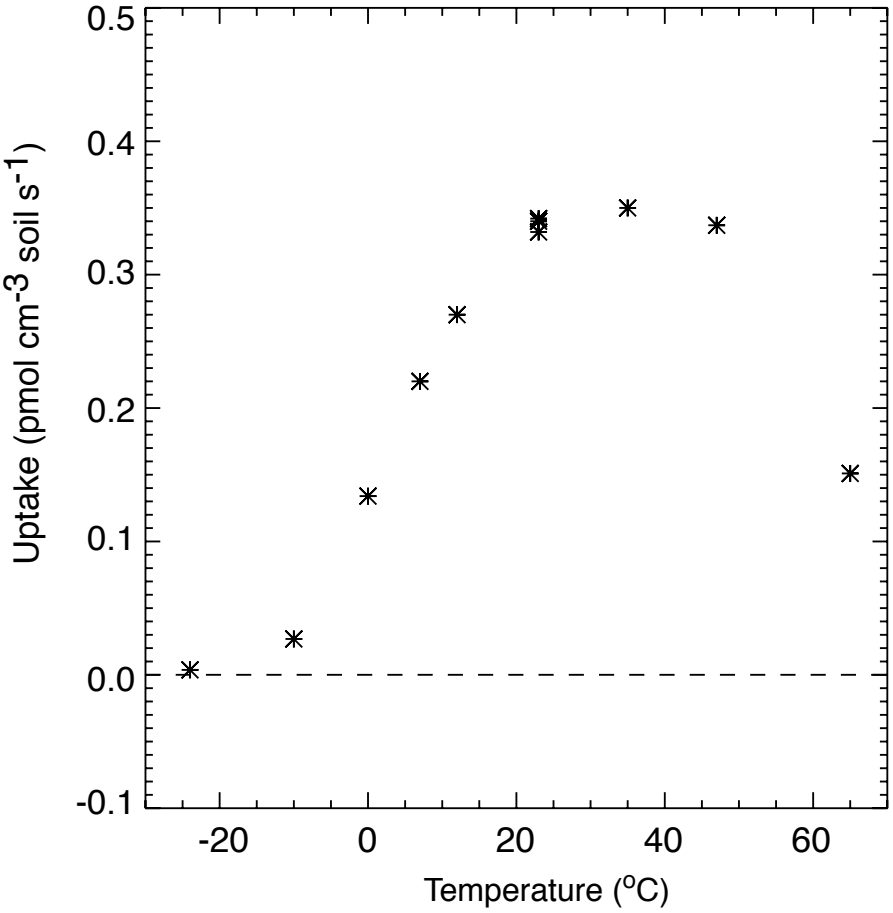

Figure S1. Hydrogen uptake rates as a function of temperature for soil from a mixed conifer and hardwood forest in the San Jacinto Mountains, CA. (33°48'N, 116°46'W). Uptake rate at 23°C was measured three times to assess reproducibility and experimental errors with our measurement system.

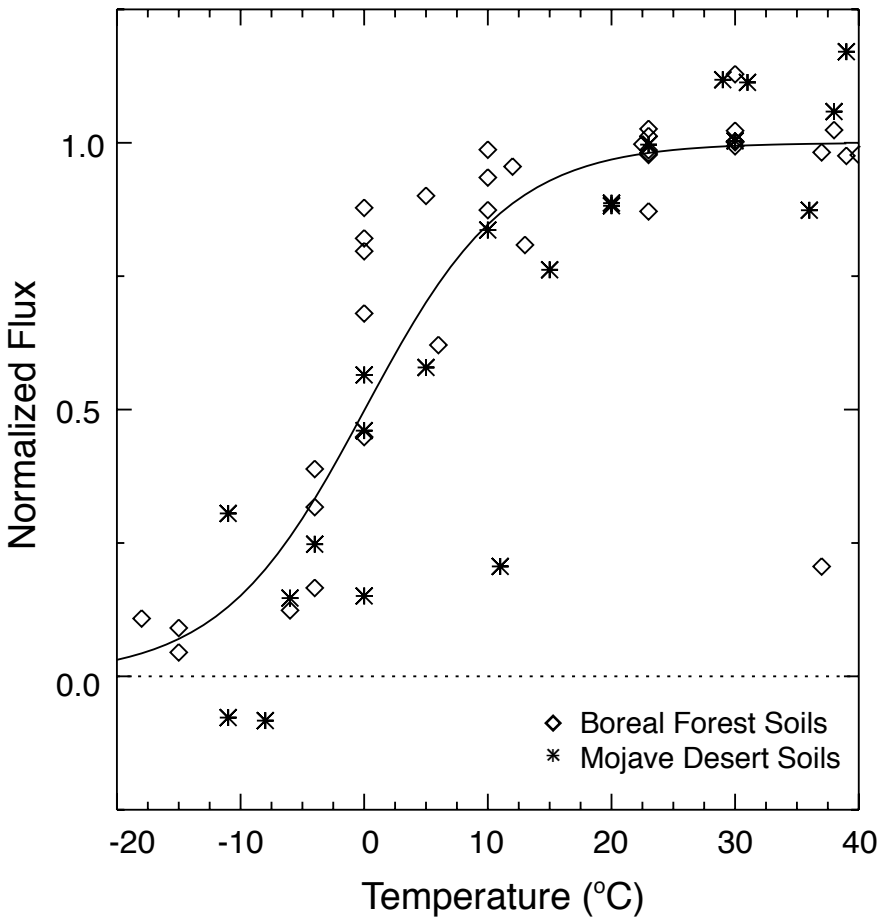

Figure S2. Normalized temperature response curve for both the Mojave Desert and boreal forest soils. Normalized temperature response was calculated as the flux from each moisture level in Figure 2 divided by the flux between 20°C and 30°C. Data from the Mojave Desert soils at 11% saturation were excluded from the temperature normalization.

Chapter 4

A Global Mechanistic Model of Molecular Hydrogen (H_2) Uptake by Soils

In preparation for Global Biogeochemical Cycles

Nicole Smith Downey, James T. Randerson and John M. Eiler

Abstract

The soil sink of molecular hydrogen (H_2) is a key component of the global H_2 budget. Here, we present a mechanistic model of global H_2 uptake by soils between 2001 and 2004. We find that soils consume 67.3 ± 5.5 Tg H_2 per year, with a range of 59.8 to 73.2 Tg yr^{-1}. This falls within previous estimates of the sink strength. The diffusion of H_2 into soils dictates the uptake rate, and changes in soil moisture and snow cover are the two largest barriers to H_2 diffusion globally. Our model reproduces the amplitude and phase of the seasonal cycle of H_2 between 50°N and 70°N, and changes in snow cover drive the seasonal cycle at these latitudes. The soil moisture and snow cover controls on H_2 uptake suggest that in the future, the global H_2 budget may be significantly altered by global climate change.

1. Introduction

Hydrogen fuel cells may become a significant source of energy in the future, and the environmental impact of a hydrogen economy remains uncertain. If emissions of NO_x decrease due to decreased fossil fuel combustion, the atmospheric lifetimes of CH_4 and CO would increase and troposphere ozone (O_3) would decrease [*Schultz, et al.*, 2003]. If significant leakage occurs in the transportation and storage of molecular hydrogen (H_2),

the tropospheric H_2 burden may increase. H_2 mixes freely across the tropopause into the stratosphere, catalyzing stratospheric O_3 loss [*Tromp, et al.*, 2003; *Warwick, et al.*, 2004]. The current concentration of H_2 in the atmosphere is ~ 530 ppb [*Novelli, et al.*, 1999]. Sources of H_2 to the atmosphere include fossil fuel combustion, biomass burning, and the oxidation of methane and non-methane hydrocarbons. The two largest sink terms are reaction with OH and uptake by soils. The concentration of H_2 is lower in the northern hemisphere than the southern hemisphere, and the amplitude of the seasonal cycle increases with latitude in the north [*Novelli, et al.*, 1999]. These features are attributed to the large role of the soil sink, which consumes between 56 and 90 Tg H_2 yr^{-1} (62 to 92% of the total) [*Seiler*, 1987; *Warneck*, 1988; *Novelli, et al.*, 1999; *Gerst and Quay*, 2001; *Hauglustaine and Ehhalt*, 2002; *Rhee, et al.*, 2006].

Previous work on the global H_2 cycle has reached the same conclusion: the soil sink is large and it is the least well-understood component of the H_2 budget. *Hauglustaine and Ehhalt* [2002] developed a 3D model of the H_2 budget, and for lack of a better option, used the distribution of Net Primary Productivity (NPP) to constrain the spatial pattern of soil uptake. Their analysis was unable to recreate the seasonal cycle of H_2, especially at northern latitudes, and they point to the uncertainties in the spatial and temporal variation of the soil sink as their major weakness.

Field and laboratory measurements show that H_2 uptake is dependent on temperature, moisture and the organic carbon content of soils [*Fallon*, 1982; *Conrad and Seiler*, 1985; *Yonemura, et al.*, 2000a; *Smith-Downey, et al.*, in prep; *Smith-Downey, et al.*, in press]. The diffusion of H_2 into soils also plays an extremely important role in controlling uptake rates [*Yonemura, et al.*, 2000a; *Yonemura, et al.*, 2000b; *Smith-*

Downey, et al., in prep]. Recently, *Rhee et al.* [2006] proposed that the seasonal cycle in the north is driven primarily by snow cover, which would limit the diffusion of H_2 to the soil surface.

Here we present a global mechanistic model of H_2 uptake by soils. Our model is based on the one-dimensional diffusion equation with a sink term, and includes the effects of temperature, moisture, and organic carbon content of soils on the biological activity of H_2 consuming microbes. We also include the effect of soil porosity, which is determined by soil type and moisture level, and snow cover on the diffusion of H_2 into soils. Our model predicts a mean annual global sink of 67.3 ± 5.5 Tg H_2 yr^{-1} over the period 2001 to 2004. The seasonal cycle in the north is driven almost entirely by snow cover, whereas soil moisture sets the uptake rate in temperate and tropical regions. These results imply that global climate change may significantly affect the soil sink of H_2.

2 Global H_2 Model

2.1 Conceptual Framework

The uptake of H_2 by soils is a diffusion-limited biological process. To correctly model the uptake by various soils over time, it is necessary to account for the environmental dependence of biological uptake and the diffusion of H_2 into soils, which regulates supply of H_2 to soil microbes. We have, therefore, designed our model in such a way that the environmental controls on biological uptake and diffusion of H_2 are treated separately. The 1D diffusion equation with a first-order loss term combines estimates of the uptake rate and diffusivity of H_2 in soils to yield an estimate of the flux of H_2.

We used the laboratory results of *Smith-Downey et al.* [in press] and soil moisture and temperature data from the CLM2 land surface model [*Rodell, et al.*, 2004]

to constrain variability in the biological uptake term. Generally, H_2 uptake requires a minimum moisture threshold for biological activity, and responds strongly to temperature between -4°C and 10°C. There is a broad temperature maximum between 10°C and 37°C [*Smith-Downey, et al.*, in press].

The diffusion of H_2 into soils is controlled by soil porosity, which is dependent on soil structure and moisture. For our model, we use global soil porosity maps [*Reynolds, et al.*, 1999] combined with monthly soil moisture data from the CLM2 land surface model [*Rodell, et al.*, 2004] to estimate changes in the diffusivity of soils over time. Mean monthly snow depth data from the United States Air Force (USAF) [*Foster and Davy*, 1988] and monthly snow cover data from MODIS (2001 to 2004) [*Hall, et al.*, 2003] were used to account for the effect of snow on diffusion of H_2 into soils.

2.2 Model Design

Our model produces a 1x1 degree globally gridded estimate of H_2 flux into soils at a monthly time-step from 2001 to 2004. Monthly mean values of $[H_2]$ were calculated for 30° latitude bands from the NOAA flask network [*Novelli, et al.*, 1999], and used as model input for hydrogen concentration at the surface for each time-step.

The flux of H_2 into soils (F) is proportional to the concentration gradient at the surface.

$$F = D_s \cdot \left. \frac{\partial [H_2]}{\partial z} \right|_{z = soil_surface} \qquad (1)$$

The gradient in $[H_2]$ with depth is driven by the uptake of H_2 in the soil profile, which is a diffusion-limited process. It can be described by the diffusion equation with a first order loss term:

$$\frac{\partial[H_2]}{\partial t} = \frac{\partial}{\partial z}\left(D_s(z) \cdot \frac{\partial[H_2]}{\partial z}\right) - \frac{\lambda}{\varepsilon} \cdot [H_2] \quad (2)$$

where $[H_2]$ is the concentration of hydrogen expressed as moles m^{-3}, t is time (s), z is depth (cm) measured negative downwards, D_s is the diffusivity of hydrogen in soil at a given depth, λ is the H_2 uptake rate (1/s) and ε is the air filled porosity of a soil.

The diffusivity of hydrogen in soils (D_s) varies with depth and is a function of the diffusivity of H_2 in air (D_g) and soil air filled porosity (ε). ε is primarily determined by soil structure and moisture content, which leads to a strong control of soil texture and saturation on the diffusivity of hydrogen in soils [*Yonemura, et al.*, 1999; *Yonemura, et al.*, 2000b; *Smith-Downey, et al.*, in press]. The uptake of hydrogen by soils (λ) is biologically controlled and varies with soil moisture, temperature, and organic carbon content of soils [*Fallon*, 1982; *Conrad and Seiler*, 1985; *Smith-Downey, et al.*, in press]. Knowing how D_s and λ change in response to soil type and environmental conditions allows us to calculate the flux of hydrogen into soils globally (Figure 1).

2.3 Estimating D_s

As noted above, the diffusivity of hydrogen in soils (D_s) varies as a function of the diffusivity of hydrogen in air (D_g), and soil air filled porosity (ε). D_g is temperature dependent and is calculated according to *Hirschfelder et al.* [1954].

Estimating D_s requires that we know the soil porosity, and how it changes with depth and time. *Moldrup et al.* [1999] proposed an empirical relationship between ε, D_g, total porosity (ϕ) and the fraction of soil particles larger than 2 μm (F_{cp}).

$$D_s = D_g \cdot \phi^2 \cdot \left(\frac{\varepsilon}{\phi}\right)^{2.9 \cdot F_{cp}} \quad (3)$$

Global maps of soil porosity (ϕ) and fraction clay content (F_{clay}) [*Reynolds, et al.*, 1999] were used for ϕ and F_{cp} ($F_{cp} = 1 - F_{clay}$) for each 1x1 degree land covered grid cell on earth at two levels, 0-30 cm and 30-100 cm. Soil moisture data from the CLM2 land surface model [*Rodell, et al.*, 2004] provided monthly mean soil moisture content (θ, m^3 water/m^3 soil) of soils at 8 levels (1.8, 4.5, 9.1, 16.6, 28.9, 49.3, 82.9 and 138.3 cm depth). In soils $\varepsilon = \phi - \theta$, so these estimates of ϕ and θ allowed us to calculate monthly values of ε and D_s that depends on soil structure and moisture conditions.

2.4 Estimating λ

Laboratory measurements of soil uptake of H_2 suggest that it is strongly temperature and moisture dependent and weakly dependent on organic carbon content of soils [*Smith-Downey, et al.*, in press]. Soil temperature and moisture at 8 depths were extracted from the CLM2 land surface model [*Rodell, et al.*, 2004]. We used the *Reynolds* [1999] organic carbon soil map for soil organic carbon content (O) at each 1x1 degree pixel. We estimated λ as a function of depth and time using the relationships proposed by [*Smith-Downey, et al.*, in press]:

$$\lambda = \lambda_{max} \cdot f(T) \cdot f(O) \cdot f(M) \quad (4)$$

where

$$f(T) = \frac{1}{1 + \exp(-0.1718 \cdot T + 46.938)} \quad (4a)$$

$$f(O) = 1.178 \cdot O + 0.3465 \quad (4b)$$

λ_{max} is the maximum possible uptake under ideal conditions, and was estimated using the maximum observed uptake in laboratory experiments ($\lambda_{max} = 0.12266\ s^{-1}$). f(M) is a function of soil moisture (M) such that at below 8% saturation f(M) =0, between 8%

and 15% saturation $f(M) = 14.286*M-1.1429$ and above 15% saturation $f(M) = 1$. Saturation (M) was defined as the ratio of water filled pore space (θ) to total pore space (ϕ). $f(T)$, $f(M)$ and $f(O)$ range between 0 and 1.

2.5 Snow cover

In the northern hemisphere, snow cover is an important component of the environment. For our purposes, snow cover can be thought of as a layer that impedes diffusion of H_2 to the soil surface, but is inactive with respect to λ. We used monthly mean snow climatology maps from the USAF [*Foster and Davy*, 1988] to constrain snow depth and monthly fractional snow cover estimates from MODIS [*Hall, et al.*, 2003] to constrain snow cover. The diffusivity of hydrogen in snow was calculated according to the relationship proposed by *Hubbard et al.* [2005] assuming a mean snow density of 300 kg m^{-3} ($D_{snow} = 0.38$).

Our model was run twice, once with no snow and again with snow covering all of the pixels with a snow depth value in the USAF dataset. The final flux (F) for each 1x1 degree pixel was calculated as:

$$F=f_{snow}*F_{snow} + (1-f_{snow})*F_{no\ snow} \quad (5)$$

where f_{snow} is the fraction of the pixel covered by snow, F_{snow} is the flux calculated for that pixel with a snow layer whose depth is constrained by the USAF data, $(1-f_{snow})$ is the snow-free fraction of the pixel, and $F_{no\ snow}$ is the flux calculated for the pixel with no snow.

2.6 Numerical approach

We used an explicit finite difference scheme (Numerical Recipes 1992) with a time step of 1 s and a depth step of 1 cm, to solve the 1D diffusion equation (2). We

utilized a specific concentration at the upper surface [*Novelli, et al.*, 1999] and zero flux at 138 cm depth as boundary conditions. We ran each calculation to steady-state for every pixel and month. Once steady-state was achieved, the flux of H_2 into the soil was calculated as the product of the concentration gradient at the air soil interface and D_s at z = soil surface (equation 1). The calculated steady-state profile for each week was passed on as the initial condition for the following week.

3 Model Results

Our model predicts a mean global H_2 sink of 67.3 ± 5.5 Tg yr^{-1} between 2001 and 2004, with a range of 59.8 to 73.2 Tg (Figure 2). The latitude band between 10°N and 40°N consumes the most H_2 on a monthly basis (1.8 Tg/month), followed by 40°N to 70°N and 20°S to 10°N then 50°S to 20°S (Figure 3). Only the latitude band between 40°N and 70°N showed a strong seasonal cycle in H_2 uptake rate, with a peak in June and a minimum in December. When compared to field measurements of H_2 uptake, the model does reasonably well reproducing the deposition velocity of H_2, but it fails to capture one very high measurement (0.13 cm s^{-1}) made in Transvaal, South Africa [*Conrad and Seiler*, 1985] (Figure 4).

Global mean patterns for four months are shown in Figure 5. The mean pattern in the southern hemisphere does not vary seasonally, but the northern hemisphere shows a distinct change in uptake rate over the course of the year. The highest uptake rates observed are in Africa, and distinct lows can be seen in the Congo Basin and the Amazon. The range of fluxes we observe, 0-13 nmol m^{-2} s^{-1} is similar to that observed in field experiments.

We chose 5 sites across the globe, including Saharan Africa, Tapajos Brazil, The Harvard Forest in Central Massachusetts, Boreas South in Manitoba, Canada and Siberia to investigate the contribution of each of our scalars to the observed uptake of H_2 (Figure 6). In Saharan Africa, the observed flux rate is primarily controlled by the effect of soil moisture on both D_s and λ. In this case, λ is moisture limited in the summer months. In Tapajos Brazil, a tropical rainforest site, the observed uptake is controlled only by the effect of soil moisture on D_s. In the winter, fluxes are lower due to increased soil moisture, whereas in summer the fluxes increase as soils dry out. At the Harvard Forest, a temperate forest site, the uptake rate is primarily controlled by the effect of soil moisture on D_s, but there is also a strong snow signal in the winter of 2002. At Boreas South, a boreal forest site, the flux is controlled by snow cover and soil moisture effects on D_s. In Siberia, the seasonal cycle is driven entirely by snow cover.

To assess the performance of our soil model, we also developed a 1-box atmospheric model of the H_2 budget between 50 °N and 70°N, using the technique developed by *Welp et al.* [in press]. For this experiment, we assumed that sources of H_2 were constant throughout the year, and were equal to the sum of the total uptake (i.e. there is no change in $[H_2]$ over one year). For each month, the mean monthly uptake from our four years was removed from the box, and a constant source term was added. We ran this model for three soil model cases: 1) the soil model with no snow cover, 2) the soil model with $f_{snow} = 1$ in pixels with snow depths > 0 in the USAF dataset, and 3) the soil model with f_{snow} varying monthly according to the MODIS fractional snow cover data, and snow depth defined by the USAF.

For the first case, almost no seasonal cycle was evident (Figure 7a), and the phase was offset from flask data by 3-4 months. In the second case, the amplitude of our modeled H_2 budget was much higher than the observed data, but the period agreed well with the flask data (Figure 7b). After the fractional snow cover data from MODIS was added to the model, the amplitude of the seasonal cycle between 50 °N and 70°N matched the flask data (Figure 7c). The spring maximum is similar, but the flask data persist at slightly higher values through the growing season. The fall minimum is captured by our simple model. The offset between our model data and the observed record may be due to variation in the sources of H_2 seasonally, or to uncertainty in the snow cover data.

4 Discussion and Conclusions

We have developed the first mechanistic model of soil H_2 uptake globally, and estimate that soils consumed 67.3 ± 5.5 Tg of H_2 per year between 2001 and 2004. This estimate falls within previous estimates of the magnitude of the soil sink (56 to 90 Tg yr^{-1} [*Seiler*, 1987; *Warneck*, 1988; *Novelli, et al.*, 1999; *Gerst and Quay*, 2001; *Hauglustaine and Ehhalt*, 2002; *Rhee, et al.*, 2006]). Our model generally reproduces observed variation in uptake rate between sites, and is able to predict the observed seasonal cycle of H_2 between 50 °N and 70°N. In northern latitudes, snow cover dictates the H_2 uptake rate and seasonal cycle, whereas south of 30°N the uptake rate is determined by soil texture and moisture.

The control of uptake by snow cover and soil moisture has important implications for the future of the H_2 soil sink under global climate change scenarios. If snow cover decreases due to global warming, soils may continue consuming H_2 throughout the

winter, especially in regions where the soil temperature does not fall below -4°C. If soil moisture decreases, the porosity of soils will increase, increasing the flux of H_2 into soils. If excessive drying occurs (i.e. below 15% saturation), uptake will begin to decrease with decreasing soil moisture. Our model is suitable for performing climate change experiments, and we plan to predict how the uptake of H_2 will respond both to changes in climate and changes in emissions.

Supplementary Material – Symbols and their definitions

D_g diffusivity of hydrogen in air ($cm^2\ s^{-1}$)

D_s diffusivity of hydrogen in soils ($cm^2\ s^{-1}$)

D_{snow} diffusivity of hydrogen in snow ($cm^2\ s^{-1}$)

F flux of hydrogen into soils from atmosphere ($nmol\ m^{-2}\ s^{-1}$)

F_{clay} fraction of soil particles smaller than 2μm

F_{cp} fraction of soil particles larger than 2μm ($F_{cp} = 1 - F_{clay}$)

O fraction organic carbon in soils

P pressure (Pa)

R universal gas constant ($8.3145\ J\ mol^{-1}\ K^{-1}$)

T temperature (K)

t time (s)

ε air filled soil porosity (m^3/m^3)

θ water filled soil porosity (m^3/m^3)

λ uptake capacity of soils (s^{-1})

λ_{max} maximum observed uptake capacity of soils ($\lambda_{max} = 0.12266\ s^{-1}$)

ϕ soil porosity (m^3/m^3) ($\phi = \varepsilon + \theta$)

f_{snow} fraction of a pixel covered by snow

F_{snow} flux of H_2 into soil with a snow layer

$F_{no\ snow}$ flux of H_2 into soil with no snow layer

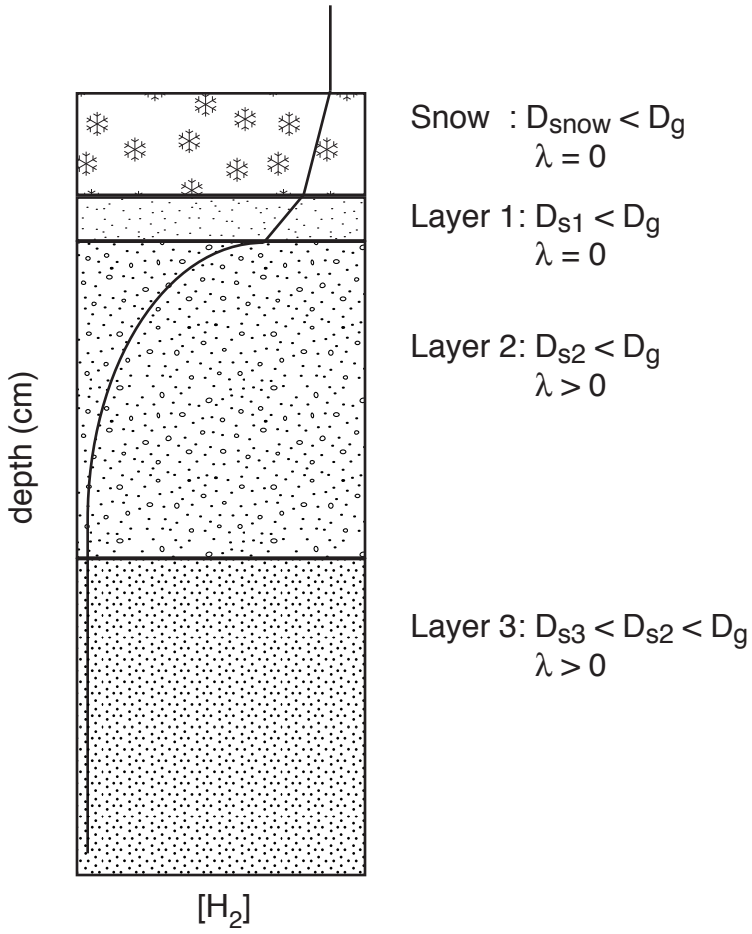

Figure 1. Simplified schematic of soil layers used in the model. The depth of the snow layer for each is pixel is determined by the USAF snow climatology database, and varies monthly. Layer 1 is the top layer of soil, which in this illustration does not actively consume H_2. This condition occurs when soil moisture is below 8% saturation.

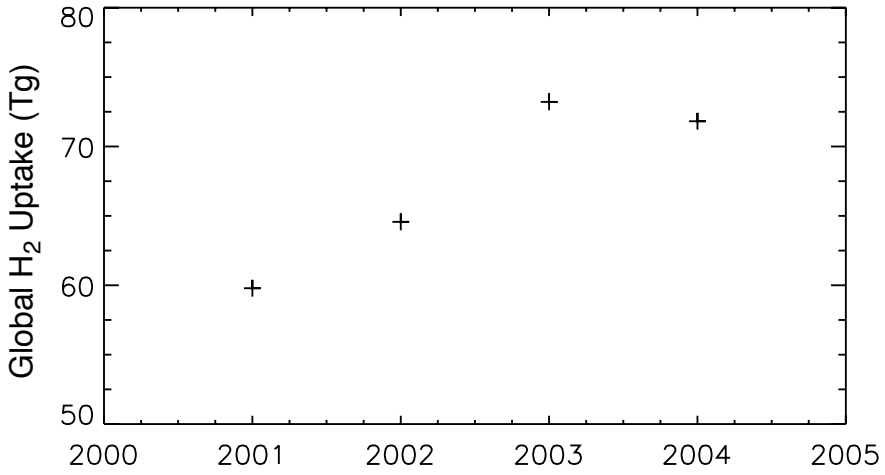

Figure 2. Global total H_2 uptake predicted by our model.

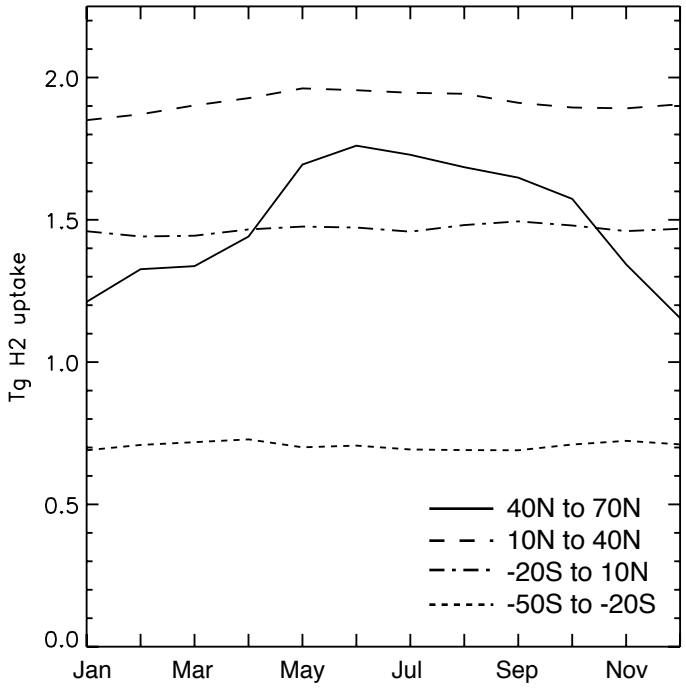

Figure 3. Mean monthly H_2 uptake separated by latitude bands averaged over 2001 to 2004.

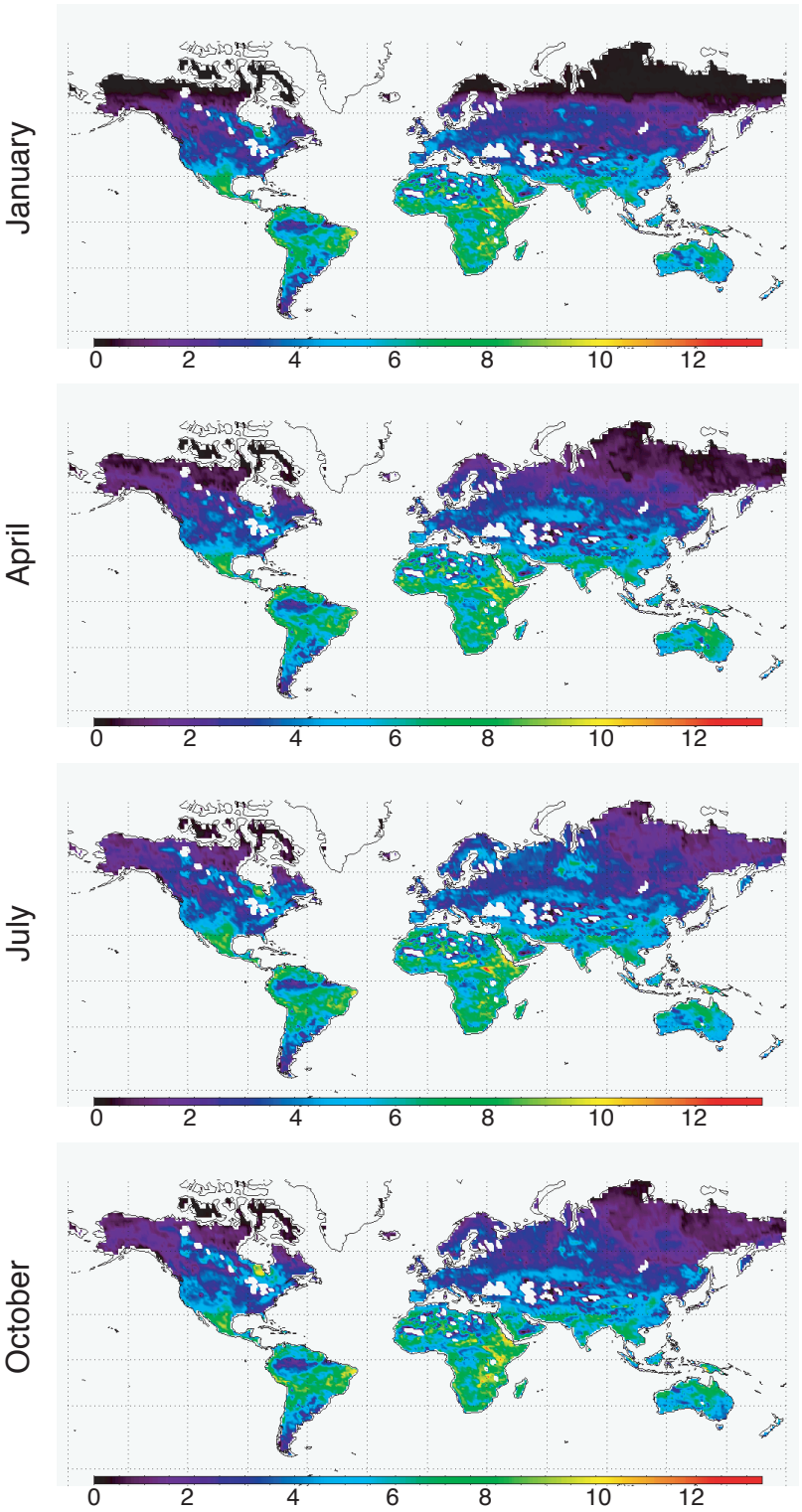

Figure 4. Maps of H_2 uptake by soils averaged for each month from 2001 to 2004. Units are10^9 g H_2 per month.

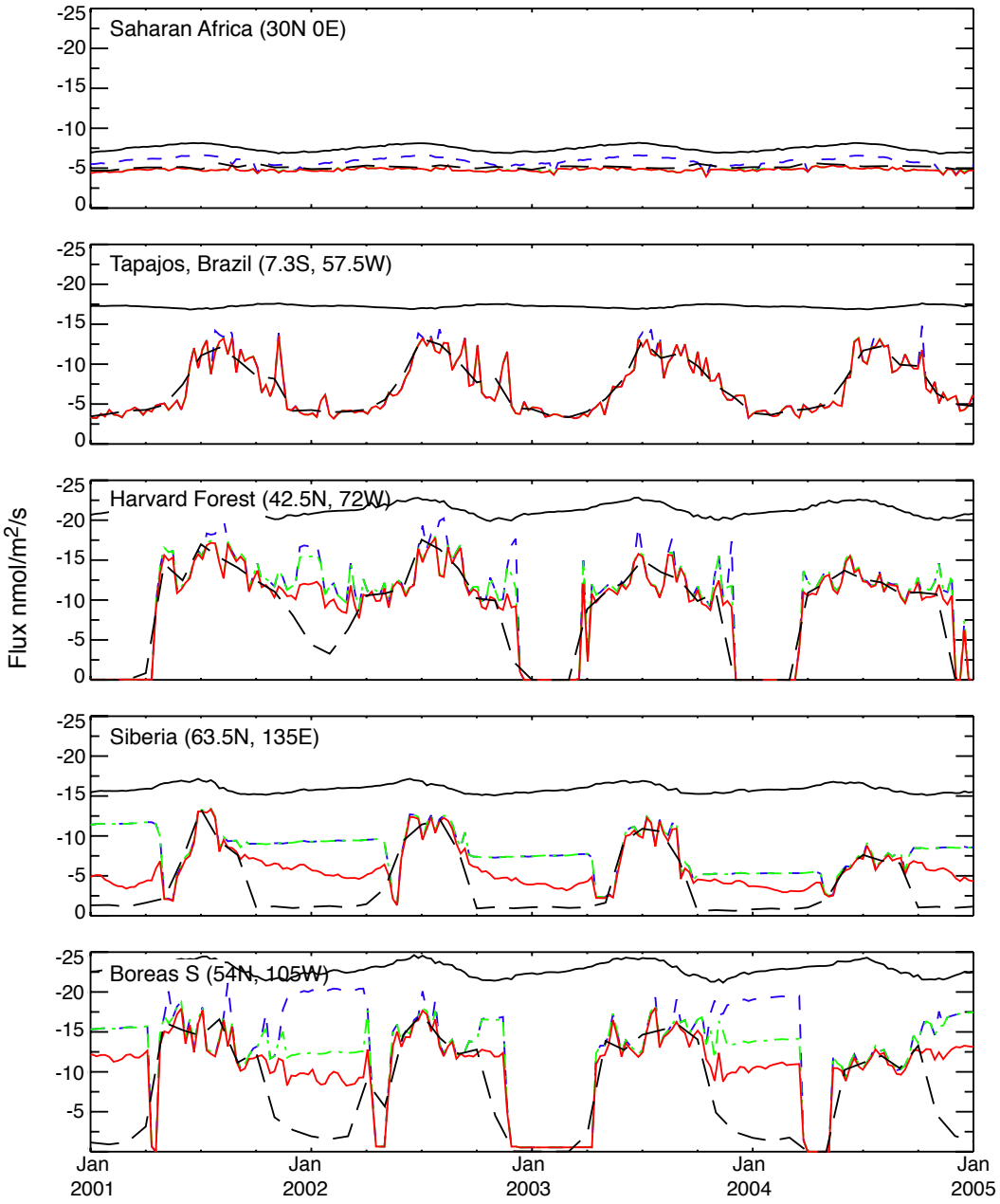

Figure 5. Scalar removal experiments for five regions:

1) Solid black line is maximum possible flux, includes temperature dependence of H_2 diffusion in air, and is driven by the H_2 mean seasonal cycle.
2) Blue Dash line is 1) + the effect of soil moisture on diffusivity of soils
3) Green Dash line is 2) + the effect of soil moisture on uptake of H_2
4) Red line is 3) + the effect of temperature on uptake of H_2
5) Black Dashed line is 4) + the effect of snow cover*

* snow data were run at 1 month timestep, whereas all other data were run at 1 week timestep

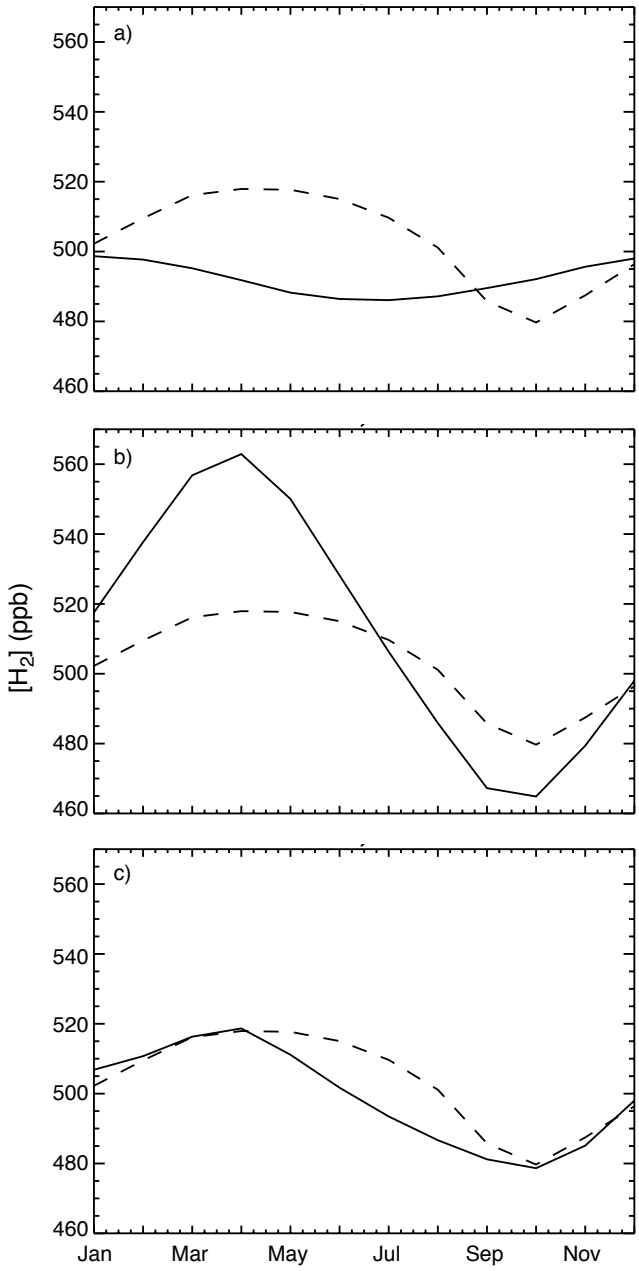

Figure 6. Mean seasonal cycle between 50ºN to 70ºN from 2001 to 2004 from a one box model. In all cases the dashed line is the mean seasonal cycle from flask measurements (*Novelli et al*. 1999). a) Seasonal cycle from our model with no snow cover. b) Seasonal cycle from our model with f_{snow} = 1 for all cells with snow in the USAF 1x1 degree dataset. c) Seasonal cycle from our model with f_{snow} set by MODIS measurements, and snow depth set by the USAF data.

Chapter 5

Trends in high northern latitude freeze and thaw cycles from 1988-2002

Reprinted from Journal of Geophysical Research v109, D12101, 2004.

Nicole V Smith, Sassan S. Saatchi and James T. Randerson

Abstract

In boreal and tundra ecosystems, the freeze state of soils limits rates of photosynthesis and respiration. Here we develop a technique to identify the timing of freeze and thaw transitions of high northern latitude land areas using satellite data from the Scanning Multichannel Microwave Radiometer (SMMR) and Special Sensor Microwave/Imager (SSM/I). Our results indicate that in Eurasia there was a trend towards earlier thaw dates in tundra (-3.3 ± 1.8 days/decade) and larch biomes (-4.5 ± 1.8 days/decade) over the period 1988-2002. In North America, there was a trend towards later freeze dates in evergreen conifer forests by 3.1 ± 1.2 days/decade that led, in part, to a lengthening of the growing season by 5.1 ± 2.9 days/decade. The growing season length in North American tundra increased by 5.4 ± 3.1 days/decade. Despite the trend towards earlier thaw dates in Eurasian larch forests, the growing season length did not increase because of parallel changes in timing of the fall freeze (-5.4 ± 2.1 days/decade), which led to a forward shift of the growing season. Thaw timing was negatively correlated with surface air temperatures in the spring, whereas freeze timing was positively correlated with surface air temperatures in the fall, suggesting that surface air temperature is one of several factors that determines the timing of soil thaw and freeze.

The high spatial resolution, frequent temporal coverage, and duration of the SMMR and SSM/I satellite records makes them suitable for rigorous time series analysis and change detection in northern terrestrial ecosystems.

1. Introduction

In high northern latitude regions, excluding the North Atlantic and Greenland, mean annual surface air temperature increased at rates of up to ~ 0.7°C per decade during the latter half of the 20th century, with the largest increase occurring during winter and spring months [*Chapman and Walsh*, 1993; *Hansen et al.*, 1999; *Hansen et al.*, 2001]. Concurrently, sea ice extent and thickness decreased in the northern hemisphere [*Cavalieri et al.*, 1984; *Chapman and Walsh*, 1993; *Cavalieri et al.*, 1997; *Vinnikov et al.*, 1999], possibly due to increases in the length of the melting season [*Laxon et al.*, 2003]. Observational studies of snow cover in Alaska find a trend towards earlier spring snow melt [*Stone et al.*, 2002], and satellite measurements indicate that snow cover area decreased over the period 1972 to 1988 in both North America and Eurasia [*Serreze et al.*, 2000].

The implications of these changes for the net carbon balance of northern ecosystems remains uncertain because many of these trends may simultaneously increase rates of ecosystem respiration and photosynthesis [*Chapin III et al.*, 2000]. Soils in northern biomes are carbon rich [*Dixon et al.*, 1994] and lie within the region expected to experience the most extreme temperature changes due to global warming over the next century [*IPCC*, 2001]. Soil carbon degradation is sensitive to changes in temperature and moisture content, thus the potential for increasing temperatures to promote carbon loss

from soils in high latitude ecosystems is large [*Schimel and Clein*, 1996; *Goulden et al.*, 1998; *Hobbie et al.*, 2000; *Mikan et al.*, 2002; *Dioumaeva et al.*, 2003].

In addition to impacts on soil respiration, increasing air temperatures may also lengthen the growing season and enhance rates of net primary production (NPP) in tundra and boreal biomes. Several studies of trends in satellite-derived Normalized Difference Vegetation Index (NDVI) report both an increase in growing season length and a "greening" of high northern latitudes [*Myneni et al.*, 1997; *Myneni et al.*, 1998; *Tucker et al.*, 2001; *Zhou et al.*, 2001; *Hicke et al.*, 2002; *Shabanov et al.*, 2002], especially in Eurasia [*Zhou et al.*, 2001; *Bogaert et al.*, 2002]. In a recent study, the increase in growing season length (1981-1999) was attributed to both a trend towards earlier spring leaf out (6 ± 2 days in Eurasia and 8 ± 4 days in North America) and later fall senescence (11 ± 3 days in Eurasia and 4 ± 3 days in North America) leading to an overall increase in the growing season length by 19-24 days in Eurasia and 4-12 days in North America [*Zhou et al.*, 2001].

Examination of trends in atmospheric CO_2 records provides additional evidence for widespread changes in northern ecosystem function. The amplitude of the CO_2 cycle increased by 40% at Point Barrow, AK, and by 20% at Mauna Loa, HI over the period 1960-1993 [*Keeling et al.*, 1996]. These trends are probably caused by a combination of increases in spring and summer NPP [*Keeling et al.*, 1996; *Randerson et al.*, 1999], increasing rates of soil respiration during fall, winter and spring [*Chapin III et al.*, 1996; *Goulden et al.*, 1998], and increasing levels of natural and human induced disturbance [*Zimov et al.*, 2001]. Concurrently, the period of the CO_2 record shifted forward 7 days

from 1960 to 1993 [*Keeling et al.*, 1996] suggesting a trend towards earlier spring thaw and forward shift in the timing of CO_2 drawdown by terrestrial ecosystems.

Although NDVI provides a means for evaluating regional trends in leaf area (and thus NPP), and atmospheric CO_2 records allow for analysis of trends in net ecosystem production (NEP), no comparable constraint is available for estimating trends in biome-level soil respiration. Soil respiration persists at temperatures below 0°C, but rates typically decrease by over an order of magnitude at temperatures below freezing [*Goulden et al.*, 1998; *Dioumaeva et al.*, 2003]. In contrast, at temperatures above 0°C, respiration is exponentially related to soil temperature [*Lloyd and Taylor*, 1994; *Raich and Potter*, 1995; *Raich et al.*, 2002; *Dioumaeva et al.*, 2003].

As proposed by *Running et al.* [1999], a global satellite product that identified soil freeze and thaw boundaries would be of broad use in determining fluxes of both soil respiration and photosynthesis in northern biomes. Here we present a method to estimate the annual timing of freeze and thaw for land north of 45°N using passive microwave satellite observations. We used data from the Nimbus-7 Scanning Multichannel Microwave Radiometer (SMMR), which operated from late 1978 to mid 1987, and the Defense Meteorological Satellite Program (DMSP) Special Sensor Microwave/Imager (SSM/I), which operated from mid 1987 to present. Our algorithm uses an iterative least-squares characterization of the difference between the brightness temperature at 37 and 19 (or 18) GHz to identify the transition from frozen to thawed soil. Using this algorithm we estimate the date of thaw and freeze for each 1° x 1° grid cell north of 45°N. As part of our analysis, we assessed regional and biome level trends in soil freeze and thaw since 1988, and analyzed interannual variability since 1979. We found a trend toward earlier

spring thaw in Eurasian tundra and larch biomes, a trend toward earlier fall freeze in Eurasian larch forests and a trend toward later fall freeze in North American evergreen conifer forests. The growing season length increased significantly in North American evergreen conifer and tundra biomes, but did not change in Eurasian biomes due to the parallel shift of the spring thaw and fall freeze to an earlier date.

2. Methods

2.1. SMMR and SSM/I Data

The SMMR and SSM/I instruments are dual polarized passive multi-channel radiometers that together span the period from late 1978 through the present (Table 1). The operational overlap period between SMMR and SSM/I (on DMSP F8) was limited to 6 weeks between 9 July 1987 and 20 August 1987. SMMR and SSM/I brightness temperature data are widely used to monitor sea ice [*Cavalieri et al.*, 1984; *Bjorgo et al.*, 1997; *Smith*, 1998; *Abdalati and Steffen*, 2001], wind speed over the ocean [*Wentz*, 1992; *Wentz*, 1997], snow cover [*Grody*, 1991; *Basist et al.*, 1998], precipitable water over the ocean [*Liu et al.*, 1992] and freeze-thaw cycles in prairie [*Judge et al.*, 1997] and North American snow free soils [*Judge et al.*, 1997; *Zhang and Armstrong*, 2001].

In our study we used the Equal Area Scalable Earth Grid (EASE-Grid) daily brightness temperature product that is publicly available from the National Snow and Ice Data Center (NSIDC) [*Armstrong et al.*, 1994, updated 2003; *Knowles et al.*, 2002]. The EASE-Grid is a global equal area projection that was developed at the NSIDC with a spatial resolution of 25 km x 25 km for all channels. Data are available twice daily (ascending and descending tracks) for the SSM/I and twice every other day for the SMMR instrument. The length and temporal frequency of the data set makes it suitable

for rigorous time series analysis and change detection. The radiometer channels included 6.6, 10.7, 18, 21 and 37 GHz for the SMMR, and 19, 22, 37, and 85 GHz for the SSM/I. Both horizontally (H) and vertically (V) polarized radiation were measured for all channels except 22 GHz. In our analysis, we used the 18 and 37 GHz channels from SSMR and the 19 and 37 GHz channels from SSM/I, and considered both horizontally and vertically polarized data from ascending and descending satellite tracks. There is little atmospheric interference in this region of the spectrum, except for a water absorption band in the 22 GHz channel [*Chahine et al.*, 1983]. Clouds are thought to have minimal impact on the channels we used, and *Judge et al.* [1997] determined that water vapor and oxygen corrections did not change their freeze-thaw classification results using the 18, 19 and 37 GHz channels. We therefore made no atmospheric corrections in our data processing.

The EASE-Grid data were compiled for the entire period between 1978 and 2002 and were processed through several stages before development and implementation of the algorithm.

2.2. Data Resampling

Our first step of data processing was to average the daily EASE-Grid data to 6-day averages. Six-day averages are necessary because the swath width of the SMMR and SSM/I instruments was not wide enough to yield complete coverage of the region north of 45°N daily. SMMR achieved complete coverage of our study area every 6 days, and SSM/I achieved complete coverage every 4 days. To maintain consistency between satellite records, we averaged both the SMMR and SSM/I data to 6-day means for our analysis. We then aggregated the global EASE-Grid data to 1° x 1° grid cells, removing

EASE-pixels with high water content and complex topography for a 'cleaner' signal prior to this step (as described below). These processing steps were performed on both H and V polarized signals from both ascending and descending satellite tracks, giving us 4 independent time series for each 1° x 1° grid cell that spanned 1 January 1979 to 31 December 2002 (24 years).

2.3. Theory of Algorithm

Brightness temperature (T_b) measured by a radiometer is the product of surface temperature (T_s) and emissivity (ε) of a surface:

(1) $T_b = T_s \cdot \varepsilon.$

ε depends on frequency (ν), polarization (H or V), incidence angle of the satellite observation, surface structure (roughness or vegetation), and moisture. Brightness temperature measurements from microwave radiometers are sensitive to surface moisture because of the relatively high dielectric constant of water. Surface roughness and vegetation cover modulate this sensitivity. For our analysis, we used the difference between the 37 and 18 GHz brightness temperatures for SMMR and the difference between the 37 and 19 GHz brightness temperatures for SSM/I as indicators of soil freeze state.

The difference between these two channels ($\Delta T_b = T_{b(37)} - T_{b(18/19)}$) reflects the difference in emissivity ($\Delta\varepsilon = \varepsilon_{37} - \varepsilon_{18/19}$) that is much larger for frozen than for thawed soils [*Basist et al.*, 1998]. The SMMR and SSM/I instruments maintained fixed incidence angles, thus by using different combinations of channels (frequency) and polarization we can estimate changes in T_s and ε. The ΔT_b signal is dominated by

changes in surface temperature and the difference between the emissivity at 37 and 18 or 19 GHz ($\Delta\varepsilon$).

$$(2) \qquad \Delta T_b = T_{b(37)} - T_{b(18/19)} = (T_s \cdot \varepsilon_{37}) - (T_s \cdot \varepsilon_{18/19}) = T_s \cdot (\varepsilon_{37} - \varepsilon_{18/19}) = T_s \cdot \Delta\varepsilon$$

As the soil surface thaws, $\Delta\varepsilon$ tends towards zero for pixels with low water content [*Basist et al.*, 1998]. T_s remains constant between two channels measured simultaneously, leading to a plateau shaped ΔT_b curve driven solely by changes in $\Delta\varepsilon$ at the freeze thaw boundary.

Our algorithm, which is described below, was designed to detect the date of thaw and freeze by identifying the edges of this annual plateau in the ΔT_b curve for each pixel. We define the growing season length (gsl) as the difference between the day of freeze and the day of thaw.

In another study, an algorithm designed to detect snow cover from the SMMR and SSM/I radiometer data used a combination of the 19, 22, 37 and 85 GHz channels [*Grody et al.*, 1998]. A threshold difference between 37 and 19 GHz and a decision tree approach for the 85-22 GHz difference were used to classify snow covered pixels [*Grody et al.*, 1998]. Although there is some correlation between snow melt and soil thaw, they can be offset by many weeks as observed by *Kimball et al.* [2001]. Although we ignore snow cover in this analysis, it remains an important question that should be addressed further.

2.4. Freeze-Thaw Algorithm

First, we fit a spline to the ΔT_b curve. The algorithm involved a two-step process of fitting a line by ordinary least squares to the plateau of the spline-fitted ΔT_b curve. The

first step was to select a horizontal line that minimized the sum of squares of the residual between the line and the plateau of the curve. This was the first estimate (e_1) of the plateau level. The second step eliminated points deviating from e_1 by more than one standard deviation (σ). The process of line fitting was repeated again, and a second line was chosen to represent the plateau (e_2). σ was then recalculated and the thaw and freeze date were chosen by finding the first and last points where the spline-fitted ΔT_b curve crossed the horizontal line $0.5 \cdot \sigma$ below e_2 (Figure 1). The factor $0.5 \cdot \sigma$ desensitized the algorithm to high frequency variability in the ΔT_b curve, which may be caused by repeated freeze-thaw events in a grid cell.

To validate our algorithm and its application to a variety of surface characteristics, we compared the estimated date of thaw and freeze to that observed directly from soil temperature records at Boreas North Study Area, Manitoba (56°N, 98°W) [*Dunn and Wofsy*, 2003], Delta Junction, AK (64°N, 145°W) [*Liu et al.*, 2004], Toolik Lake, AK (68°N, 149°W) [*Shaver and Laundre*, 2003], and Happy Valley, AK (69°N, 148°W) [*Hinkel*, 1998, updated 2002] (Figure 2, Figure 3). Notice that the algorithm performs better at Happy Valley than at Toolik Lake (Figure 3). Soil temperatures were measured at 8 cm depth in Happy Valley, and at 20 cm depth in Toolik Lake, which may explain the difference in algorithm performance. The microwave emissions measured by the SMMR and SSM/I originate in the upper few (~5) cm of the soil surface, depending on surface wetness. We would expect to see some offset between the Toolik Lake measured and satellite estimated dates of freeze and thaw because of this depth offset.

For the global analysis we computed the date of freeze and thaw for each of the 4 time series (horizontally or vertically polarized and ascending or descending tracks) at each 1° x 1° pixel, giving us 4 independent estimates of soil thaw and freeze date. Despite the fact that the data were originally aggregated to 6-day intervals, we were able to detect trends at a much finer resolution because we fit a spline to the ΔT_b curve with a short temporal resolution. We averaged the 4 estimates of date of freeze and date of thaw for each pixel and aggregated the results to biome and regional scales for the period 1988-2002. Vegetation classifications were based on *DeFries et al.* [1998]. The biomes analyzed here were evergreen conifer forest and tundra in both North America and Eurasia and larch forest in Eurasia (Table 2).

2.5. Pixels with Open Water

EASE 25 km x 25 km pixels with greater than 40% open water cover were excluded from our analysis. We chose the 40% cutoff as a compromise between reducing the failure rate of our algorithm and retaining a high data volume in all of our major biomes (Table 2). With a 40% cutoff, we eliminated virtually all algorithm failures, but kept at least 86% of all pixels in each biome (Table 2).

We generated a water fraction map by aggregating the pixels of a 1 km x 1 km resolution land cover map developed by *Hansen et al*. [2000] to the EASE pixels and 1° x 1° grid cells. Each EASE pixel was assigned a water percentage based on the number of 1 km land cover pixels identified as water. 1° x 1° grid cells were constructed from EASE-Grid pixels that had less than 40% water cover. In addition, any 1° x 1° grid cell with greater than 40% water cover was eliminated from the analysis.

The physical basis of this exclusion is that $\Delta\varepsilon$ does not tend towards zero as water cover of a pixel increases [*Basist et al.*, 1998]. Instead, $\Delta\varepsilon$ becomes larger, destroying the plateau observed in pixels with low water content. Figure 4 illustrates the difference between average signals for each biome with varying water contents. At the 40% level, the shape of the ΔT_b curve degraded to a degree that prevented accurate detection of freeze and thaw (Figure 4) without eliminating significant portions of any major biome. Because our algorithm was based on the shape of the curve rather than the absolute value of the curve, we can safely include pixels with some water, but must remove those that are greater than 40% (Figure 4). A total of 7880 (6.7%) pixels at the EASE-Grid resolution were excluded from our analysis, and the maximum portion of any biome excluded was 14% in the tundra of North America (Table 2).

2.6. High Elevation Pixels

Pixels with high elevations (> 1250 m) had a very high rate of algorithm failure compared with pixels at lower elevations. This is probably due to complex topography and in some instances, snow and ice cover that persisted over the entire year in some pixels. With this threshold, we excluded a maximum of 7% of any biome (Table 2). We therefore filtered out all pixels above 1250 m elevation, as identified by the United States Geological Survey's (USGS) GTOPO30 elevation map [*LP-DAAC*, 2003] averaged to the EASE grid resolution. A total of 2018 EASE pixels were excluded from the three biomes, or 1.7% of the total (Table 2).

2.7. Cross Platform Changes

The SMMR and SSM/I satellites have differences in their viewing angles, overpass time, and frequency (channels) that can introduce bias in the analysis of time

series extending across the period covered by the two satellites. The viewing angles of SMMR and SSM/I are 50.2° and 53.1°, respectively. The warm and cold overpass of SMMR occur at noon (ascending) and midnight (descending), whereas for SSM/I the timing is shifted to 0600 hours and 1800 hours for the F8 satellite, and 1800 and 0600 hours for the F11 and F13 satellites. These differences are particularly important because of the variation in freezing and thawing caused by diurnal variations in temperature. Furthermore, SMMR collected data at 18 GHz, and SSM/I collected data at 19 GHz. There are small differences between atmospheric absorption and surface emissivity at these frequencies, leading to differences in measured brightness temperature.

We observed a large offset between the SMMR (1979-1986) and SSM/I (1988-2002) freeze-thaw record. *Derksen and Walker* [2003] suggest that there is a systematic bias between the measured brightness temperatures of SMMR and SSM/I, primarily caused by differences in overpass time and instruments, but the short (~10 day) period of overlap between the two EASE-Grid records does not permit the development of correction terms that would be both spatially and seasonally valid. For this reason, we did not combine the records to study trends over the complete 24-year measurement period. Instead, we generated averages and trends based only on the 1988-2002 period (14 years). We did, however, utilize the SMMR record to compare interannual variability of freeze/thaw transitions to that of the surface temperature record during 1979-1986.

2.8. Surface Air Temperature Comparison

Using the Goddard Institute for Space Studies (GISS) 2001 surface air temperatures [*Hansen et al.*, 2001], we calculated a correlation between seasonal surface

air temperature anomalies (with a base period of 1951-1980) and the freeze-thaw anomalies. We divided the complete 1979 to 2002 record into two periods, 1979 to 1986 for the SMMR and 1988-2002 for the SSM/I. 1987 was excluded from the analysis because the SMMR to SSM/I shift occurred in the middle of the year. The mean for each satellite period (SMMR or SSM/I) was used separately to compute annual anomalies in thaw and freeze transitions. Thaw transitions were compared with surface air temperatures during the spring, while freeze transitions were compared with surface air temperatures during the fall. For the spring, we averaged air temperature anomalies from April and May. For the fall, we averaged air temperature anomalies from September and October for tundra biomes, and from October and November in evergreen conifer and larch biomes.

2.9. Analysis approach

We produced annual dates of freeze, thaw and length of growing season for each 1° x 1° grid cell from 1979 to 2002. We used these data to examine the spatial and temporal patterns of spring thaw, fall freeze and growing season length. To compare with NDVI trends and other metrics of ecosystem function, we averaged our results to biome levels and separated each biome by continent. For both the global and biome level analysis, we computed mean statistics along with trends over the period from 1988 through 2002. Interannual variability was analyzed for the entire satellite record (1979-2002) and compared to variability in surface air temperature over the same period. Spatial patterns of the freeze-thaw anomalies were also compared to the spatial patterns of the surface air temperature record.

3. Results

3.1. Mean Patterns

In Eurasia, the timing of the mean thaw progressed from west to east, with a distinct transitional border at the Ural Mountains in Russia. The mean thaw date was delayed with increasing latitude. The latest mean thaw dates occurred in central Siberia along the coast of the Arctic Ocean (Figure 5a). In Eurasia, the date of thaw occurred first in evergreen conifer forests (Julian day 120 ± 25), followed by larch forests (131 ± 15) and tundra (151 ± 21) (Table 3). In North America, the area west of the Hudson Bay in Canada had the latest mean thaw (Figure 5a). North American evergreen conifer thawed first (132 ± 20), followed by tundra (157 ± 21) (Table 3).

The timing of the freeze occurred in the reverse order of the thaw across Eurasia and North America. In Eurasia, freeze timing occurred later from East to West, again with a distinct border at the Ural Mountains. The freeze occurred earlier with increasing latitude (Figure 5b). In Eurasia the date of the freeze occurred first in tundra (272 ± 17) followed by larch (276 ± 16) and evergreen conifer forests (289 ± 23) (Table 3). The Brooks Range in Alaska was the first part of North America to freeze, with eastern Canada following much later (Figure 5b). In North America the date of freeze occurred first in tundra (285 ± 20) then in evergreen conifer forests (293 ± 23).

The mean gsl in Eurasia decreased from West to East and from South to North. It was shortest in central Siberia on the Arctic coast (Figure 5c). The gsl in Eurasia was shortest in tundra biomes (121 ± 30 days) followed by larch forest (146 ± 26) and evergreen conifer forest (170 ± 42) biomes (Table 3). In North America, the Brooks Range in Alaska had the shortest gsl. Tundra had a shorter gsl (128 ± 31) than evergreen conifer forests (160 ± 34) in North America (Table 3).

3.2. Trends

In all biomes north of 45° N there was either a trend towards earlier spring thaw, or no significant change over the 14-year period from 1988 through 2002 (Figure 5d; Table 3). There was a trend towards earlier spring thaw throughout much of Eurasia east of the Ural Mountains, but a trend towards later thaw in areas west of the Urals (Figure 5d). Eurasian larch forest thaw exhibited the greatest rate of change (-4.5 ± 1.8 days/decade, where the negative sign convention indicates earlier thaw) followed by tundra (-3.3 ± 1.8 days/decade) (Figure 6a, Table 3). In North America, Alaska demonstrated a mixed response with some positive and negative trends in the date of thaw (Figure 5d).

Trends in the timing of the fall freeze were substantially different for North America and Eurasia. In Eurasia there was a trend towards earlier fall freeze in the larch biome by –5.4 ± 2.1 days/decade, whereas in the North American evergreen conifer biome, there was a 3.1 ± 1.2 days/decade trend towards later fall freeze . (Figure 6e, Table 3). While there were some areas of Eurasia with a trend towards later fall freeze, such as Scandinavia and the Ural Mountain region of Russia, most of eastern Eurasia experienced a trend towards earlier fall freeze similar in magnitude to the trend in spring thaw (Figure 5e). In contrast, there was a trend towards later fall freeze in many areas of North America (Figure 6e, Table 3). The area east of the Canadian Rockies between 50 and 60° N experienced the greatest trend towards later fall freeze (Figure 5e).

In Eurasian larch forests the parallel movement of spring thaw and fall freeze to an earlier date led to a shift in the phase of the growing season to an earlier period but resulted in no net change in gsl (Figure 6f, Table 3). In contrast, North America's

growing season length increased significantly for both evergreen conifer forests (5.1 ± 2.1 days/decade) and tundra (5.4 ± 3.1 days/decade). These changes were driven by a trend towards both earlier spring thaw and later fall freeze. Some areas in Alaska showed a negative trend in growing season length, but nearly all of Canada showed a large positive trend (Figure 5f).

3.3. Interannual Variability and Comparison with Surface Air Temperature Records

Mean surface air temperature patterns were similar to patterns in freeze and thaw (Table 4). There was a strong negative correlation between spring air temperature anomalies and thaw dates, and a strong positive correlation between fall air temperature anomalies and freeze dates (Table 5, Figure 7). The single largest anomaly in the timing of the fall freeze occurred in 1998, where the timing of the freeze was ~ 10 days earlier than average in all of the Eurasian biomes (Figure 7). This was matched in the surface air temperature record by a strong negative anomaly (Figure 7). In addition, the spatial pattern of the 1998 freeze anomaly had a very similar structure to that of the surface air temperature anomaly during this time (Figure 8). The freeze date captured widespread cooling in central Eurasia, and more localized warming in northern Canada. Because of the high resolution of the SMMR and SSM/I data we identified an area with slightly positive freeze anomalies over the Ural Mountains in Russia, a feature that the surface air temperature record could not resolve.

4. Discussion

Passive microwave measurements reflect changes in the emissivity of a pixel, which incorporates information from both the soil surface and vegetation. It provides a

direct measurement of the freeze state of a pixel that is independent of surface air temperature measurements. Air temperature and freeze-thaw timing can, in fact, be decoupled by several factors such as ground cover (i.e. insulating mosses vs. bare ground), vegetation that shades the soil surface, or water content of vegetation and soils [*Baldocchi et al.*, 2000]. Vegetation and ground cover may be particularly important in mature evergreen conifer forests, which have a perennial canopy and thick insulating moss ground cover [*Beringer et al.*, 2001; *Chambers and Chapin*, 2001].

As a validation of our predicted trends, it was important to assess whether our results reproduced expected mean patterns of thaw, freeze, and growing season length. Generally, we expected that evergreen conifer ecosystems would thaw earlier and freeze later than tundra and that the date of thaw would increase with increasing latitude, and date of freeze would decrease with increasing latitude based on surface soil temperature measurements (Figure 2, Figure 3). Our biome-level results support these assumptions (Table 3), and give confidence that our algorithm captured the large-scale trends and interannual variability in the freeze-thaw record.

The trends observed in this study are interesting to consider in the context of ecosystem function and the surface energy budget of northern biomes. In Eurasia, there was little net change in the growing season length, but there was a trend towards earlier spring thaw in both tundra and larch biomes and a trend towards later fall freeze in the larch biome. Because northern ecosystems are light and temperature limited, an earlier spring thaw may allow plants to become photosynthetically active at earlier periods, when light levels are relatively high. Earlier spring thaw may also increase soil respiration. Although there was also a trend towards earlier fall freeze, it may have

impacted plant productivity less because of light limitation during this time of year. An earlier fall freeze could, however, reduce fall fluxes of CO_2 from soils. In contrast, the trend towards later fall freeze in North America may not significantly change plant productivity due to limited light, but could increase fall efflux of CO_2 from soils. Earlier spring thaw also allows transpiration to occur earlier in the year, increasing early season latent heat fluxes. Because much of the latent heat fluxes in evergreen conifer ecosystems are modulated by mosses and trees with shallow rooting systems [*Baldocchi et al.*, 2000], changing freeze thaw patterns may have a disproportionately large effect on the energy budget of these biomes.

Our freeze-thaw trends show substantial differences with reported NDVI time series, although the different time periods for the published NDVI analyses make it challenging to construct a direct comparison. A recent NDVI analysis by *Zhou et al.* [2001] over the 1981 to 1999 period concluded that there was a trend of 3.1 days/decade towards earlier spring leaf-out in Eurasia and 4.2 days/decade in North America. *Zhou et al.* also found a trend of 5.8 days/decade towards later fall senescence in Eurasia and 2.1 days/decade in North America. They concluded that the growing season length had increased by 9.5 days/decade in Eurasia and 6.3 days/decade in North America. Our freeze-thaw analysis over the period 1988-2002 yields similar results for the trend towards an earlier spring, but our results differ significantly for the fall freeze. Where the NDVI analysis showed a large trend towards later fall in Eurasia (5.8 days/decade), we detected a 5.4 days/decade trend towards earlier fall freeze in the larch biome. We found no net change in the gsl of Eurasia, and a 5 days/decade lengthening trend in North American tundra and evergreen conifer biomes. A hypothesis to reconcile these results

could be that in Eurasia colder temperatures were accompanied by later snow cover. In evergreen conifer and tundra ecosystems, a change in NDVI during the fall may be due in part to changes in the timing of snow cover.

High latitude atmospheric CO_2 observations suggest that there is a trend towards earlier spring uptake of CO_2 by 3.3 days/decade from 1975-1996 [*Keeling et al.*, 1996]. There is, however, less evidence in the CO_2 record of significant changes in the zero crossing time during the fall [*Keeling et al.*, 1996; *Randerson et al.*, 1997; *Randerson et al.*, 1999]. This may be due to the opposite trends in the timing of soil freeze (and thus rates of soil respiration) in Eurasia and North America that would cancel out their net contribution to the seasonal cycle of atmospheric CO_2.

Limitations on the application of SMMR and SSM/I data to the study of freeze thaw transitions stems from several sources. The large pixel size prohibited including small scale topography in our analysis, a variable that is significant for soil respiration fluxes [*Goulden et al.*, 1998; *Dioumaeva et al.*, 2003]. In addition, the effect of vegetation and canopy cover on our algorithm was not explicitly examined in this study. However, grouping data by vegetation type and region allowed for an internally consistent analysis of trends across years.

We did not account for snow cover of pixels, although soil freeze and thaw dates chosen with this method compare well to field data in areas with seasonal snow cover (Figure 3). The ΔT_b curve primarily reflects changes in surface emissivity and has a strong correlation with the soil freeze state. At the four field sites we compared our algorithm to, our algorithm worked reasonably well for most years but does not capture

the interannual variability perfectly at all sites (Figure 4). Despite these limitations, this approach provides a new metric of soil freeze and thaw timing since 1988.

5. Conclusions

The freeze-thaw product developed here represents a new and independent measurement of soil freeze state. We found that there was a trend towards earlier spring thaw in Eurasian larch and tundra biomes, and a trend towards earlier fall freeze larch forests in Eurasia but there was a trend towards later fall in evergreen conifer forests in North America. The net effect on gsl was minimal in Eurasia, but was on the order of 5 days/decade in North American tundra and evergreen conifer biomes. Although the growing season length did not change in Eurasia, the shift in the timing of freeze and thaw may have important implications for ecosystem carbon fluxes because of increased net primary productivity in spring, when light is plentiful. In contrast, the extended growing season in North America may increase plant productivity and soil respiration in spring, and increase soil respiration in fall.

Acknowledgements

The authors thank W. Chapman and J. Walsh for providing them with surface air temperature data. We also thank S. Wofsy and A. Dunn for soil temperature data at the BOREAS North Study Area. NVS thanks L. Caspar, J.D. Godchaux, and N. Downey for their helpful comments on the manuscript. This work was supported by the following grants: NSFOPP-0097439 and NASA_NAG5-11200. In addition, NVS is supported by the NCER STAR program, EPA.

Table 1. Satellite data included in this study

Satellite	Instrument	Time Period		Overpass Time (Equator)	
		Start	End	Ascending	Descending
Nimbus 7	SMMR	25 October 1978	20 August 1987	12:00	0:00
DMSP - F8	SSM/I	1 August 1987	3 December 1991	6:00	18:00
DMSP - F11	SSM/I	4 December 1991	2 May 1995	18:00	6:00
DMSP - F13	SSM/I	3 May 1995	31 December 2002*	18:00	6:00

* These data continue to be collected

Table 2. Characteristics of northern biomes including number of 1x1 degree pixels, water content and elevation masking properties. Each biome is divided by continent, North America (NA) and Eurasia (EA). Water fraction distribution describes the percent of pixels in each biome with a given water content. The pixels with greater than 40% water cover or 1250m elevation were excluded from our analysis.

Biome	Number of Pixels		Area	Water Fraction Distribution				EASE Pixels Eliminated		
	EASE Grid	1∞ x 1∞	10^6 km^2	0-5%	5-20%	20-60%	60-100%	Water	Elevation	Total
Evergreen Conifer NA	9257	905	5.8	55%	31%	10%	3%	6%	7%	13%
Evergreen Conifer EA	10853	1078	6.7	80%	13%	5%	2%	3%	7%	10%
Tundra NA	4920	632	3.0	38%	35%	18%	9%	14%	4%	17%
Tundra EA	6495	896	4.0	73%	16%	8%	4%	6%	4%	10%
Larch EA	8532	886	5.3	87%	10%	2%	1%	2%	2%	3%
All Evergreen conifer	20110	1983	12.5	69%	22%	7%	3%	4%	7%	11%
All Tundra	11415	1528	7.0	58%	24%	12%	6%	10%	4%	13%
North America [a]	20629	2130	12.8	56%	27%	12%	6%	6%	7%	13%
Eurasia [a]	38974	3941	24.3	83%	11%	4%	2%	5%	7%	12%

[a] For all areas north of 45° N excluding Greenland

Table 3. Summary of freeze-thaw averages and trends by biome and continent.

	Average Julian Day [b]			Trends (days/decade) [b]		
	Thaw	Freeze	GSL	Thaw	Freeze	GSL
Evergreen conifer NA	132 ± 20	293 ± 23	160 ± 34	-2.0 ± 2.5	3.1 ± 1.2*	5.1 ± 2.9*
Evergreen conifer EA	120 ± 25	289 ± 23	170 ± 42	-3.2 ± 2.5	0.9 ± 2.4	2.3 ± 3.0
Tundra NA	157 ± 21	285 ± 20	128 ± 31	-4.2 ± 2.8	1.2 ± 2.1	5.4 ± 3.1*
Tundra EA	151 ± 21	272 ± 17	121 ± 30	-3.3 ± 1.8*	-3.9 ± 2.3	-0.7 ± 2.6
Larch EA	131 ± 15	276 ± 16	146 ± 26	-4.5 ± 1.8*	-5.4 ± 2.1*	-0.9 ± 3.2
All Evergreen conifer	125 ±24	291 ± 23	165 ± 39	-2.7 ± 1.7	0.9 ± 1.4	3.6 ± 2.1
All Tundra	154 ±17	277 ± 22	124 ± 34	-3.6 ± 1.4*	-1.9 ± 1.5	1.8 ± 1.7
North America [a]	133 ±38	288 ± 33	155 ± 59	-0.8 ± 2.3	2.2 ± 1.5	3.1 ± 2.2
Eurasia [a]	119 ±42	288 ± 30	169 ± 122	-3.9 ± 2.4	-3.1 ± 2.2	0.8 ±2.7

* indicates statistically significant trend at the = 0.1 level

[a] For all areas north of 45° N excluding Greenland

[b] Standard deviations are calculated as the average deviation of each pixel from the mean value

Table 4. Summary of surface air temperature averages and trends by biome and continent.

	Average [a, e]			Trends (degrees C/decade) [b, e]		
	Spring [d]	Fall [d]	Year [d]	Spring [d]	Fall [d]	Year [d]
Evergreen conifer NA	1.1 ± 4.2	-2.1 ± 4.8	-2.6 ±2.2	-0.2 ± 0.8	1.4 ± 0.7	0.8 ± 0.6
Evergreen conifer EA	4.2 ± 5.1	-4.4 ± 7.7	-1.1 ± 2.8	0.4 ± 0.9	-0.1 ± 1.8	-0.4 ± 1.2
Tundra NA	-3.4 ± 5.1	0.1 ± 4.0	-3.4 ± 2.0	0.7 ± 1.5	1.9 ± 0.9	1.4 ± 0.9
Tundra EA	-2.1 ± 4.5	-1.6 ± 4.3	-6.9 ± 2.1	0.2 ± 0.7	0.3 ± 1.4	-0.3 ± 1.1
Larch EA	0.2 ± 4.2	-9.5 ± 6.5	-6 ± 2.6	0.5 ± 0.9	-0.9 ± 2.4	-0.6 ± 1.4
All Evergreen conifer	2.8 ± 5.0	-3.4 ± 6.7	-1.8 ± 5.2	0.1 ± 0.8	0.6 ± 1.1	0.1 ± 0.7
All Tundra	-2.6 ± 4.8	-0.9 ± 4.3	-5.5 ± 6.2	0.4 ± 0.9	0.9 ± 1.2	0.4 ± 1.0
North America [c]	0.7 ± 5.4	1.1 ± 5.5	-1.6 ± 5.4	0.0 ± 1.0	1.3 ± .8	0.8 ± 0.7
Eurasia [c]	3.7 ± 6.5	-0.3 ± 6.9	-1.6 ± 7.1	0.5 ± 0.8	-0.1 ± 1.7	-0.3 ± 1.2

[a] Average surface air temperatures are for 1988-2002, and were generated from *Chapman and Walsh* 1993.

[b] Trends in surface air temperature are for 1988-2001, and were generated from *Hansen et al.* 2001

[c] For all areas north of 45° N excluding Greenland

[d] Spring values are average of April and May for all biomes and continents. Fall values are average of October and November for Evergreen Conifer and Larch, and are average of September and October for Tundra. North America and Eurasian fall surface temperatures are average of September, October and November.

[e] Standard deviations are calculated as the average deviation of each pixel from the mean value

Table 5. Correlation of surface temperature and freeze-thaw anomalies by biome.

	Spring Thaw				Fall Freeze				Number of Stations [2]
	r[1]		r[1]		r[1]		r[1]		
	SMMR (1979-1986)	p-value	SSM/I (1988-2002)	p-value	SMMR (1979-1986)	p-value	SSM/I (1988-2002)	p-value	
Evergreen Conifer NA	-0.38	0.34	-0.51*	0.05	0.72*	0.05	0.65*	0.02	353
Evergreen conifer EA	-0.50	0.2	-0.75*	< 0.01	0.62	0.13	0.66*	0.02	126
Tundra NA	-0.19	0.65	-0.41	0.15	0.55	0.12	0.43	0.13	33
Tundra EA	-0.05	0.91	-0.65*	0.06	0.39	0.36	0.55*	0.04	26
Larch EA	-0.93*	< 0.01	-0.71*	< 0.01	0.73*	0.04	0.71*	< 0.01	58

* indicates significance at = 0.1 level

[1] r is the correlation coefficient

[2] Number of stations available in the GISS surface air temperature analysis (www.giss.nasa.gov/data)

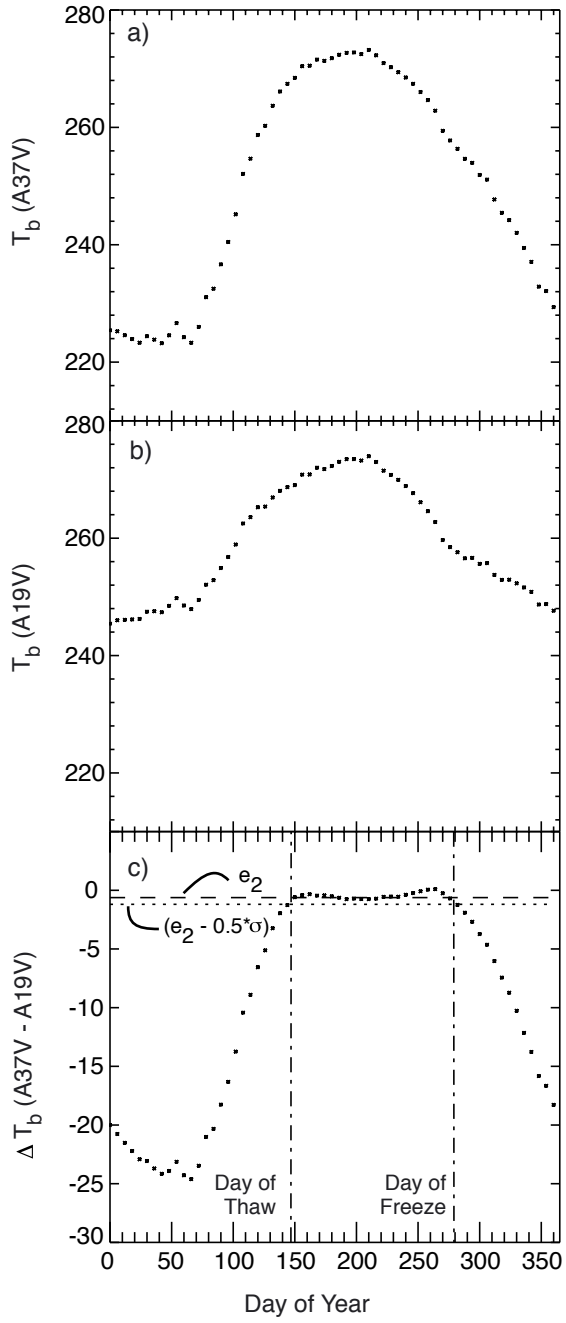

Figure 1. Average ascending 37V (a), 19V (b) and 37V-19V (c) annual time series for the evergreen conifer biome in North America. Each point represents a six-day average signal. The horizontal dashed line in (c) represents the level of the plateau identified by our algorithm. The vertical dashed lines represent the dates of thaw and freeze.

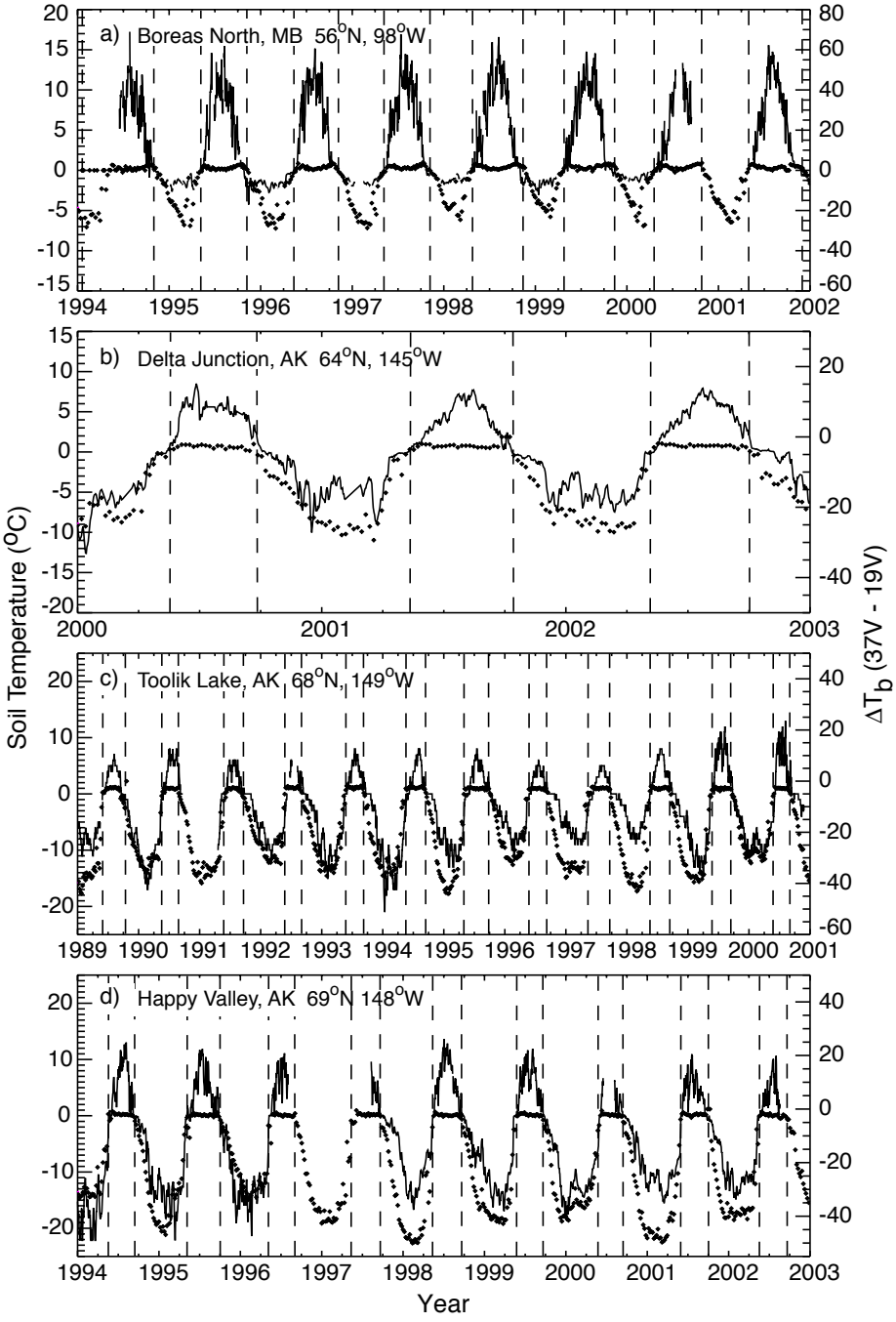

Figure 2. Observed soil temperatures (solid lines) and ΔT_b curves (dots) for Happy Valley, Alaska (8 cm), Boreas North, Manitoba (10 cm), Toolik Lake, Alaska (20 cm), and Delta Junction, Alaska (11 cm). The width of the plateau in the ΔT_b signal corresponds to the length of time that the soil is thawed at each site. Dashed vertical lines represent the thaw and freeze transitions identified by our algorithm based on the ΔT_b signal.

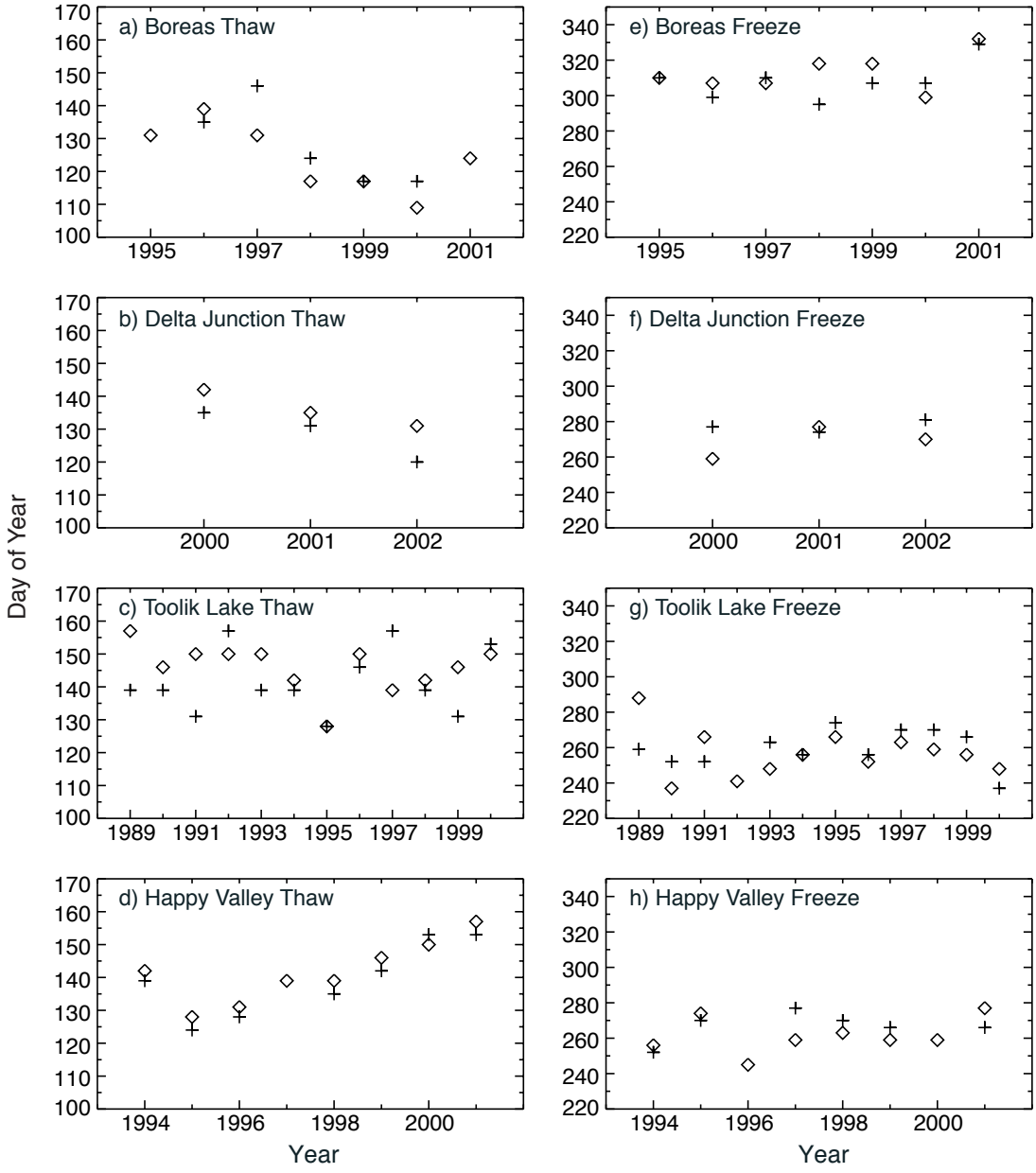

Figure 3. Estimates of thaw (a-d) and freeze day (e-h) for each site in Figure 2 from the soil temperature data (+) and from our satellite analysis (◇). For the in situ soil temperature we defined the date of thaw as the earliest date that the soil temperature is greater than 0^{o}C for 3 consecutive days and date of freeze as the latest date that soil temperature is less than or equal to 0^{o}C for 3 consecutive days.

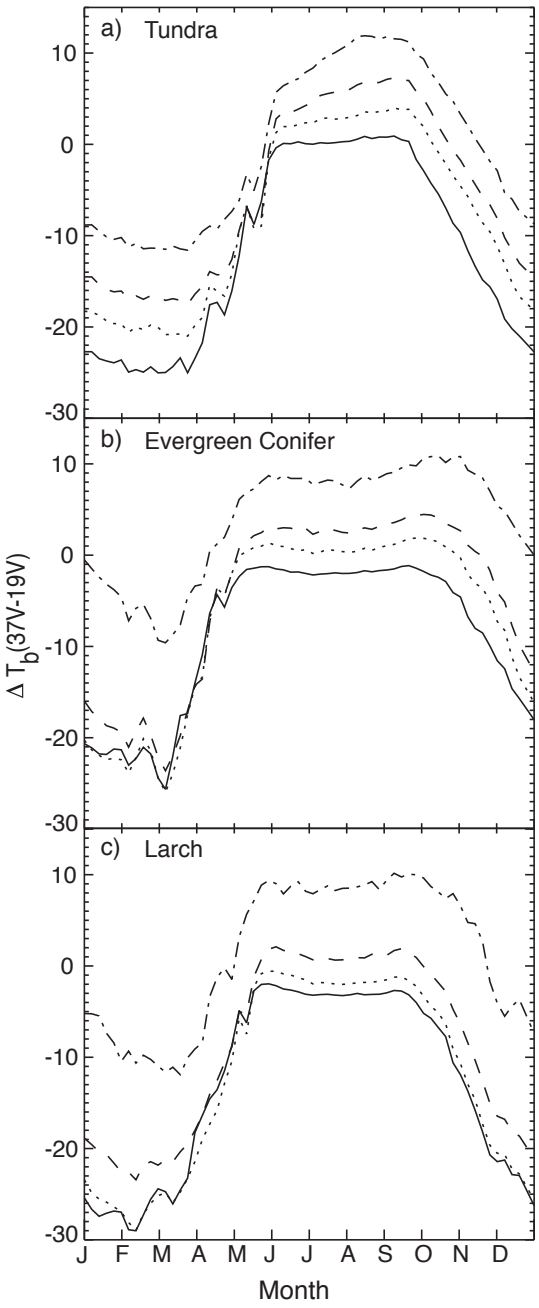

Figure 4. Average ΔTb signal for tundra (a), evergreen conifer (b), and larch (c) in 1998 separated by pixel water content. 0.0-5% (solid lines), 5.01-20% (dotted lines), 20.01-60% (dashed lines) and 60.01-100% (dash-dot lines) water cover. The plateau shape degrades as the water content of a pixel increases, especially in the tundra ecosystem. This is due to an increase in $\Delta\varepsilon$ for water vs. thawed soil.

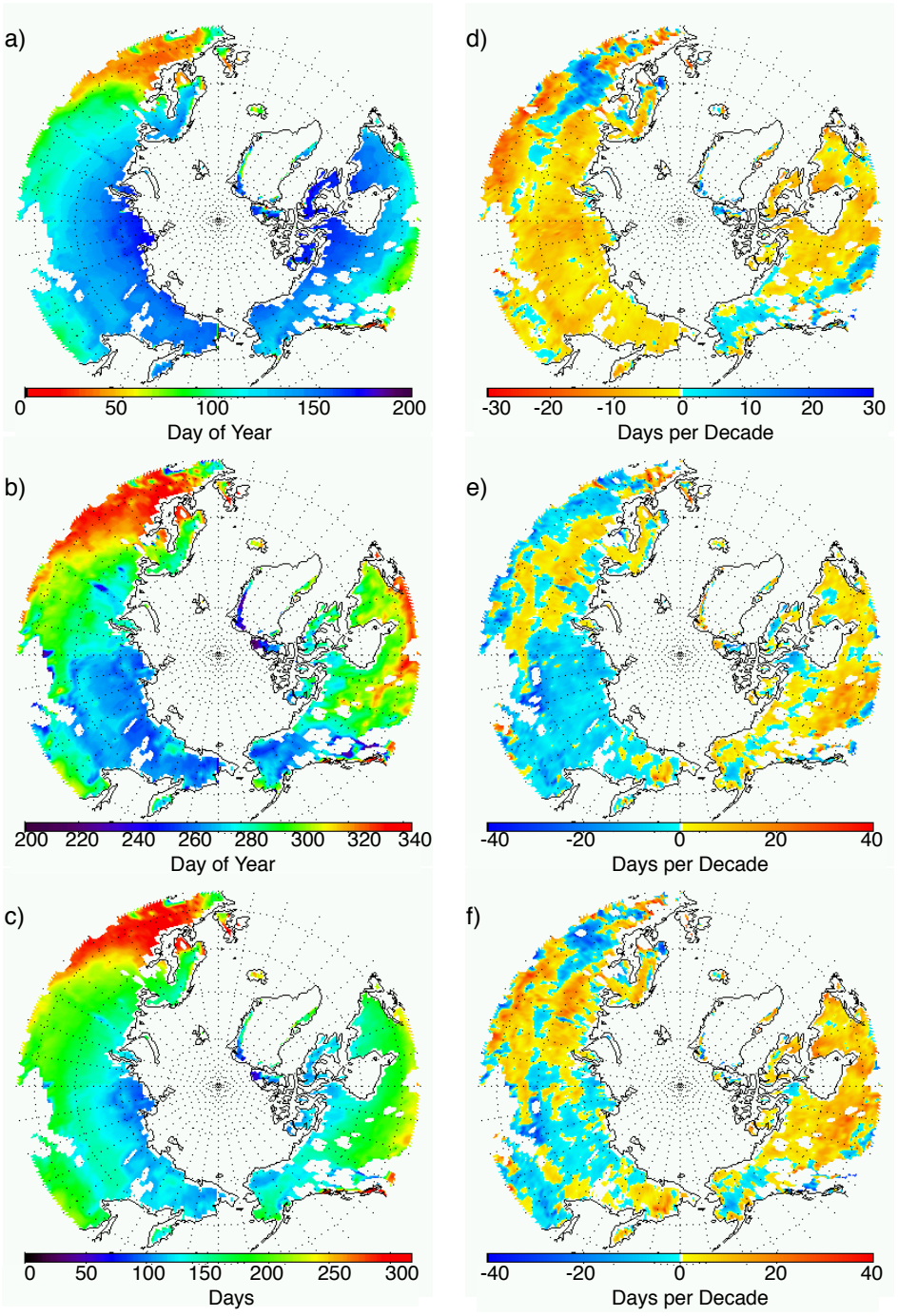

Figure 5. Maps of thaw, freeze and growing season length for all areas north of 45 degrees N. (a) average Julian Day of thaw, (b) average Julian Day of freeze, (c) average growing season length (days), (d) trends in thaw (days/decade) 1988-2001, (e) trends in freeze (days/decade) 1988-2001, and (f) trends in growing season length (days/decade).

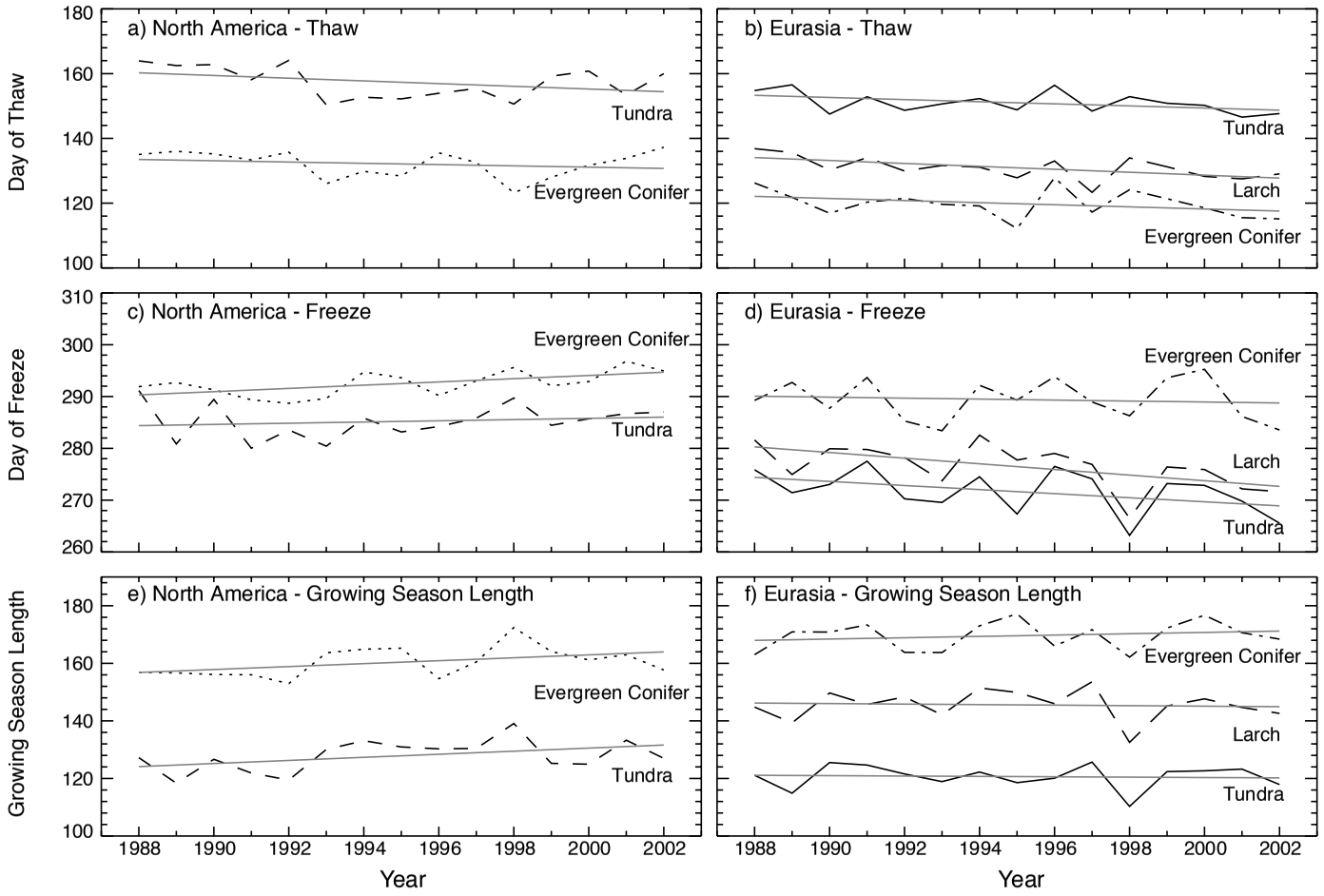

Figure 6. Biome level trends for freeze, thaw, and growing season length in North America and Eurasia. (a) North America thaw date for evergreen conifer (dotted line) and tundra (dashed line) (b) Eurasia thaw date for evergreen conifer (dash-dot line), tundra (solid line) and larch (dashed line). (c, d) North America and Eurasia freeze dates, (e,f) Growing season length for North America and Eurasia. Light grey lines represent the least squares fit to the data.

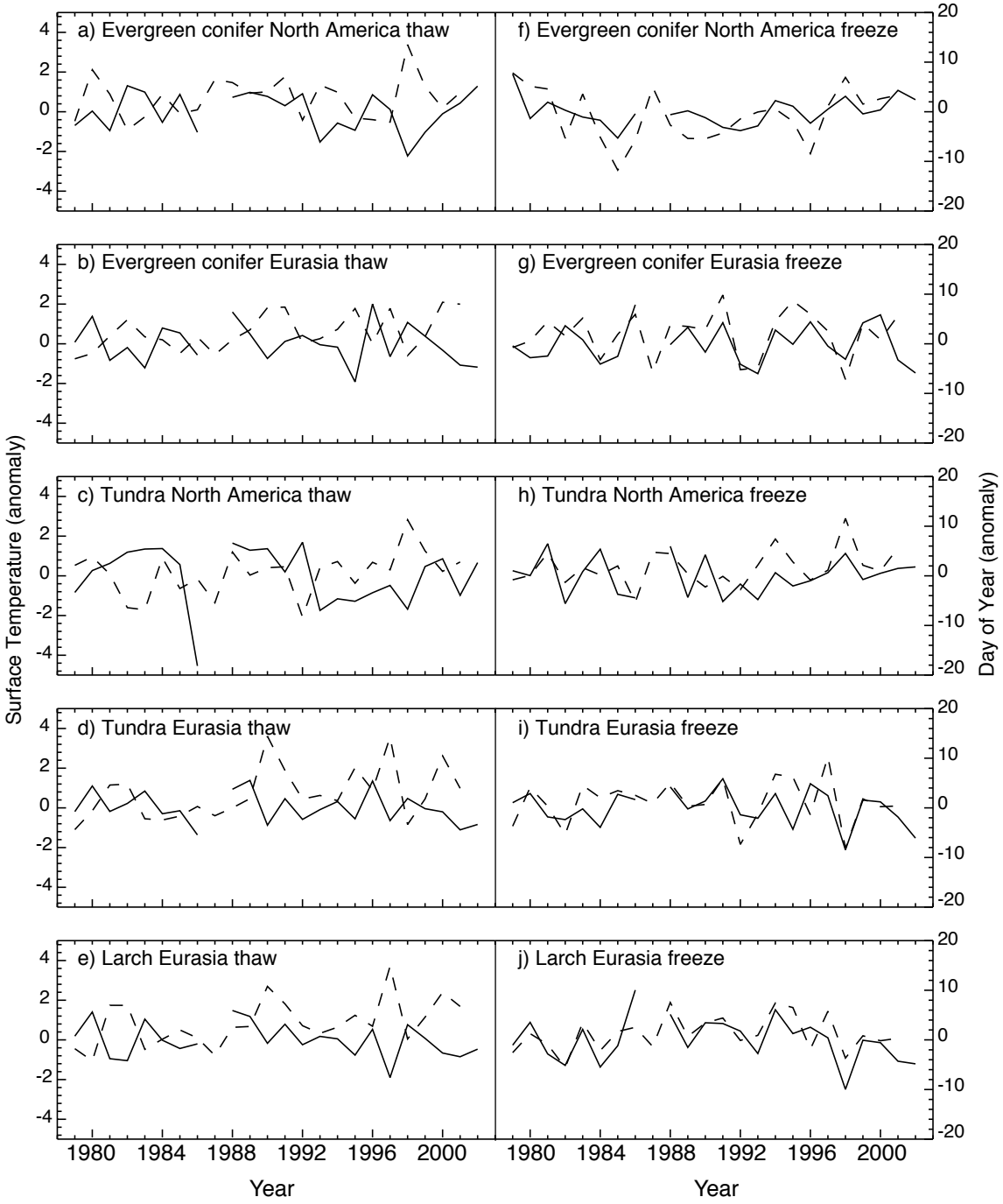

Figure 7. Freeze-thaw anomalies (solid line) and monthly surface temperature anomalies (dotted line) for 1979-1986 and 1988-2002. The spring thaw is negatively correlated with spring temperatures, and the fall freeze is correlated with fall temperatures. See Table 5 for correlation coefficients.

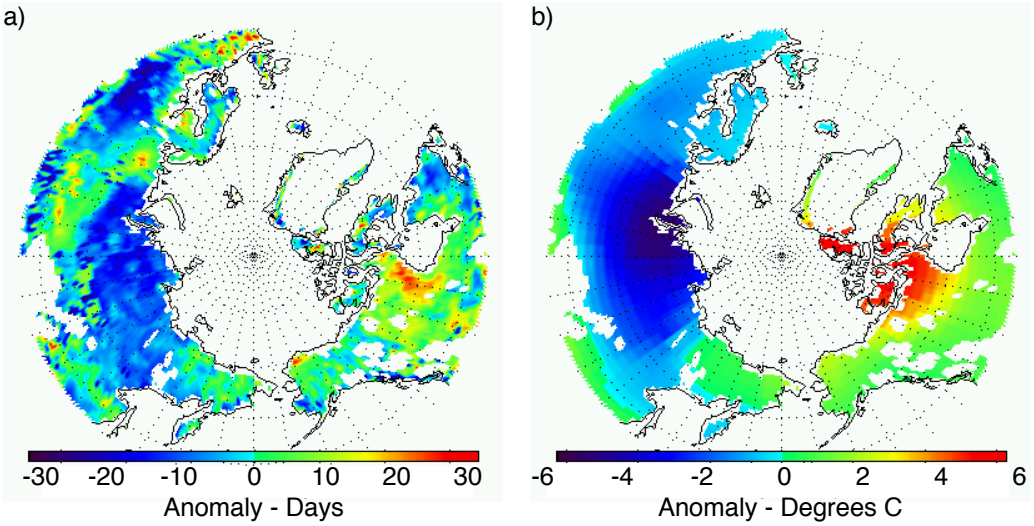

Figure 8. Maps of anomaly of 1998 freeze (a) and fall temperature (b). Fall temperature data are the average of September, October and November surface air temperature anomalies in 1998 from the GISS 1200 km smoothed dataset [Hansen et al., 2001].

Appendix I

Update to "Trends in High Northern Latitude Freeze and Thaw Cycles from 1988 to 2002"

Since the original publication of this paper in 2004, three years of SSM/I data have been released. We extended our record to include the new data and the average dates of spring thaw, fall freeze and growing season length for North America and Eurasia are plotted in Figure 1. The mean patterns observed in our original analysis did not change substantially, and we found significant increases in the growing season length in all boreal and tundra regions (4.2 and 3.1 days/decade respectively), and for North America as a whole (Table 1).

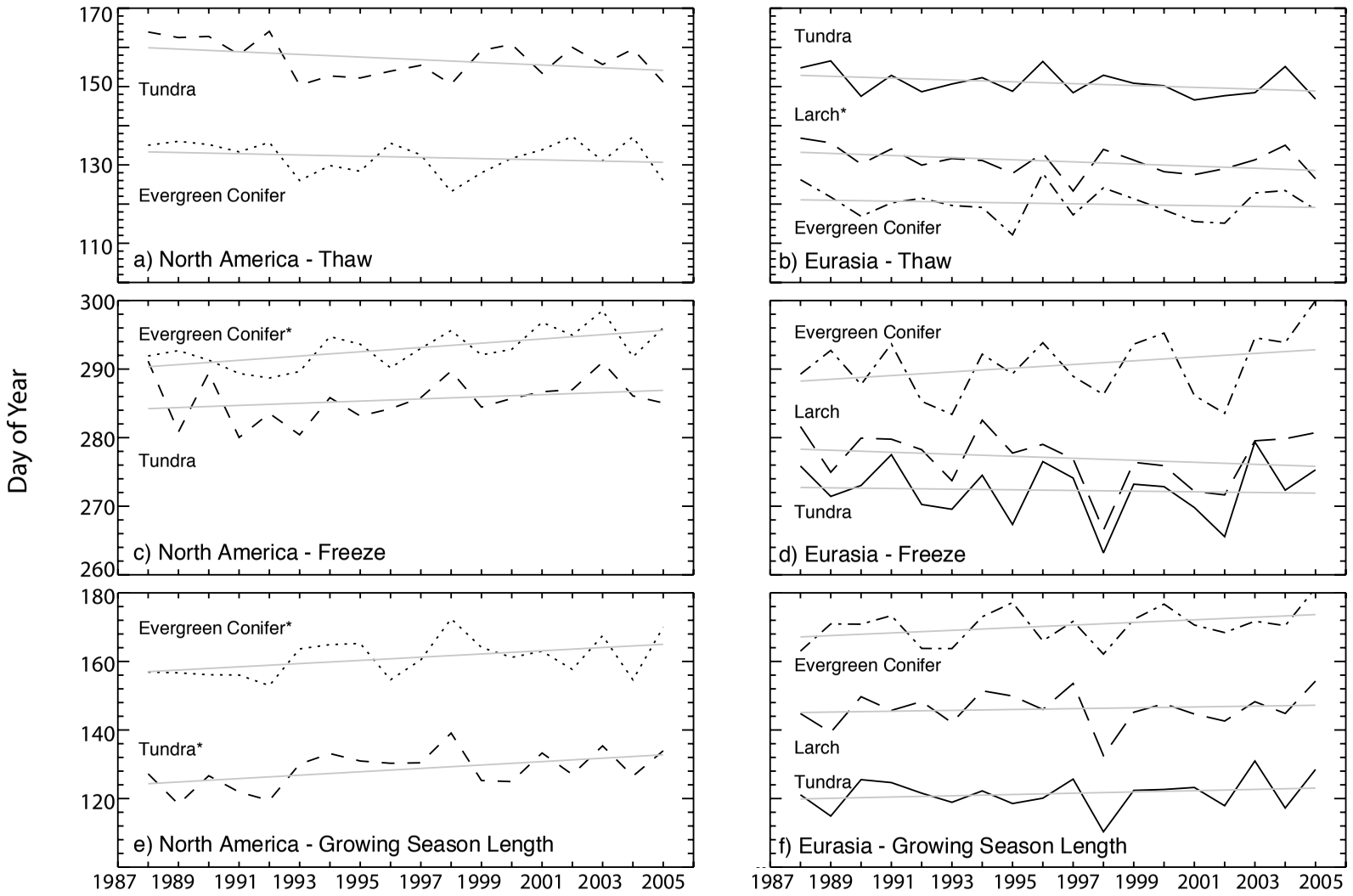

Figure 1. Updated freeze, thaw and growing season length trends through 2005.

	Region	Trends days/decade	p-value
Thaw	Boreal NA	-1.56	0.43
	Boreal EA	-1.13	0.55
	Tundra NA	-3.38	0.12
	Tundra EA	-2.34	0.12
	Larch EA	-2.71	0.09
	All Boreal	-1.33	0.35
	All Tundra	-2.76	0.04
	North America	-1.35	0.46
	Eurasia	2.26	0.22
Freeze	Boreal NA	3.12	0.01
	Boreal EA	2.69	0.20
	Tundra NA	1.56	0.31
	Tundra EA	-0.48	0.81
	Larch EA	-1.46	0.44
	All Boreal	2.88	0.03
	All Tundra	0.34	0.80
	North America	2.47	0.04
	Eurasia	0.25	0.89
GSL	Boreal NA	4.68	0.07
	Boreal EA	3.82	0.11
	Tundra NA	4.95	0.04
	Tundra EA	1.85	0.42
	Larch EA	1.24	0.61
	All Boreal	4.21	0.03
	All Tundra	3.10	0.07
	North America	3.82	0.06
	Eurasia	2.51	0.23

Table 1. Updated freeze and thaw trends through 2005.

BIBLIOGRAPHY

Abdalati, W., and K. Steffen, (2001), Greenland ice sheet melt extent: 1979-1999, Journal of Geophysical Research, 106 (D24), 33983-33988.

Armstrong, R.L., K.W. Knowles, M.J. Brodzik, and M.A. Hardman, (2003), DMSP SSM/I Pathfinder daily EASE-Grid brightness temperatures, National Snow and Ice Data Center, Boulder, CO.

Baldocchi, D., F.M. Kelliher, A. Black, and P. Jarvis, (2000), Climate and vegetation controls on boreal zone energy exchange, Global Change Biology, 6 (Suppl. 1), 69-83.

Basist, A., N.C. Grody, T.C. Peterson, and C. Williams, N., (1998), Using the special sensor microwave/imager to monitor land surface temperatures, wetness and snow cover, Journal of Applied Meteorology, 37, 888-911.

Beringer, J., A.H. Lynch, F.S. Chapin, M. Mack, and G.B. Bonan, (2001), The representation of arctic soils in the land surface model: the importance of mosses, Journal of Climate, 14, 3324-3335.

Bjorgo, E., O.M. Johannessen, and M.W. Miles, (1997), Analysis of merged SMMR-SSMI time series of Arctic and Antarctic sea ice parameters 1978-1995, Geophysical Research Letters, 24 (4), 413-416.

Bogaert, J., L. Zhou, C.J. Tucker, R.B. Myneni, and R. Ceulemans, (2002), Evidence for a persistent and extensive greening trend in Eurasia inferred from satellite vegetation index data, Journal of Geophysical Research, 107 (D10), art# 4119.

Cavalieri, D.J., P. Gloerson, and W.J. Campbell (1984), Determination of sea ice parameters with the NIMBUS 7 SMMR, Journal of Geophysical Research, 89 (D4), 5355-5369.

Cavalieri, D.J., P. Gloerson, C.L. Parkinson, J.C. Comiso, and H.J. Zwally, (1997) Observed hemispheric asymmetry in global sea ice changes, science, 272, 1104-1106.

Chahine, M.T., D.J. McCleese, P.W. Rosenkranz, and D.H. Staelin, (1983), Interaction Mechanisms Within the Atmosphere, in Manual of Remote Sensing, edited by R.N. Colwell, pp. 165-230, American Society of Photogrammetry, Falls Church, Virginia.

Chambers, S., and F.S. Chapin, (2001), Fire effects on surface-atmosphere energy exchange in Alaskan black spruce ecosystems: Implications for feedbacks to regional climate, Journal of Geophysical Research, 108 (D1), art# 8145.

Chapin III, F.S., A.D. McGuire, J.T. Randerson, R. Pielke, D. Baldocchi, S.E. Hobbie, N. Roulet, W. Eugster, E. Kasischke, E.B. Rastetter, A. Zimov, and S.W. Running, (2000), Arctic and boreal ecosystems of western North America as components of the climate system, Global Change Biology, 6 (Suppl. 1), 211-223.

Chapin III, F.S., S.A. Zimov, G. Shaver, and S.E. Hobbie, (1996), CO2 fluctuation at high latitudes, Nature, 383 (6601), 585-586.

Chapman, W.L., and J.E. Walsh, (1993), Recent variations of sea ice and air temperature in high latitudes, Bulletin American Meteorological Society, 74 (1), 33-47.

Conrad, R., and W. Seiler (1981), Decomposition of atmospheric hydrogen by soil microorganisms and soil enzymes, Soil Biol. Biochem., 13, 43-49

Conrad, R., and W. Seiler (1985), Influence of temperature, moisture, and organic carbon on the flux of H2 and CO between soil and atmosphere: Field studies in tropical regions, J. Geophys. Res., 90, 5699-5709

DeFries, R.S., M. Hansen, J.R.G. Townshend, and R. Sohlberg, (1998), Global land cover classifications at 8km spatial resolution: The use of training data derived from Landsat imagery in decision tree classifiers, International Journal of Remote Sensing, 19, 3141-3168.

Derksen, C., and A.E. Walker, (2003), Identification of systematic bias in the cross-platform (SMMR and SSM/I) EASE-Grid brightness temperature time series, IEEE Transactions on Geoscience and Remote Sensing, 41 (4), 910-915.

Dioumaeva, I., S.E. Trumbore, E.A.G. Schuur, M.L. Goulden, M. Litvak, and A.I. Hirsch, (2003), Decomposition of peat from upland boreal forest: temperature dependence and sources of respired carbon, Journal of Geophysical Research, 108 (D3), art# 8222.

Dixon, R.K., S. Brown, R.A. Houghton, A.M. Solomon, M.C. Trexler, and J. Wisniewski, (1994), Carbon pools and flux of global forest ecosystems, Science, 263, 185-189.

Dunn, A., and S.C. Wofsy, (2003), Boreal Forest CO2 flux, soil temperature, and meteorological data, edited by N.V. Smith, Harvard University, Department of Atmospheric Sciences.

Ehhalt, D. H. (1999), Gas phase chemistry of the troposphere, in Global aspects of atmospheric chemistry, edited by R. Sellner, pp. 21-109, Springer-Verlag, New York.

Fallon, R. D. (1982), Influences of pH, temperature, and moisture on gaseous tritium uptake in surface soils, Appl. Env. Microbiol., 44, 171-178

Foster, J. D. J., and R. D. Davy (1988), Global Snow Depth Climatology, in USAF Publication, edited by USAF, Scott Air Force Base, Illinois.

Gerst, S., and P. Quay (2001), Deuterium component of the global molecular hydrogen cycle, J. Geophys. Res., 106, 5021-5031

Godde, M., et al. (2000), Hydrogen consumption and carbon monoxide production in soils with different properties, Biol. Fert. Soils, 32, 129-134

Goulden, M.L., S.C. Wofsy, J.W. Harden, S.E. Trumbore, P.M. Crill, S.T. Gower, T. Fries, B.C. Daube, S.-M. Fan, D.J. Sutton, A. Bazzaz, and J.W. Munger, (1998), Sensitivity of boreal forest carbon balance to soil thaw, Science, 279, 214-217.

Grody, N.C., A. Basist, T.C. Peterson, and C. Williams, N., (1998), Using the Special Sensor Microwave/Imager to Monitor Land Surface Temperatures, Wetness and Snow Cover, Journal of Applied Meteorology, 37 (9), 888-911.

Grody, N.C., (1991), Classification of snow cover and precipitation using the special sensor microwave imager, Journal of Geophysical Research, 94 (D4), 7423-7435.

Grody, N.C., (1988), Surface identification using satellite microwave radiometers, IEEE Transactions on Geoscience and Remote Sensing, 26 (6), 850-859.

Hall, D. K., et al. (2003), MODIS/Aqua Snow Cover Daily L3 Global 0.5Deg CMG

Hansen, J., R. Ruedy, J. Glascoe, and M. Sato, (1999), GISS analysis of surface temperature change, Journal of Geophysical Research, 104 (D24), 30997-31002.

Hansen, J., R. Ruedy, M. Sato, M. Imhoff, W. Lawrence, D. Easterling, T.C. Peterson, and T.R. Karl, (2001), A closer look at United States and global surface temperature change, Journal of Geophysical Research, 106 (D20), 23947-23963.

Hansen, M., R.S. DeFries, J.R.G. Townshend, and R. Sohlberg, (2000), Global land cover classification at 1km spatial resolution using a classification tree approach., International Journal of Remote Sensing, 21 (6-7), 1331-1364.

Hauglustaine, D. A., and D. H. Ehhalt (2002), A three-dimensional model of molecular hydrogen in the troposphere, J. Geophys. Res., 107, 4330, doi:10.1029/2001JD001156.

Hicke, J.A., G.P. Asner, J.T. Randerson, C.J. Tucker, S.O. Los, R. Birdsey, J.C. Jenkins, and C.B. Field, (2002), Trends in North American net primary productivity derived from satellite observations, 1982-1998, Global Biogeochemical Cycles, 16 (2), 2-1 - 2-14.

Hinkel, K.M., (1998), Soil Temperatures for Happy Valley and Barrow, Alaska, USA, National Snow and Ice Data Center, Boulder, CO.

Hirschfelder, J. O., et al. (1954), Molecular theory of gases and liquids, John Wiley and Sons, Inc., New York.

Hobbie, S.E., J.P. Schimel, S.E. Trumbore, and J.T. Randerson, (2000), Controls over carbon storage and turnover in high-latitude soils., Global Change Biology, 6 (Suppl. 1), 196-210.

Hubbard, R. M., et al. (2005), Seasonal patterns in soil surface CO2 flux under snow cover in 50 and 300 year old subalpine forests, Biogeochemistry, 73, 93-107

IPCC, Climate Change 2001: (2001) IPCC Third Assessment Report, Intergovernmental Panel on Climate Change.

Judge, J., J.F. Galantowicz, A.W. England, and P. Dahl, (1997), Freeze/Thaw classification for prairie soils using SSM/I radiobrightnesses, IEEE Transactions on Geoscience and Remote Sensing, 35 (4), 827-832.

Keeling, C.D., J.F.S. Chin, and T.P. Whorf, (1996), Increased activity of northern vegetation inferred from atmospheric CO2 measurements, Nature, 382, 146-149.

Kimball, J.S., K.C. McDonald, A.R. Keyser, S. Frolking, and S.W. Running, (2001), Application of the NASA Scatterometer (NSCAT) for determining the daily frozen and nonfrozen landscape of Alaska, Remote Sensing of Environment, 75, 113-126.

Knowles, K.W., E. Njoku, R.L. Armstrong, and M.J. Brodzik, (2002), Nimbus-7 SMMR Pathfinder daily EASE-Grid brightness temperatures, National Snow and Ice Data Center, Boulder, CO.

Laxon, S., N. Peacock, and D. Smith, (2003), High interannual variability of sea ice thickness in the Arctic region, Nature, 425, 947-950.

Liu, H.P., J.T. Randerson, J. Lindfors, and F.S. Chapin, (2004), Changes in the surface energy budget in boreal ecosystems following fire in interior Alaska., in preparation for J.G.R.

Liu, W.T., W.Q. Tang, and F.J. Wentz, (1992), Precipitable water and surface humidity over global oceans from special sensor microwave imager and European Center for Medium Range Weather Forcasts, Journal of Geophysical Research, 97, 2251-2264.

Lloyd, J., and J.A. Taylor, (1994), On the temperature dependence of soil respiration, Functional Ecology, 8 (3).

LP-DAAC, Land Processes Distributed Active Arcive Center (LP DAAC), U.S. Geological Survey EROS Data Center http://edcdaac.usgs.gov, (2003).

Mikan, C.J., J.P. Schimel, and A.P. Doyle, (2002), Temperature controls of microbial respiration in arctic tundra soils above and below freezing, Soil Biology and Biochemistry, 34, 1785-1795.

Moldrup, P., et al. (1999), Modeling diffusion and reaction in soils: IX. The Cuckingham-Burdine-Campbell equation for gas diffusivity in undisturbed soil, Soil Science, 164, 542-551

Myneni, R.B., C.D. Keeling, C.J. Tucker, G. Asrar, and R.R. Nemani, (1997), Increased plant growth in the northern high latitudes from 1981 to 1991, Nature, 386, 698-386.

Myneni, R.B., C.J. Tucker, G. Asrar, and C.D. Keeling, (1998), Interannual variations in satellite-sensed vegetation index data from 1981-1991, Journal of Geophysical Research, 103 (D6), 6145-6160.

Novelli, P. C., et al. (1999), Molecular hydrogen in the troposphere: Global distribution and budget, J. Geophys. Res., 104, 30427-30444

Rahn, T., et al. (2002), Concentration and dD of molecular hydrogen in boreal forests: Ecosystem-scale systematics of atmospheric H2, Geophys. Res. Letters, 29, 1888, doi:10.1029/2002GL015118.

Raich, J.W., and C.S. Potter, (1995), Global patterns of carbon dioxide emissions from soils, Global Biogeochemical Cycles, 9 (1), 23-36.

Raich, J.W., C.S. Potter, and D. Bhagawati, (2002), Interannual variability in global soil respiration, 1980-94, Global Change Biology, 8, 800-812.

Randerson, J.T., C.B. Field, I.Y. Fung, and P.P. Tans, (1999), Increases in early season ecosystem uptake explain recent changes in the seasonal cycle of atmospheric CO2 at high northern latitudes, Geophysical Research Letters, 26 (17), 2765-2768.

Randerson, J.T., M.V. Thompson, T.J. Conway, I.Y. Fung, and C.B. Field, (1997), The contribution of terrestrial sources and sinks to trends in the seasonal cycle of atmospheric carbon dioxide, Global Biogeochemical Cycles, 11 (4), 535-560.

Reynolds, C. A., et al. (1999), Estimating available water content by linking the FAO Soil Map of the World with global soil profile databases and pedo-transfer functions, paper presented at AGU 1999 Spring Conference, Boston, MA, May 31 - June 4, 1999.

Rhee, T. S., et al. (2006), The overwhelming role of soils in the global atmospheric hydrogen cycle, Atmospheric Chemistry and Physics, 6, 1611-1625

Rodell, M., et al. (2004), The global land data assimilation system, Bulletim of the American Meteorological Society, 85, 381-394

Running, S.W., J.B. Way, and K.C. McDonald, (1999), Radar remote sensing proposed for monitoring freeze thaw transitions in boreal regions, EOS, Transactions, American Geophysical Union, 80 (19).

Schimel, J.P., and J.S. Clein, (1996), Microbial response to freeze-thaw cycles in tundra and taiga soils, Soil Biology and Biochemistry, 28 (8), 1061-1066.

Schuler, S., and R. Conrad (1991), Hydrogen oxidation activities in soil as influenced by pH, temperature, moisture and season, Biol. Fert. Soils, 12, 127-130

Schultz, M. G., et al. (2003), Air pollution and climate-forcing impacts of a global hydrogen economy, Science, 302, 624-627

Seiler, W. R., Conrad (1987), Contribution of tropical ecosystems to the global budgets of trace gases, especially CH4, H2, CO and N2O, in The geophysiology of Amazonia: Vegetation and Climate Interactions, edited by R. E. Dickerson, pp. 33-62, John Wiley, New York.

Serreze, M.C., J.E. Walsh, F.S. Chapin, T.E. Osterkamp, M. Dyurgerov, V.E. Romanovsky, W.C. Oechel, J. Morison, T. Zhang, and G. Barry, (2000), Observational evidence of recent change in the northern high-latitude environment, Climatic Change, 46, 159-207.

Shabanov, N.V., L. Zhou, Y. Knyazikhin, R.B. Myneni, and C.J. Tucker, (2002), Analysis of interannual changes in northern vegetation activity observed in AVHRR data from 1981 to 1994, IEEE Transactions on Geoscience and Remote Sensing, 40 (1), 115-130.

Shaver, G., and J. Laundre, (2003), Toolik Lake, AK soil temperature data, Arctic LTER,.

Smith, D.M., (1998), Recent increase in the length of the melt season of perennial Arctic sea ice, Geophysical Research Letters, 25 (5), 655-658.

Smith-Downey, N., et al. (in prep), Field observations of H2 uptake by soils

Smith-Downey, N., et al. (in press), Temperature and moisture dependence of soil H2 uptake measured in the laboratory, Geophys. Res. Letters

Stone, R.S., E.G. Dutton, J.M. Harris, and D. Longenecker, (2002), Earlier spring snowmelt in northern Alaska as an indicator of climate change, Journal of Geophysical Research, 107 (D10), 10-1 - 10-13.

Streig, R. G., et al. (1992), Consumption of atmospheric methane by desert soils, Nature, 357, 145-147

Trevors, J. T. (1985), Hydrogen consumption in soil, Plant and Soil, 87, 417-422

Tromp, T. K., et al. (2003), Potential environmental impact of a hydrogen economy on the stratosphere, Science, 300, 1740-1742

Tucker, C.J., D.A. Slayback, J.E. Pinzon, S.O. Los, R.B. Myneni, and M.G. Taylor, (2001), Higher northern latitude normalized difference vegetation index and growing season trends from 1982-1999, International Journal of Biometeorology, 45, 184-190.

Vinnikov, K.Y., A. Robock, R.J. Stouffer, J.E. Walsh, C.L. Parkinson, D.J. Cavalieri, J.F.B. Mitchell, D. Garrett, and V.F. Zakharov, (1999), Global warming and northern hemisphere sea ice extent, Science, 286, 1934-1937.

Warneck, P. (1988), Chemistry of the Natural Atmosphere, in International Geophysics Series, edited, p. 757, Academic, San Diego.

Warwick, N. J., et al. (2004), Impact of a hydrogen economy on the stratosphere and troposphere studied in a 2-D model, Geophys. Res. Letters, 31, L05107, doi:10.1029/2003GL019224.

Welp, L. R., et al. (in press), Seasonal exchange of CO2 and d18O-CO2 varies with post-fire succession in boreal forest ecosystems, J. Geophys. Res.

Wentz, F.J., (1997), A well-calibrated ocean algorithm for Special Sensor Microwave/Imager, Journal of Geophysical Research, 102 (8703-8718).

Wentz, F.J., (1992), Measurement of oceanic wind vector using satellite microwave radiometers, IEEE Transactions on Geoscience and Remote Sensing, 30 (5), 960-972.

Yonemura, S., et al. (1999), Continuous measurements of CO and H2 deposition velocities onto an andisol: uptake control by soil moisture, Tellus, 51B, 688-700

Yonemura, S., et al. (2000a), Carbon monoxide, hydrogen and methane uptake by soils in a temperate arable field and a forest, J. Geophys. Res., 105, 14347-14362

Yonemura, S., et al. (2000b), Model analysis of the influence of gas diffusivity in soil on CO and H2 uptake, Tellus, 52B, 919-933

Zhang, T., and R.L. Armstrong, (2001), Soil freeze/thaw cycles over snow-free land detected by passive microwave remote sensing, Geophysical Research Letters, 28 (5), 763-766.

Zhou, L., C.J. Tucker, R.K. Kaufmann, D.A. Slayback, N.V. Shabanov, and R.B. Myneni, (2001), Variations in northern vegetation activity inferred from satellite data of vegetation index during 1981 to 1999, Journal of Geophysical Research, 106 (D17), 20069-20083.

Zimov, A., S.P. Davidov, G.M. Zimova, A.I. Davidova, F.S. Chapin, M.C. Chapin, and J.F. Reynolds, (2001), Contribution of disturbance to increased seasonal amplitude of atmospheric CO2, Science, 284, 1973-1976.